Edinburgh Napier UNIVERSITY

Processing and Characterisation of Tubular Solid Oxide Fuel Cell (SOFC) Cathodes using a Novel Manufacturing Technique

Dong Wang

Doctor of Philosophy

A thesis submitted in partial fulfilment of the requirements of Edinburgh Napier University, for the award of Doctor of Philosophy, April 2015

Abstract

This thesis investigates a novel method for manufacturing a tubular solid oxide fuel cell cathode. The work involved depositing a lanthanum nickel ferrite / lanthanum strontium manganite cathode onto an yttria stabilized zirconia electrolyte using an electroless co-deposition technique. The lanthanum nickel ferrite is a promising cathode material but suffers from degradation at the high temperatures encountered during the sintering process which is required during conventional cathode processing.

The novel technique employed in this work does not involve these high temperatures so the investigation was focused on whether co-deposition could be employed to use the lanthanum nickel ferrite (LNF). The experimental work involved co-deposition of conventional cathode materials – lanthanum strontium manganite and yttria stabilized zirconia onto both planar and tubular sections of alumina substrates, under the environment of both acid and alkaline baths. This was followed by repeating the procedure using lanthanum nickel ferrite onto tubular and planar yttria stabilized zirconia substrates.

The performance of these co-deposited cathodes was characterized using optical and scanning electron microscopy, energy dispersive X-ray analysis and electrochemical analysis. These were planar fuel cells so as to allow basic testing of the cells. The work thus demonstrated that electroless co-deposition of tubular cathodes incorporating LNF was successful – both via SEM / EDX characterisation and basic electrical testing.

Factors which affected the coating deposition and performance were also investigated and a comprehensive overview of the development of solid oxide fuel cells is also detailed.

Acknowledgements

I sincerely express my deepest gratitude to my supervisors, Mr. Alan Davidson and Dr Mike Barker, for their valuable supervision, continuous encouragement, and especially sacrifice of part of holiday throughout this project.

I thank Edinburgh Napier University and the School of Engineering and the Build Environment for offering me full research facilities used in this programme.

I thank the staff members and the research team; in particular, Dr Callum Wilson, Dr Neil Shearer, Mrs Lynn Chalmers, Dr Nwosu Nkem and Mr Yanzhao Zhang for their patient encouragement and continuous help in my work.

Especially I would like to acknowledge Lanying Lu, from School of Chemistry, University of St. Andrews, for her help and support.

Finally, my grateful thanks are due to my family for their understanding, encouragement, support, and help.

Contents List

List of figures

List of tables

1. Introduction

1.1 Background

The demand for energy has kept increasing by the acceleration of global industrialization since last century. Energy is an important factor to increase the economy development and to improve people's living standard. The energy consumption is increasing dramatically with the economic development, the rise of population. This is shown in table 1[1].

Table 1 Population, energy and electricity demands

Year	Population (billions)	Energy demand, MBDOE [a]	Electricity demand, % Energy demand
1940	2.4	70	/
1960	3.0	90	/
1970	3.6	100	6
1985	4.8	200	12
1995	5.3	300	15
2000	6.1	350	30
2001	7.2	410	50

a: Millions of Barrels per Day of Oil Equivalent

Meanwhile, because of immoderate or illegal mining, the fossil fuel resources, which are the foundation of modern science, technology and civilization, are gradually diminishing; but environmental pollution is getting increasingly serious at the same time. Nowadays, most of the current global energy is coming from fossil fuel combustion process, which causes the continuous growth of fossil fuel consumption. The rising emissions of greenhouse gases, especially CO_2 have become a big issue over the world.

Global warming is taking place due to the huge amount of effluent gas emission, CO_2 etc. It is established global surface temperatures have increased at a rate near

0.6°C/century [2]. Furthermore, this trend has dramatically increased in the past decades. Today, the rapidly developing fuel cells could be a good solution to this important environmental problem because of the efficiency and effectively. The total CO_2 emissions of the top 15 nations are shown in tables 2[3]; the CO_2 emissions of top industrial nations per capita are shown in table 3[3]. Table 4[3] shows the CO_2 emissions of top 9 nations by unit Gross National Product (GNP).

Table 2 Emissions of the top 15 nations by CO2 volume (billions of tonnes)

Rank	Nation	CO_2	Rank	Nation	CO_2	Rank	Nation	CO_2
1	USA	1.13	6	India	0.19	11	Mexico	0.09
2	Russia	0.98	7	UK	0.16	12	Poland	0.08
3	China	0.69	8	Canada	0.11	13	S. Africa	0.08
4	Japan	0.30	9	Italy	0.11	14	S. Korea	0.07
5	Germany	0.27	10	France	0.10	15	Australia	0.07

Table 3 Emissions of the top 15 nations by CO2 volume per capita (tonnes)

Rank	Nation	CO_2	Rank	Nation	CO_2	Rank	Nation	CO_2
1	USA	19.1	6	UK	10.1	11	France	6.3
2	Russia	18	7	Japan	8.8	12	S. Korea	5.8
3	Australia	14.4	8	Poland	7,7	13	Mexico	3.6
4	Canada	13.9	9	Italy	7.1	14	China	2.1
5	Germany	12.2	10	S.Africa	7.1	15	India	0.8

Table 4 Emissions of the top 9 nations by CO2 volume per unit GNP

Rank	Nation	CO_2	Rank	Nation	CO_2	Rank	Nation	CO_2
1	Russia	7591	4	Canada	708	7	Italy	366
2	China	4015	5	UK	549	8	Japan	271
3	USA	740	6	Germany	477	9	France	255

Because of the increase of individual energy consumption, the reduction of energy resources, and the huge amount of emissions, the new power generation technologies are becoming increasingly important. Indeed, fuel cells could be one solution. As a kind of environmental-friendly energy technology, fuel cells could achieve energy conservation by improving energy efficiency and reducing in the consumption of fossil fuels.

1.2 Fuel cells

A fuel cell is an energy conversion device that produces electricity from converting the chemical energy of a fuel gas directly to electrical energy and heat without direct combustion. It gives high conversion efficiencies which could not be achieved by conventional thermo mechanical methods. The operating principles of fuel cells are very similar to other batteries. Generally, the electrochemical combination of reactants generates electricity. The combination made of any kind of fuel gases (for example hydrogen) and an oxidant gas (normally oxygen from air) flows through electrodes and an ion conducting electrolyte. A fuel cell could keep running without reduction in power or recharging problems, what it needs are the fuel gas and air support to the electrodes.

Fuel cells have been more and more important because of these great potential for power generation and other various applications. The high efficiency, very low emissions and negligible influence on surrounding environment provide great advantages for fuel cells; and fuel cells are becoming commercially viable. The main factor is the ultimate cost of fuel cell technology. However, significant researches on manufacturing process cost reduction and properties improvement carried out in decades would help fuel cells gain a commercial footing for conventional power generation and further.

1.2.1 Fuel cells history

Despite the modern high-tech aura, fuel cells actually have been well known since 1980s'.Furthermore, fuel cells have become fervent research subject since World War II. The concept of the fuel cell goes back to 1839; it is described by William Grove [4]

(1811–1896), an English lawyer turned scientist. The ‘Grove cell’, as it was called, is a type of wet-cell battery based on reversing the electrolysis of water. Grove observed that there was a small current flowing through the electrolysis products (hydrogen and oxygen), catalysed by the platinum electrodes, when the current was switched off. Grove considered the possibility of a gaseous voltaic battery between the ‘three-phase boundary’, the gaseous reagent, the electrolyte, and the electrode. [5] Ceramic fuel cells came out in 1899, after Nernst’s discovery of solid oxide electrolytes [6]. Ludwig Mond (1839–1909) and assistant Carl Langer described that they attained 6 amps per square foot (surface area of the electrode) at 0.73 V with a hydrogen–oxygen fuel cell which had a porous platinum black electrode structure, and used a diaphragm made of a porous non-conducting substance to hold the electrolyte[7]. Fuel cells development accelerated after the World War II, and beginning the mid-1980s’, governments started to get more investment and founding in fuel cells research and development. Today fuel cells are commonly used in home power generation, transportation, spaceflight (Space shuttle, Skylab, Spacecraft, etc.), and power generation.

1.2.2 Fuel cells types

Fuel cells could be generally classified by the chemical characteristics of the electrolyte, which is the ionic conductor in the cell. The main types are shown in table 5 [8], [9]. Alkaline fuel cell (AFC) has high efficiency; needs low cost metal as catalyst; but the alkaline electrolyte may react with CO_2 to form deposit, which will seriously reduce the performance of the fuel cell. Phosphoric acid fuel cell (PAFC) and molten carbonate fuel cell (MCFC) have been commercialized. But PAFC has low power density, and needs high cost metal as catalyst; MCFC has high efficiency, but also has serious corrosion problems; CO_2 circulation system, which is used to reduce the corrosion, is very expensive. Polymer electrolyte membrane fuel cell (PEMFC) has high power density but needs high cost metal as catalyst, high cost proton exchange membrane, and is intolerant to impure fuel. Solid oxide fuel cell (SOFC) has high efficiency; and more importantly, it could use direct fossil fuel. SOFC is developing fast for low cost and has huge potential market competitiveness.

Table 5 Types of fuel cells

Fuel cell	Temp (°C)	Efficiency (%)	Fuel	Application	Advantages	Disadvantages
Alkaline fuel cell (AFC)	50–90	50–70	pure hydrogen, or hydrazine	Space application	High efficiency	Intolerant to CO2, in impure H_2 and air, corrosion, expensive
Phosphoric acid fuel cell (PAFC)	175–220	40–45	hydrogen from hydrocarbons	Stand-alone, combined heat and power	Tolerant to impure H_2, commercial	Low power density, corrosion & sulphur poisoning
Molten carbonate fuel cell (MCFC)	600–650	50–60	hydrogen, carbon monoxide, natural gas, propane, marine diesel	Central, standalone, combined heat and power	High efficiency, commercial	Electrolyte instability, corrosion & sulphur poisoning
Solid oxide fuel cell (SOFC)	800–1000	50–60	natural gas or propane	Central, standalone, combined heat and power	High efficiency, direct fossil fuel	High temperature, thermal stress failure, coking & sulphur poisoning
Polymer electrolyte membrane fuel cell (PEMFC)	60–100	40–50	less pure hydrogen from hydrocarbons or methanol	Vehicle, portable	High power density, low temperature	Intolerant to CO in impure H_2 and expensive
Direct methanol fuel cell (DMFC)	50–120	25–40	liquid methanol	Vehicle, small portable	No reforming, high power density, low temperature	Low efficiency, methanol crossover & poisonous by product

2. Aims and Objectives

The main aim is to manufacture a SOFC tubular cathode by electroless nickel co-deposition with yttria-stabilised zirconia (YSZ), lanthanum strontium manganate (LSM) and lanthanum nickel ferrite (LNF).

Other objectives of this research were:

1) To control the structure of the tubular fuel cell cathode surface, components proportion and porosity proportion in co-deposition process.
2) To analyse the performance and properties of the cathode using scanning electron microscopy, energy dispersive X-Ray analysis, optical microscope, etc.
3) To replace LSM with novel material, lanthanum nickel ferrite (LNF), which is a more competent cathode material at intermediate temperature (600°C - 800°C). Electroless nickel co-deposition with LNF/YSZ ceramic powders was carried out onto tubular substrate.
4) To build a planar cell, which is easy to test, using the novel technique and test it using electrochemical analysis.

3. Literature Review

3.1 Solid Oxide Fuel cells

3.1.1 Historical background

In 1899, after the discovery of solid oxide electrolytes, the solid oxide fuel cell was first conceived by Nernst [6]. Nernst reported that the conductivity of pure metal oxides rose very slowly with temperature and remained only relatively low; and the mixtures of metal oxides can possess dramatically higher conductivities. He suggested that this result was very similar to the well-known liquid electrolytes behaviour. Furthermore, he found that mixed oxides of zirconium oxide 85%, stabilised with 15% yttrium oxide, could get high conductivity at elevated temperatures. In 1905 Haber filed the first patent on fuel cells with a solid electrolyte. He used glass and porcelain as the electrolyte materials of his cell, and platinum and gold as the electrode materials (depending on the operation temperature). [10] In 1935, Schottky suggested that yttria stabilised zirconia could be used as a solid fuel cell electrolyte. In 1937, by giving up any liquid electrolytes, and using a completely dried solid oxide fuel cell, Baur and Preis achieved the first solid oxide (or ceramic) fuel cell with an yttria-stabilised zirconia electrolyte, at 1000 °C. [11] The serious materials problems coming from the high operating temperature and the reducing nature of the fuel gas hindered the development of the solid oxide fuel cell for decades. In 1960s, the biggest problem was that the efficiency of SOFCs was very poor because of the thick electrolyte layers and high losses due to internal resistance. Through continued advances in preparation and production methods through the 1970s, considerably thinner electrolytes were developed, which gave a significant improvement in performance of SOFCs. Recently, large scale SOFCs have been developed for power generation systems. Since December 1997, testing of a 100 kW SWH SOFC power generation system has been carried out by a consortium of Dutch and Danish utilities. [12]

3.1.2 Advantages

SOFC is a kind of advanced electrochemical fuel cell which could operate at a high temperature (round 1000°C). SOFC, which offers a clean and pollution-free

technology, is presently developing for electric power generation applications with high energy conversion efficiency. There are lots of significant advantages [9]:

- SOFCs are able to use a wild range of fuel gases, such as carbon-based fuels, natural gas, etc., which could be low cost.
- Currently, SOFCs are the most efficient (fuel input to electricity output) fuel cell electricity generators over the world.
- SOFC technology is most suited to applications in distributed generation (i.e. stationary power) because of the high conversion efficiency, which could reduce the cost of long fuel delivery systems to customer premises.
- SOFCs have a modular and solid state construction without moving parts, which is beneficial to indoor installation.
- The high SOFCs operating temperature provides high quality heat, which can be used for co-generation or for use in combined cycle applications.
- SOFCs do not contain noble metals; this is relatively low cost, also friendly to environment.
- SOFCs have an easy handling solid electrolyte which is not as corrosive as liquid ones.
- SOFCs have extremely low emissions by eliminating the danger of carbon monoxide in exhaust gases. This is because any CO produced is converted to CO_2 at the high operating temperature.
- SOFCs have a potential long life expectancy of more than 4.5 to 9 years.

3.1.3 Principle of SOFCs

The operating principle of a SOFC with an oxide ion conductor is shown in Figure 1[13]. When an external load is applied to the fuel cell, the oxygen and air go through the cathode and anode separately. At the porous air electrode, oxygen is reduced to oxide ions. These ions migrate through the solid electrolyte to the fuel electrode, where they react with the fuel H_2 (or CO or whatever), to produce H_2O (or CO_2 or others).

Following reactions happen on anode side:

$$H_2 + O^{2-} \rightarrow H_2O + 2e^- \text{ , which uses } H_2 \text{ as fuel;}$$

$$CO + O^{2-} \rightarrow CO_2 + 2e^- \text{ , which uses CO as fuel;}$$

$$CH_4 + 4O^{2-} \rightarrow 2H_2O + CO_2 + 8e^- \text{ , which uses } CH_4 \text{ as fuel}$$

And the reaction happens on cathode side is

$$O_2 + 4e^- \rightarrow 2O^{2-}$$

The theoretical maximum efficiency of this cell is very high, excess of 80% (combined heat and power, CHP) [14], SOFC practical application could get efficiency higher than 60%.

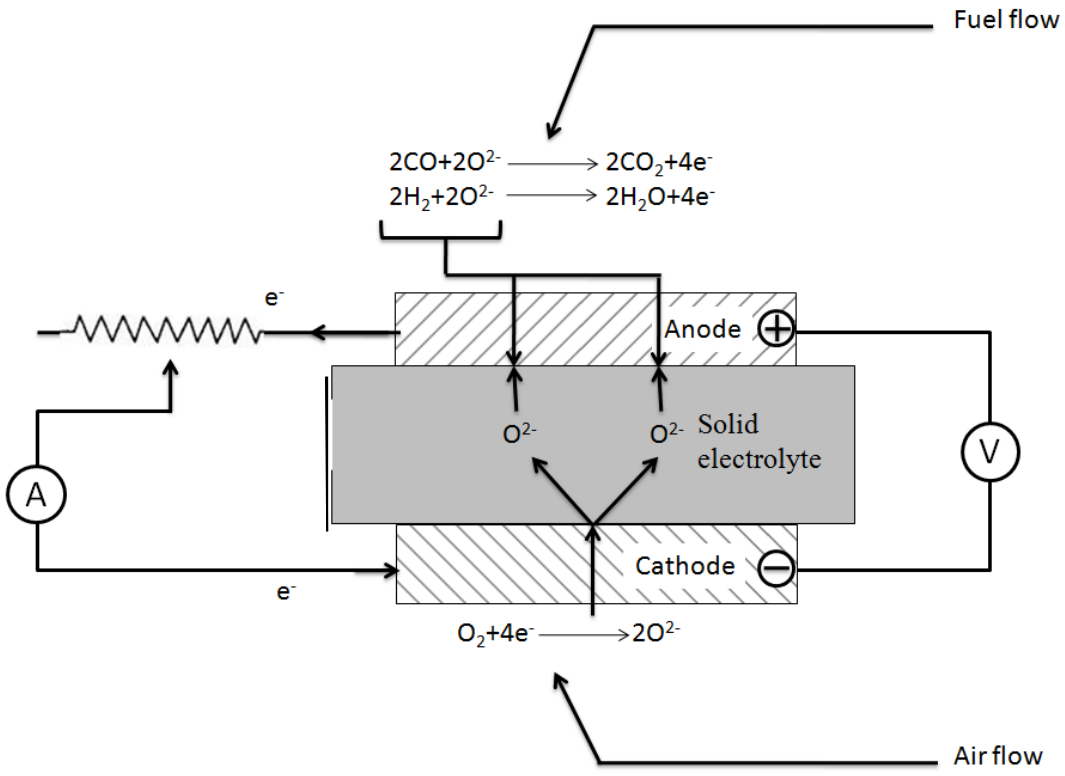

Figure 1 Principle of operation of SOFC

3.2 SOFCs Designs

Solid oxide fuel cells can be generally classified into tubular and planar designs. Both types include one or more single cells per stacking unit, single one or stack one. Furthermore, the planar designs can be divided by different interconnect materials (metallic or ceramic), and also by thickness. Table 6 presents the cell designs and current developments of the companies over the world. [15]

Table 6 Current SOFC designs

Tubular		Planar				
One cell per tube	Several cells per tube	One cell per tube			Several cells per tube	
Ceramic interconnect	Ceramic interconnect	Metallic interconnect		Ceramic interconnect	Metallic interconnect	
		Thick electrolyte	Thin electrolyte	Thick electrolyte	Thick electrolyte	Thin electrolyte
SWPC (D/USA)	MHI+EPDC (Nagasaki)(JP)	Sulzer (CH)	FZJ (D)	SOFCo (USA)	CFCL (AUS)	Rools-Royce (GB)
Toto (JP)		ECN (NL)	ECN (NL)	Tokyo Gas(JP)	Sanyo (JP) (terminated)	
		TMI (USA)	Riso (DK)	MHI+CEPC (Himeji) (JP)	Siemens (D) (terminated)	
		Ztek (USA)	Global			
		Fuji Electric (JP) (terminated)	Thermo electric (CAN)	Mitsui (JP)		
		Murata + Osaka gas (JP) (terminated)	Allied Signal (USA)	Riso (DK) (terminated)		
			CFCL(AUS)	Toho Gas (JP)		
				Dornier (D) (terminated)		

Furthermore, SOFCs could be divided into several cell configurations by different current paths. SOFCs are generally divided into two kinds: self-supporting and external-supporting. Self-supporting SOFCs could be electrolyte-supported, cathode-supported, and anode-supported; the external-supporting configuration could be porous substrate-supported and interconnect-supported. These are shown in figure 2. [16] Also the cell configurations and advantage & disadvantages are shown in table 7. [17]

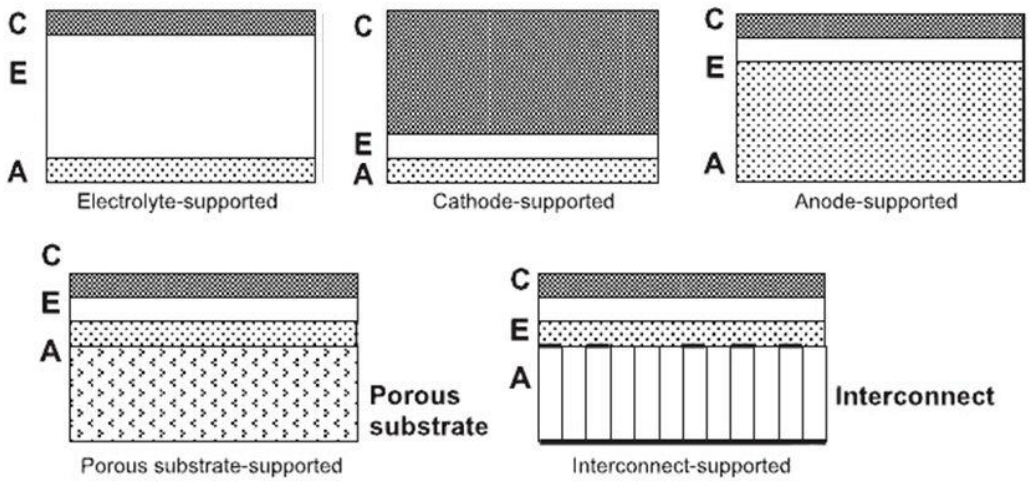

Figure 2 SOFC single cell configurations

Table 7 *Features of single cell configurations*

Cell configuration	Advantage	Disadvantage
Self-supporting		
Electrolyte-supported	Relatively strong structural support from dense electrolyte Less susceptible to failure due to anode reoxidation (Ni/YSZ anode) and cathode reduction (LSM cathode)	Higher resistance due to low electrolyte conductivity Higher operating temperatures required to minimize electrolyte ohmic losses
Anode-supported	Highly conductive anode Lower operating temperature via use of thin electrolytes	Potential anode reoxidation Mass transport limitation due to thick anodes
Cathode-supported	No oxidation issues but potential cathode reduction Lower operating temperature via use of thin electrolyte	Lower conductivity Mass transport limitation due to thick cathodes
External-supporting		
Interconnect-supported	Thin cell components for lower operating temperature Stronger structures from metallic interconnects	Interconnect oxidation Flowfield design limitation due to cell support requirement
Porous substrate	Thin cell components for lower operating temperature Potential for use of non-cell material for support to improve properties	Increased complexity due to addition of new materials Potential electrical shorts with porous metallic substrate due to uneven surface

By different stack design, SOFCs could be divided into several kinds. **Tubular design,** which is normally cathode-supported, has a tube made by cathode material, electrolyte and anode formed outside, and closed at one end. **Segmented-cell-in-series design,** which is normally porous substrate-supported, has each tube as a stack of cell arranging as a thin banded structure. **Planar design,** which could be either self-supported or external-supported, has flat plates connected electrically in series. **Monolithic design,** which is normally electrolyte-supported, has components forming into a corrugated structure.

3.2.1 Tubular Design

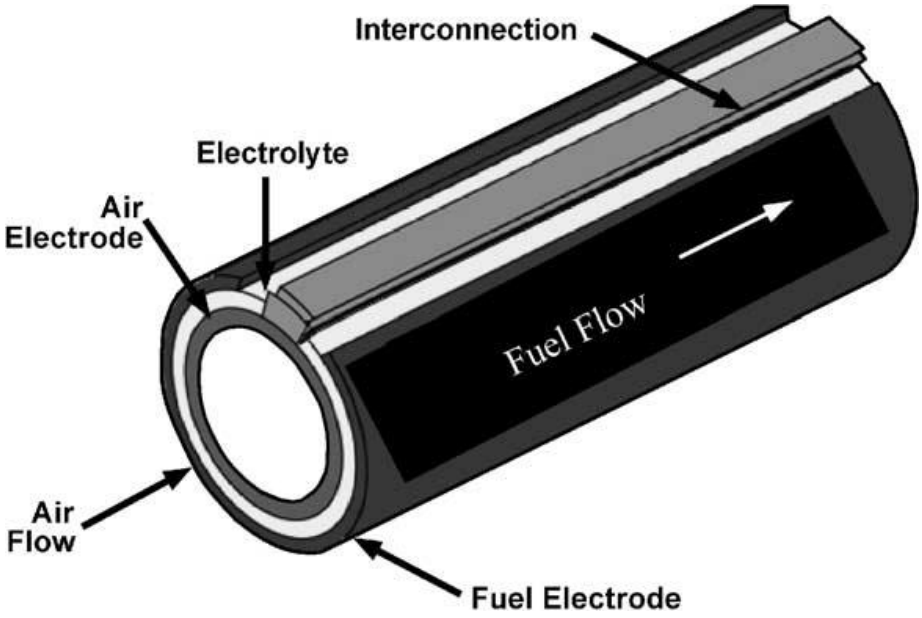

Figure 3 Tubular SOFC design.

The tubular cell design by the Siemens Westinghouse is shown in Figure 3. [18] The tubular SOFC design could be cathode-supported, anode-supported, or electrolyte-supported. The other two components are deposited on to the substrate. For example, the cathode tube of the cell, fabricated by extrusion and sintering, could be doped lanthanum manganite. The yttria-stabilised zirconia (YSZ) electrolyte is deposited in the form of about 40 μm thick dense layer by electrochemical vapour deposition [19]. The Ni/YSZ anode is deposited either by nickel slurry application or electrochemical vapour deposition of YSZ. (Sintering of Ni/YSZ slurry could also achieve this deposition). The doped lanthanum chromite interconnection strip along

the length of the cell is deposited by plasma spraying [20]. A large number of tubular cells have been electrically tested for over 25,000 hours [18]. These cells perform satisfactorily for extended periods of time under a variety of operating conditions with less than 0.1% per 1000 hours performance degradation. Such tubular cells have a power density at 1000°C of about 0.25–0.30 W/cm^2.

Table 8 shows the developers of SOFC tubular cell design.

Table 8 developers of SOFC tubular cell design

Company	Country	Component	Materials	Thickness
SWPC [21]	USA	Cathode tube	Doped $LaMnO_3$	2200μm
		Electrolyte	YSZ	40μm
Toto+KEPC [22],[23]	JP	Anode	Ni/YSZ	100μm
		Interconnect	Doped $LaCrO_3$	85μm
		Cathode tube	$(La,Sr)MnO_3$	ns
		Electrolyte	YSZ	40μm
MHI+EPDC [24],[25],[26],[27]	JP	Anode	Ni/YSZ	thick film
		Interconnect	$(La,Ca)CrO_3$	ns
		Substrate tube	Ca-SZ	21mm (out diameter)
		Cathode	$LaCoO_3$ $(La,Sr)MnO_3$	150-200μm
		Electrolyte	YSZ	100-150μm
Rolls-Royce [28]	GB	Anode	Ni/YSZ	80-100μm
		Interconnect	$NiAl/Al_2O_3$ $(Ln,AE)TiO_3$	80-100μm
		Substrate tube	ns	ns
		Electrolyte	ns	<20μm
		Cathode	ns	ns

3.2.2 Planar Design

Figure 4 shows the planar SOFC design. This sandwich structure simple planar cell is comprised with many thin, flat plates (anode, electrolyte, and cathode). The interconnection, which is ribbed on both sides, gives enough space for gas flowing, and serves as a bipolar gas separator contacting the anode and the cathode of adjoining cells.

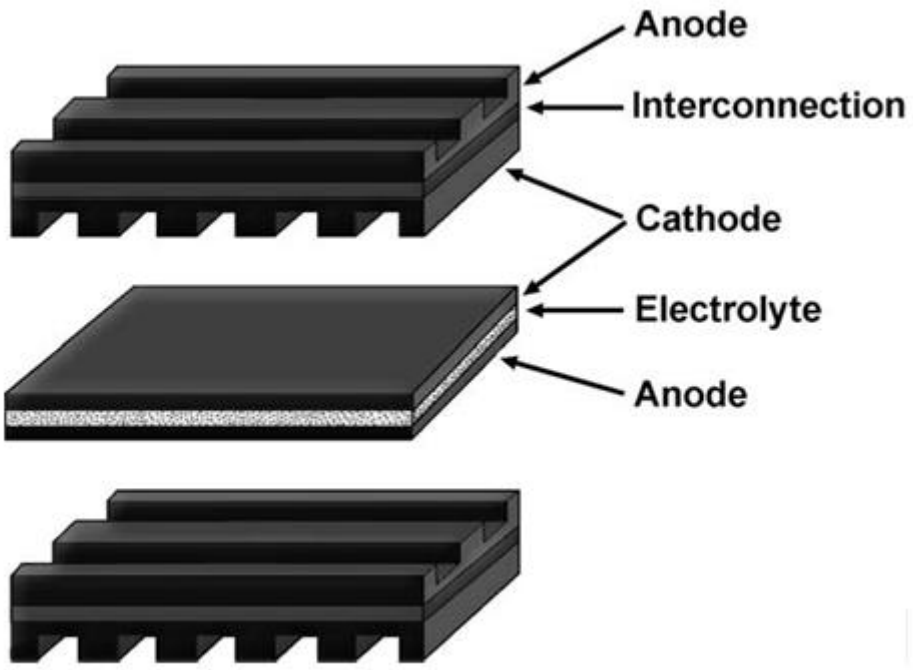

Figure 4 Planar SOFC Design

3.3 Components

Because SOFC will be working at a high temperature, and it is a solid state, the thermal expansion coefficient of each material must be very close, the closer the better. This could avoid some mechanical failure or cracking. And on the other hand, the cathode, anode, and interconnects must have high electrical conductivity. There are also other properties beside these, which narrow the range of SOFC materials. Though there are various designs of SOFCs, the materials for cell components in these are very similar. The functions dictate these properties: [29]

- Good stability (chemical, phase, morphological, and dimensional)
- Proper conductivity
- Chemical compatibility with other components
- Similar thermal expansion coefficient to avoid cracking during the cell operation
- Dense electrolyte to prevent gas mixing
- Porous anode and cathode to allow gas transport to the reaction sites
- High strength and toughness properties
- Fabricability
- Amenable to particular fabrication conditions
- Compatibility at higher temperatures at which the ceramic structure are fabricated
- Low cost

3.3.1 Cathode

The cathode is normally the air electrode, where the oxygen reduction reaction happens. The oxygen in gas phase consumes two electrons, and is reduced to oxide ions.

$$1/2\ O_2 + 2e^- \rightarrow O^{2-}$$

Because of the high operating temperature (around 1000°C) of the SOFC, only noble metals, which have prohibitive cost and insufficient long term stability, or electronic conducting oxide, could be used as a cathode.

The electrode material depends on the application, the specific electrolyte material, the desired operating temperature range, the electrochemical cell design, and the specific fabrication methods. The most common materials for cathode applications of SOFCs are lanthanum manganite suitably doped with alkaline and rare earth elements. This perovskite-type lanthanum manganite shows reversible oxidation-reduction behaviour. The perovskite lattice structure is shown in figure 5 [30]. This oxide consists of three element, large cations A^{n+}, the small cations, $B^{(6-n)+}$, and

the oxide ions, O^{2-}, where n is the positive charge of A, cations $B^{(6-n)+}$ are surrounded by 6 O^{2-}s.

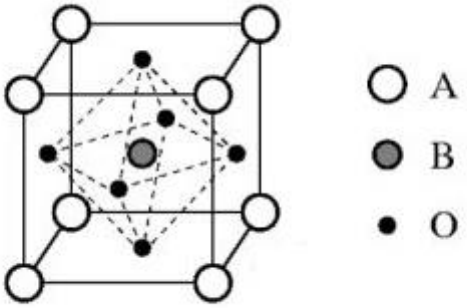

Figure 5 Schematic representation of lattice structure of perovskite. ABO_3

Lanthanum manganite doped with alkaline and rare earth elements can have oxygen excess or deficiency depending upon the ambient oxygen partial pressure and temperature. It is stable in air, and could dissociate at 1000°C when the oxygen pressure is less than 10^{-14} atm. The oxides show deficiency from the stoichiometric composition, and, the oxygen vacancies are formed by the representing as:

$$2Mn_{Mn}^{\cdot}+O_o^x=2Mn_{Mn}^x+V_o^{\cdot\cdot}+\frac{1}{2}O_2 \qquad [30]$$

The electronic conductivity of lanthanum manganite is due to hopping of an electron hole between the +3 and +4 valence stats of Mn, and this conductivity is enhanced by doping with a divalent ion such as calcium or strontium. [31],[32] The electrical conductivity comes from a La^{3+} ion being replaced by a Sr^{2+} ion, an electric hole is formed on the Mn^{3+} site to maintain electroneutrality and increases the electrical conductivity, which could be presented as:

$$LaMnO_3 \xrightarrow{xSrO} La_{1-x}^{3+}Sr_x^{2+}Mn_{1-x}^{3+}Mn_x^{4+}O_3 \qquad [30]$$

Lanthanum strontium manganite, $LaSrMnO_3$ (LSM) and lanthanum calcium manganite, $LaCaMnO_3$ (LCM) offer excellent thermal expansion coefficient which matches with zirconia electrolytes, and provide good performance at operating temperatures above 800°C. The reactivity and interdiffusion studies between doped Lanthanum manganite and yttria stabilized zirconia (YSZ) electrolyte have minimal interactions between these two materials at 1000°C [33], [34]. There are a range of alternative perovskite-structured ceramic electrode materials built on lanthanum manganite. The commonly use materials are

- Lanthanum strontium ferrite (LSF), $(LaSr)(Fe)O_3$
- Lanthanum strontium cobaltite (LSC), $(LaSr)CoO_3$
- Lanthanum strontium cobaltite ferrite (LSCF), $(LaSr)(CoFe)O_3$
- Lanthanum strontium manganite ferrite (LSMF), $(LaSr)(MnFe)O_3$
- Samarium strontium cobaltite (SSC), $(SmSr)CoO_3$
- Lanthanum calcium cobaltite ferrite (LCCF), $(LaCa)(CoFe)O_3$
- Praseodymium strontium manganite (PSM), $(PrSr)MnO_3$
- Praseodymium strontium manganite ferrite (PSMF), $(PrSr)(MnFe)O_3$

To improve electrode performance, electrolyte materials (for example YSZ) powder could be mixed with the perovskite-structured ceramic (for example LSM). The incorporation of electrolyte material and the cathode material could increase the volume of active sites available for electrochemical reactions, which could improve electrode performance at lower temperatures. [35] This would be mentioned in the laboratory work of this report.

3.3.2 Electrolyte

The electrolyte of SOFC must be conducting, could let the oxide ions (O^{2-}) migrate from air electrode (cathode) to fuel electrode (anode). There is a range of oxide combinations that could be used for solid non-porous electrolytes. The most common used has been the fluorite-structured stabilised zirconia with conductivity based on oxygen ions (O^{2-}), especially yttria-stabilised zirconia (Y_2O_3-stabilized ZrO_2 or YSZ). A tiny amount of yttrium (normally with a form of Y_2O_3), is added to the zirconia during manufacture. YSZ offers purely oxygen ionic conduction (with no electronic

conduction). ZrO_2 crystalline array has two oxide ions to every zirconium ion. But Y_2O_3 has only 1.5 oxide ions to every yttrium ion. The result is vacancies in the crystal structure where oxide ions are missing.

An oxygen vacancy is created for every mole of the Y_2O_3. Yttrium oxide stabilizes the high temperature cubic phase in zirconia and generates oxygen vacancies. The high oxide ion conductivity in YSZ is attributed to these oxygen vacancies. Furthermore, besides YSZ, the other commonly used oxide based ceramic electrolytes include:

- Cerium oxide doped with samarium (SDC), $(Ce_{0.85}Sm_{0.15})O_{1.925}$
- Cerium oxide doped with gadolinium (GDC), $(Ce_{0.90}Gd_{0.10})O_{1.95}$
- Cerium oxide doped with yttrium doped Ceria (YDC), $(Ce_{0.85}Y_{0.15})O_{1.925}$
- Cerium doped with calcium (CDC), $(Ce_{0.88}Ca_{0.12})O_{1.88}$
- Lanthanum gallate ceramic that include lanthanum strontium gallium magnesium
- (LSGM), $(La_{0.80}Sr_{0.20})$ $(Ga_{0.90}Mg_{0.10})O_{2.85}$ or $(La_{0.80}Sr_{0.20})$ $(Ga_{0.80}Mg_{0.20})O_{2.80}$
- Bismuth yttrium oxide (BYO), $(Bi_{0.75}Y_{0.25})_2O_3$
- Barium Cerate (BCN), $(Bi_{0.75}Y_{0.25})2O_3$ and
- Strontium Cerate (SYC), $Sr(Ce_{0.95}Yb_{0.05})O_3$

3.3.3 Anode

The anode (fuel electrode) could be made of variety of materials but should have good electronic conductivity. Thus, there should be a metallic content of around 40% by volume. Less content of metal will cause a poor conductivity, and too much will cause a failure at operating temperature because the thermal expansion coefficient differs too much at high temperature. The fuel oxidation reaction below takes place on the anode:

$$O^{2-} + H_2 \rightarrow H_2O + 2e^-$$

Suitable metals are nickel, cobalt, and ruthenium as the anode, but because of their higher coefficient of thermal expansion, yttria-stabilised zirconia (YSZ) is mixed with nickel, in most cases, to get a closer thermal expansion coefficient to the electrolyte.

Particularly in tubular cells, a 100-150μm thick layer of nickel/YSZ cermet is used as the anode.

3.3.4 Interconnect

The interconnect could be ceramic or metal, depends on the working temperature of the SOFC. The ceramic is suitable for high temperature usage; and metal or metallic alloys are for intermediate temperature. In ceramic, primarily doped lanthanum and yttrium chromites [36] have an increasing electric conductivity with temperature, are candidates for interconnect material, but not for intermediate temperature SOFC usage. But the ceramic is relatively high cost and fragile, which are the disadvantages. At intermediate temperature, the low cost and easy processed metallic alloy like ferritic stainless steels, which have close thermal expansion coefficient to zirconia electrolyte [37], is a good choice.

To overcome the corrosion problem, which is a big problem that the interconnect has at the SOFC working temperature, chromia is usually used to combat the situation. It reduces the corrosion well. However, the evaporated Cr causes electrode poisoning. Coating the interconnect with a perovskite material, like lanthanum strontium manganite or cobaltite could help this. [36]

3.4 SOFCs materials manufacture technologies

There are lots of options existing in the process. The techniques are present separately by different process steps.

.

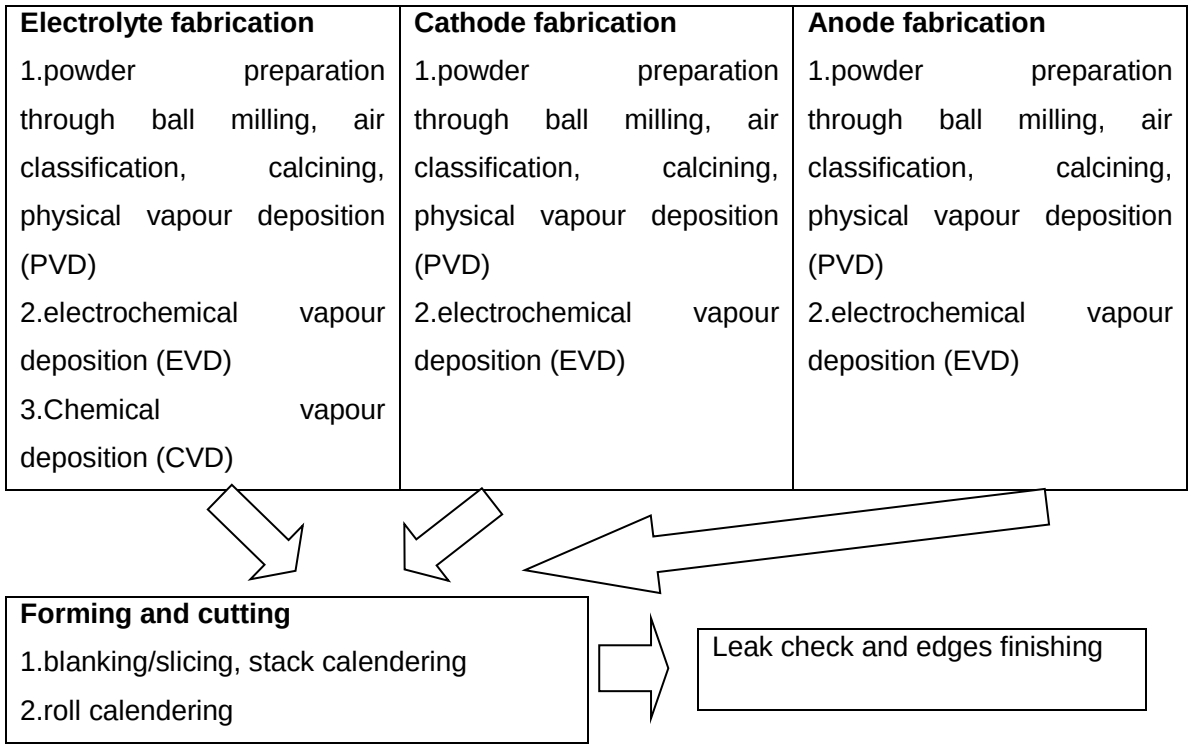

Figure 6 Simple production processes

There are a number of techniques used in SOFCs manufacturing, shown below, and also, some manufacturing techniques are discussed later.

I. Component formation without requiring subsequent firing

i) For planar and tubular

Chemical Vapour Deposition (CVD)

ii) For planar only

Interconnect layup; interconnect metal formation & shearing; sputtering (Physical vapour deposition PVD)

II. Component formation requiring subsequent firing

i) For planar and tubular

Compaction; extrusion;

ii) For planar only

Slip casting; tape calendering; tape casting

III. Deposition onto formed component requiring subsequent firing

i) For planar and tubular

Slurry spraying; vacuum plasma spraying; thermal spraying

ii) For planar only

Dip coating; screen printing;

iii) Unspecified

Flame assisted vapour deposition; Electrophoretic Deposition (EPD); Pulsed Laser Deposition (PLD); spray pyrolysis; transfer printing

3.4.1 Wet chemical or ceramic technologies

3.4.1.1 Screen printing

J L li et al. [38] built a LBSM (($La_{0.74}Bi_{0.10}Sr_{0.16}$) $MnO_{3-\delta}$) EBS ($Bi_{0.7}Er_{0.3}O_{1.5}$) cathode layer by screen printing. D. Montinaro et al. [39] screen printed LSM20 powders as a current collector onto the cathode and sintered for 2 hours at 1150°C.

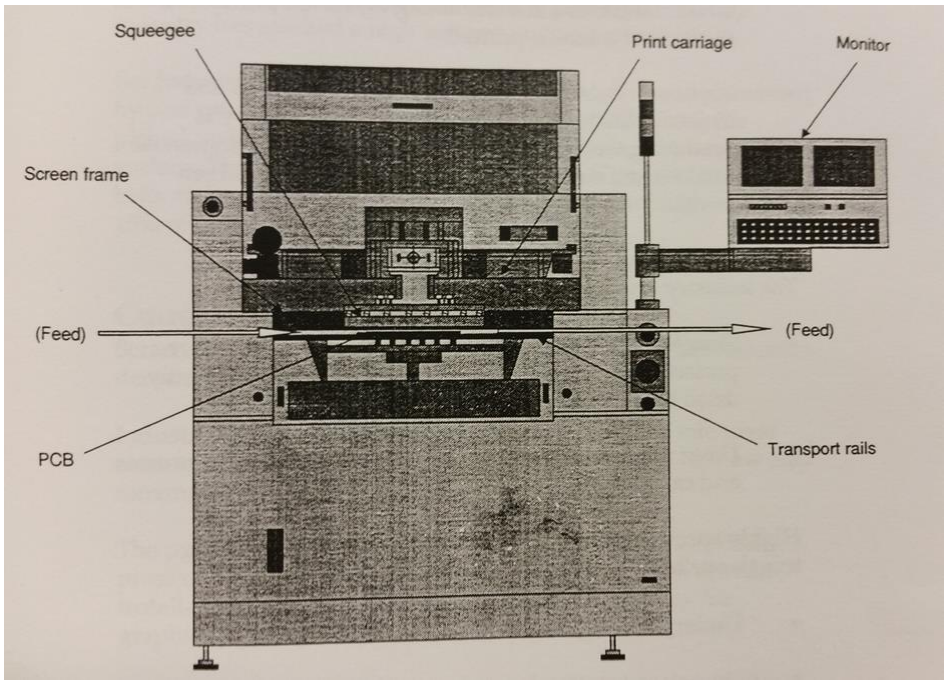

Figure 7 DEK Printing Machines Ltd, Dorset, UK [40]

There are many advantages of screen printing [41]

- Highly flexible and adaptable process,
- Prints practically any size, shape or substrate,
- Can print bright, bold and clean solids,

- Produces consistent colours on all surfaces,
- Controllable high quality print, line and tone,
- Can print solids and fine tones in the same pass,
- Can print any viscous medium ink, varnish, coatings or exotic finishes,
- Prints short runs economically,
- Economic process running costs.

In the middle of the 1800s, the ‘lalyonnaise decoration’ is used in UK and France, which is screen printing of fabrics. In 1887, Charles Nelson Jones patented a process, ‘silk screening’. It was in commercial use by the 1910s. [42].

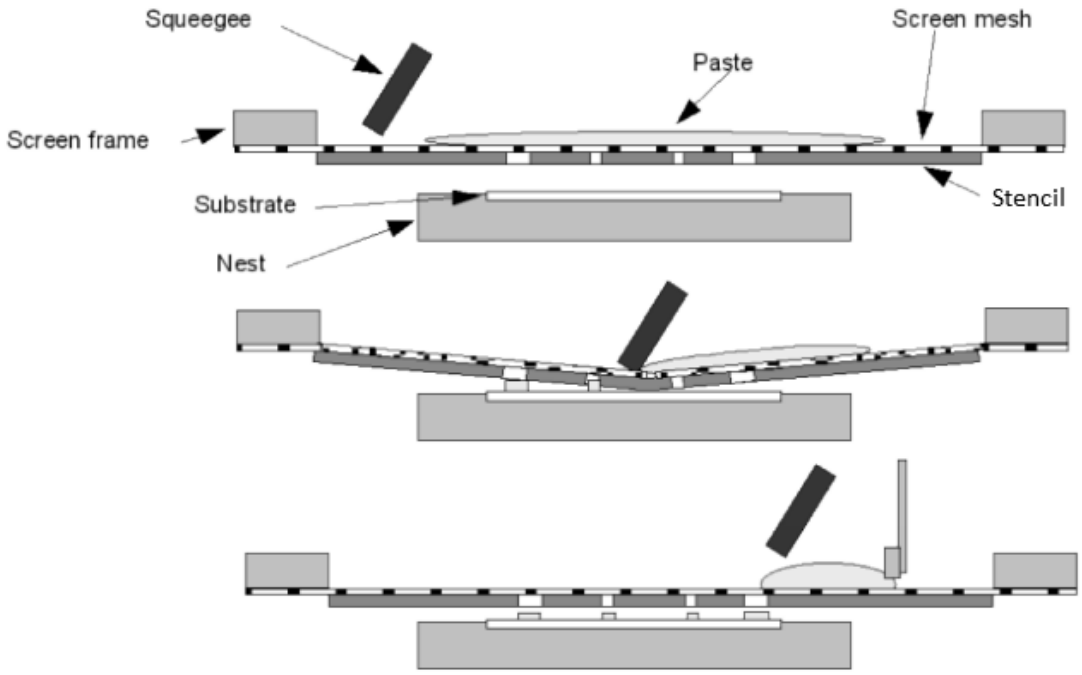

Figure 8 Principle of screen printing [40]

The sketch shows the principle of screen printing. The stencil and mesh always work together, and they control the job detail. The squeegee presses the ink, which is placed on the top of the mesh, onto the substrate.

The mesh could be polyester or nylon, could be coloured and any shape as well.

3.4.1.2 Tape-casting

Z R Wang et al. [43] use multilayer tape casting to assemble a green tape of nickel/yttria-stabilized zirconia (Ni/YSZ) and nickel/scandia-stabilized zirconia (Ni/ScSZ). X L Zhou et al. [44] fabricated an electrolyte/anode half-cell including electrolyte layer, anode functional layer (AFL), anode substrate layer (ASL), and anode by co-tape casting process. D. Montinaro et al. [39] used tape casting to achieve the half-cell with NiO/YSZ anode.

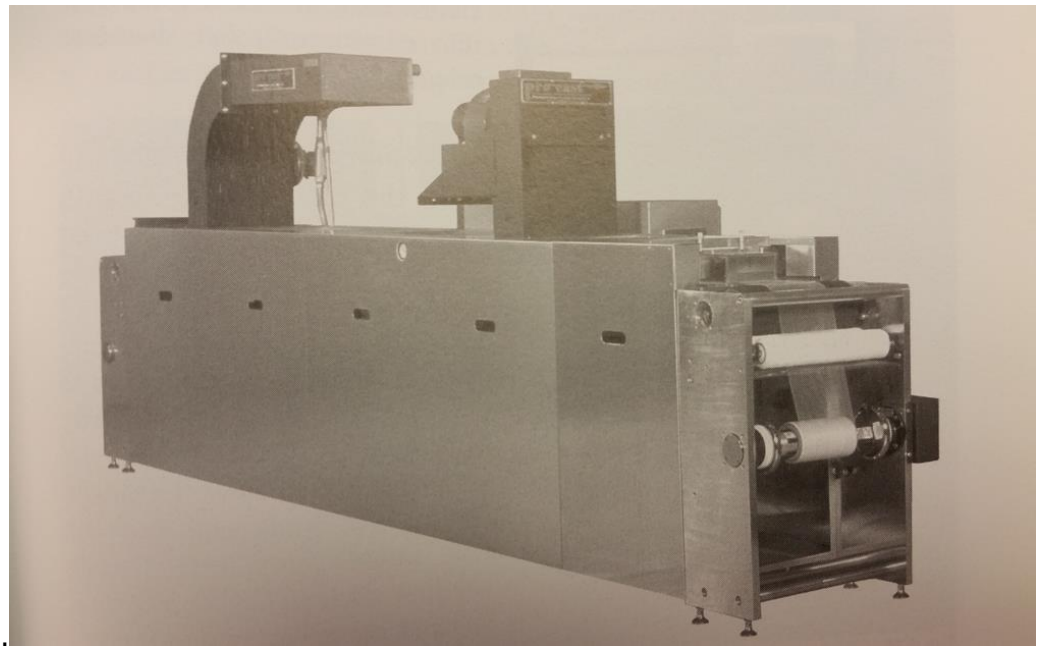

Figure 9 Pro-Cast tape casting machine [45]

Figure 10 Continuous style tape caster [45]

Tape casting, also known as ‘knife coating’ or ‘doctor blading’, is well known in various industries, like, paper, plastic, ceramic, paint, etc. In the 1940s, the first tape casting machine was designed. In 1947, the first publication of tape casting came out. [46] In the 1950s, the American Lava Corporation developed nonabsorptive surface to replace porous casting surface; and also, John L. Park, Jr. used a moving polymer carrier. [47] This is a huge step forward in tape casting technology.

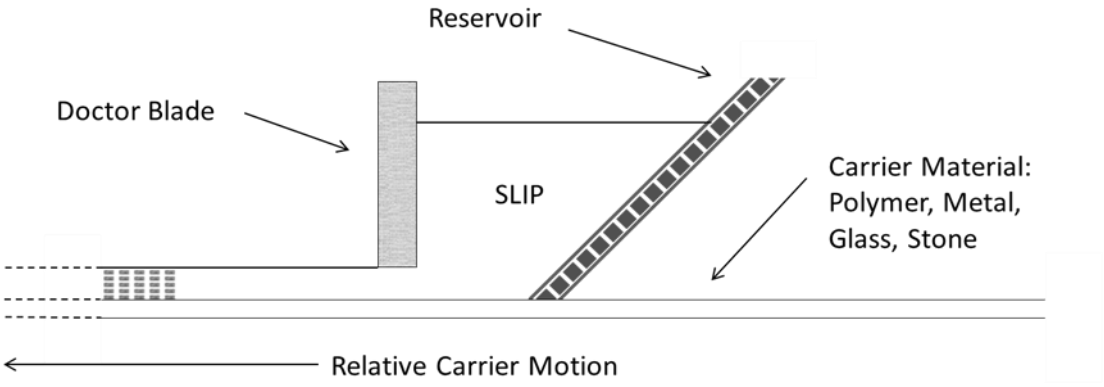

Figure 11 the basic principle of tape casting process

The picture shows the tape casting principle. It is based on a moving carrier, some slip or slurry as sort, and a blade (roll).

In this tape casting system, the powder is very important. The density, particle size, particle size distribution, particle shape, and surface Area are all suggested to effect the processing in many books and articles. [48], [49], [50].

And also, the solvent, surfactant, blinder, plasticizer, and organic interaction could effect this processing. [51], [52], [53], [54]

The surfactants used in tape casting are deflocculants, as known as dispersants. The reason why deflocculants are important in tape casting is they could keep particles apart. They achieve this is five ways.

- To separate or hold separate the primary particles
- To increase solids loadings in the suspension
- To save solvent by decreasing its amount
- To help drying process, make it fast and with less shrinkage
- To burn out cleanly

The binders are probably the most important thing in tape casting. Binders connect the whole chemical system together by acting as the only continuous phase in the tape. There are two families in the majority of binders: polyvinyls (vinyl) and polyacrylates (acrylic). Beside these, cellulose is a kind of common binder as well. The existent of plasticizers could enable the tape to bent, without cracking.

3.4.1.3 Tape Calendaring

M F Han et al. [55] build an Yttria stabilized zirconia (YSZ) electrolyte by tape calendaring. The ceramic powders (could be mixture) is mixed with plasticizers, binders, and also solvent. After it is squeezed out it passes the rolling calendars. Tape shape product is achieved, then the solvent is evaporated and the tape is cut before sintering.

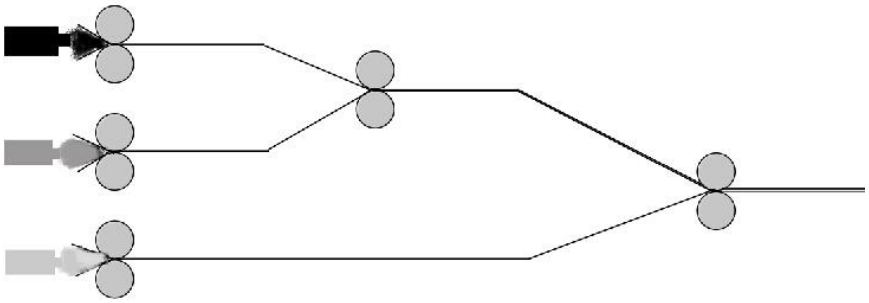

Figure 12 The basic principle of tape calendaring process

3.4.1.4 Spraying

W Zhou, et al used wet powder spraying to prepare anode-supported Yttia-Stabilized Zirconia (YSZ) thin film in China. [56] C J Li et al. use $Ar–H_2$ atmospheric plasma spraying (APS) to deposit an anode layer of NiO–4.5YSZ, and LSM cathode. [57] H G Shi et al. prepared Scandia-stabilized zirconia (ScSZ) thin film electrolyte by a wet powder spraying technique. [58]

Spray painting, a painting technique, has a device spraying a coating (varnish, paint, ink) onto a 3-dimensional surface. Powder and additives are flowed out from a nozzle by compressed gas (normally air) to particles. It is widely used in SOFC manufacturing as a PC controlled x-y-axis system and a rotational system could complete various geometries. Wet powder spraying is an easy and low-cost technology to get a 5 and 100μm thick coating. It has flexibility to size and shape of the samples which are coated, and easy integration in product manufacturing processes.

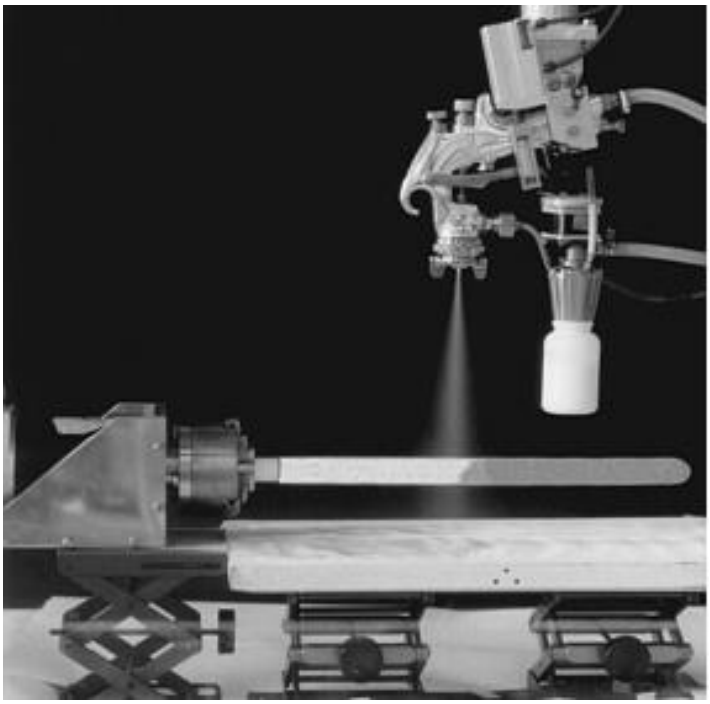

Figure 13 Wet powder spraying process

3.4.2 Chemical Vapour Deposition (CVD)

Chemical Vapour Deposition (CVD) [59] is widely used in new materials engineering. [60] G Y Meng, et al. used CVD techniques to prepare SOFC thin films. [61] M V F Schlupp et al prepared gadolinia doped ceria thin films by aerosol assisted Chemical Vapour Deposition Intermediate-Temperature Solid Oxide Fuel Cell [62]. Organometallic chemical vapour deposition was used by Bobrenok, OF et al, too. [63]

Chemical vapour deposition (CVD) is a relatively mature chemical process, is widely used to fabricate semiconductor devices. Generally speaking, CVD could transform gaseous precursor into solid surface, which could be thin film or powder form. CVD could be used to produce high-purity, high-performance solid materials.

In a typical CVD process, the substrate is exposed in a chamber to one or more precursors which react and/or decompose on the substrate surface to produce the desired deposit. A gas flowing through the chamber is used to remove by-products.

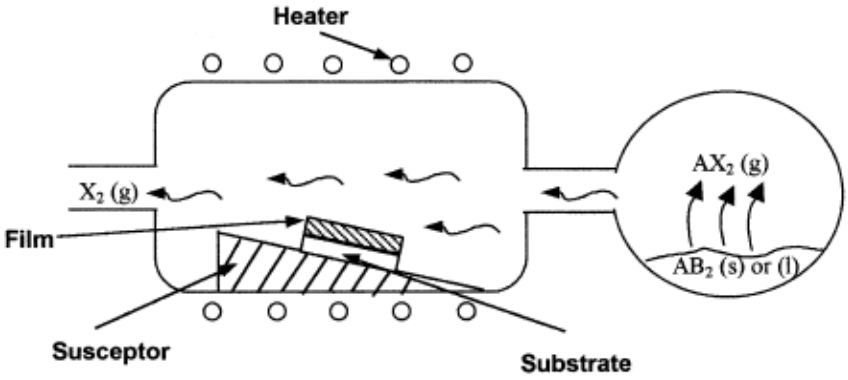

Figure 14 Schematic diagram of the CVD coating [59]

The products of CVD is highly dense, uniform, and pure, has good reproducibility and adhesion. CVD could finish complex shaped components, and has the ability to control crystal structure, surface morphology, and orientation by process parameters. Wide range of chemical precursors could be used and deposition rate is flexible for thickness or specific application. However, CVD has to be operated under flammable, toxic, corrosive, and/or explosive precursors. It has limitations when doing multi-component materials, and/or multi-precursors (different vaporisation rates).

3.4.3 Physical vapour deposition (PVD)

Physical Vapour Deposition (PVD) is widely used in new materials engineering, too. [60] B Meng, et al. [64] used physical vapour deposition to prepare YSZ electrolyte coatings for SOFC. Paul Gannon [65] used advanced PVD coatings to protect SOFC interconnects. X D He [66] used electron beam physical vapour deposition to prepare YSZ electrolyte coatings for SOFCs. Pulsed laser deposition was used by Sebastian Heiroth et al. [67] to achieve an YSZ thin film.

Physical Vapour Deposition (PVD) is a physical process, producing a thin pure film of materials (metal, alloy, or carbon, etc.) coating by depositing on a substrate. It is carried out in a vacuum chamber (10-6 torr), and needs an arc source as a cathode. The material to be deposited is vaporised by some physical means, and then the vapour is transported (or vaporised) in a vacuum chamber which locates the substrate. Then the vapour undergoes condensation on the substrate to form the thin film.

3.4.3.1 Pulsed Laser Deposition (PLD)

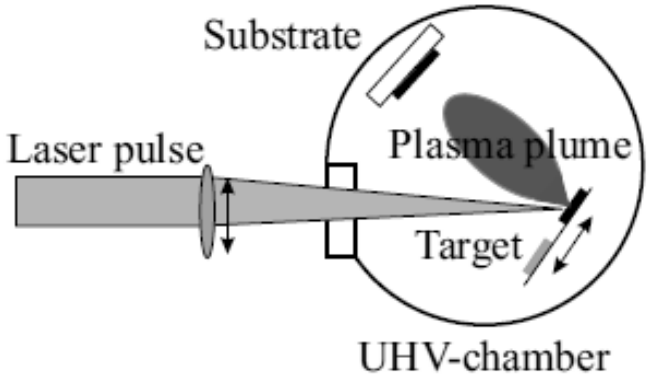

Figure 15 Schematic of Pulsed Laser Deposition (PLD) process

Pulsed laser deposition (PLD) is one of the physical vapour deposition (PVD) methods. This technique has a high power pulsed laser beam which strikes a target material in a vacuum chamber. This material is vaporised from the target and deposits a thin film onto a substrate. This process needs ultra high vacuum or in the presence of a background gas. In latter case, oxygen is mostly used when depositing oxides films.

This deposition method is similar to other PVD technique. When the target material absorbs the complex laser pulse, energy is converted to electronic excitation and then into thermal, chemical, and mechanical energy, finally generates evaporation, ablation, plasma formation, and exfoliation. All of these are brought into the vacuum chamber; form a plume containing various species (atoms, molecules, electrons, ions, clusters, particulates, and molten globules). Finally the compound deposits onto the surface of the hot substrate.

PLD is relatively simple, fast, and easy to modify. It has good compatibility with oxygen or other reactive gases. But the composition and thickness which depend on deposition conditions are not easy to control; and is hard to apply on large components.

3.4.4 Thermal spraying

Thermal spraying has relatively similar fundamental principles. Oxy-fuel combustion coming from flame or High Velocity Oxy-fuel (HVOF), or electrical process coming from arc or plasma, heat the consumable materials (powder or wire) to molten or soft, and projects these materials onto a substrate with high speed to form a coating. The bond between the coating and the substrate is primarily mechanical, not metallurgical or fused.

Thermal spray may be applied both manually and automatically, with no or little pre-/post- heats. It has comprehensive choices of coating materials (metals, alloys, ceramics, cermets and carbides), and could make thick coatings at relatively high deposition rates.

Coatings are mechanically bonded to the substrate—can often spray coating materials which are metallurgically incompatible with the substrate, e.g., materials with a higher melting point than the substrate. Parts can be rebuilt quickly and at low cost, and usually at a fraction of the price of a replacement.

Thermal spraying has been widely used for lots of years; and divided into several categories: Flame spraying, Plasma spraying, Arc spraying, and High Velocity Oxy-fuel (HVOF) spraying.

Plasma spraying

Plasma spraying is widely used in SOFC manufacturing. [68], [69], [70]

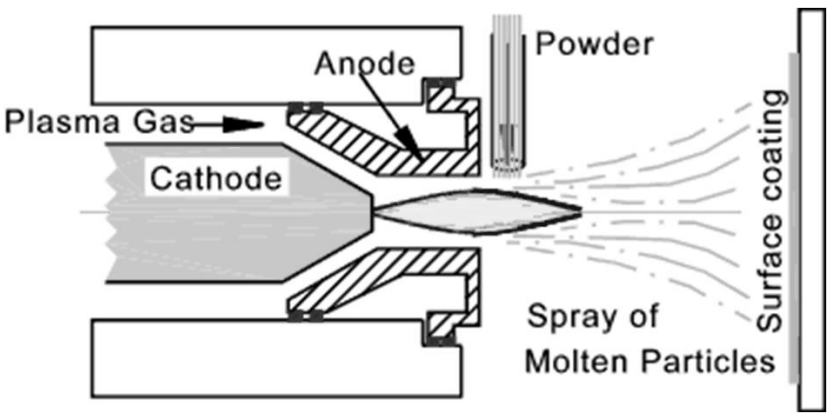

Figure 16 Schematic of Plasma spraying process

The Plasma spray could spray molten or heat softened material onto a substrate surface to form a coating. The plasma gun comprises a copper anode and a tungsten cathode; both of them are water cooled. Plasma gas (argon, nitrogen, hydrogen, helium, etc.) flows through a constricting nozzle. The plasma is initiated by a high voltage discharge; it generates a stream of high temperature ionised plasma gas (spraying heat source) by electric arc. The plasma jet is in very high speed of around 2000 m/sec, and very high temperature of 12000–16000 K. Powder form material is injected into the high temperature plasma flame; is heated and accelerated to a high speed. The hot material hits on the substrate surface and rapidly cools as a coating. The spray distances can be in the order of 25 to 150 mm.

Plasma spraying could deposit high melting point materials such as tungsten or ceramics, etc. The coatings are generally dense, strong and clean though it is a relatively high cost and complex process.

3.4.5 Electrophoretic Deposition (EPD)

Electrophoretic deposition (EPD) [71] is used in manufacturing of SOFCs, by Motohide Matsuda [72], and M.J. Santillán [73] in both reducing operation temperature and cathode preparation. Electrophoretic deposition (EPD) is a broad range of industrial processes, which includes electro coating, cathodic electrodeposition, and electrophoretic coating. The process is used in applying materials onto any electrically conductive surface. Colloidal particles suspended in a liquid medium migrate under the influence of an electric field (electrophoresis) and are deposited onto an electrode. All colloidal particles which could form stable suspensions and also could carry a charge are used in electrophoretic deposition; can be polymers, pigments, dyes, ceramics and metals.

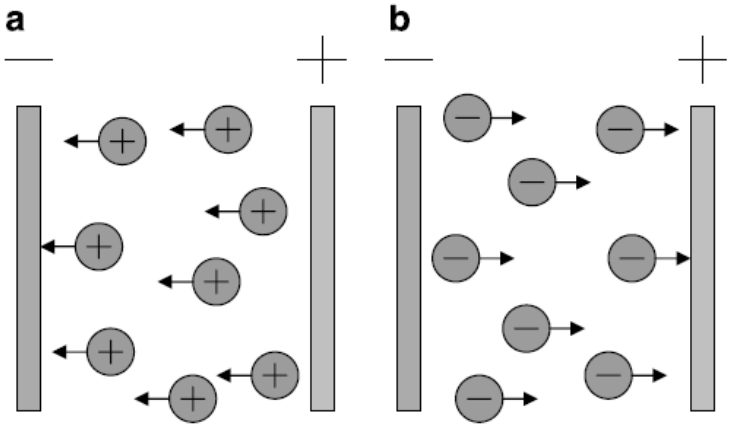

Figure 17 Schematic illustration of electrophoretic deposition process

(a) Cathodic EPD and (b) anodic EPD

There are two types of electrophoretic deposition depending on which electrode are coated. When the particles are positively charged, the deposition happens on the cathode, which called cathodic electrophoretic deposition. The deposition of negatively charged particles on positive electrode (anode) is called as anodic electrophoretic deposition. Figure 17 presents a schematic of the two electrophoretic deposition process. EPD has very high versatility of use with different materials and combinations. It is relatively low cost and requires simple apparatus.

3.4.6 Gel casting

Gel casting **[74]** is a ceramic forming technique based on the casting of slurry, which contains powder, water, and organic monomers. After casting the monomer, the mixture is polymerised to form gel, followed by drying, burning, and sintering. The process is generic; and is used for a wide range of ceramic and metallic powders. It is suitable for net shape prototypes or small series with a cheap mould. It is quite similar to slip casting and injection moulding. Typical research in this area is D H Dong [75] and H.T. Wang [76], and G J Li [77].

The gel casting process is easy and with low capital equipment. Firstly, the monomer and cross-linker(s) are dissolved in an aqueous or non-aqueous solution. It takes some time to become a premix. Then the powder material(s) and suitable dispersing

agent(s) are added into this premix. It takes some time to disperse and becomes a suspension. Initiator(s) and catalyst(s) are added into this suspension, after mixing, the suspension must be de-aired. After casting, the gelation could be triggered by catalyst or heat. When gelation completes, the product is de-moulded; drying, is always carried out separately at room temperature and sintering at high temperature.

Gel casting products have better homogeneity and higher green strength than slip casting; have better flexibility of moulds binder, suspension medium, etc., which is relatively low cost and convenient. Gel casting could produce complex parts, is relatively low cost of equipment and mould, and has the capability of mass production. The products of gel casting have high green strength and good homogeneity.

3.5 Redox / aging / degradation

Redox is the shorthand for Reduction-Oxidation reactions. All the reactions having a change of oxidation number (oxidation state) could be reduction-oxidation reactions. It could be very easy process, such as H_2 burning in O_2: $H_2 + O_2 \rightarrow H_2O$, or very complex process such as the oxidation of sugar ($C_6H_{12}O_6$), or iron rusting process. The two concepts could be presents as:

Oxidation is the loss of electrons or an increase in oxidation state by a molecule, atom, or ion. Shown below:

Reductant → Product + e^-

(Electrons lost; oxidation number increases)

Reduction is the gain of electrons or a decrease in oxidation state by a molecule, atom, or ion. Shown below:

Oxidant + e^+ → Product

(Electros gained; oxidation number decreases)

3.5.1 Cathode

The advanced materials for SOFC cathode are Lanthanum strontium manganite, $LaSrMnO_3$ (LSM). This is because it has high electronic conductivity, high electrocatalytic activity at high temperature, and the structural stability and thermal compatibility with YSZ electrolyte. When the SOFCs are operating at an intermediate temperature range of 600–800 °C, in order to increase the performance and long-term stability, the area specific resistance (ASR) and overpotential of LSM electrodes for the O_2 reduction reaction increase sharply due to the fact that LSM is almost a pure electronic conductor with negligible oxygen ion conductivity [78], and the three phase boundary (TPB) for the reaction is limited to the electrode/electrolyte interface [79]. Mixing LSM with ionic conducting phase of YSZ or Gd-doped ceria (GDC) can extend the TPB into the electrode bulk and reduce the ASR of the cathodes for the O_2 reduction reaction [80]. However, perovskite-structured LSM oxides would react with YSZ to form lanthanum zirconate ($La_2Zr_2O_7$) resistive phase at temperatures higher than 1000 °C. The equations of reactions are shown below. In these reactions, M^{n+}, as a valence state of the transition metal ion, may change and lead to other transition metal binary oxides. [30]

$$LaMO_3 + ZrO_2 = 0.5La_2Zr_2O_7 + MO + 0.25O_2(g)$$

$$LaMO_3 + ZrO_2 = 0.5La_2Zr_2O_7 + 0.5M_2O_3$$

$$LaMO_3 + ZrO_2 + 0.25O_2(g) = 0.5La_2Zr_2O_7 + MO_2$$

There is another reaction equation which shows the reaction without A site deficient (see figure 5). In this reaction, manganese ions are oxidized and oxygen is involved as a reactant. [30]

$$LaMnO_3 + x(ZrO_2 + 0.25O_2) = 0.5xLa_2Zr_2O_7 + La_{1-x}MnO_2$$

The complex interdiffusion between perovskite and oxides is shown in figure 18. [30]

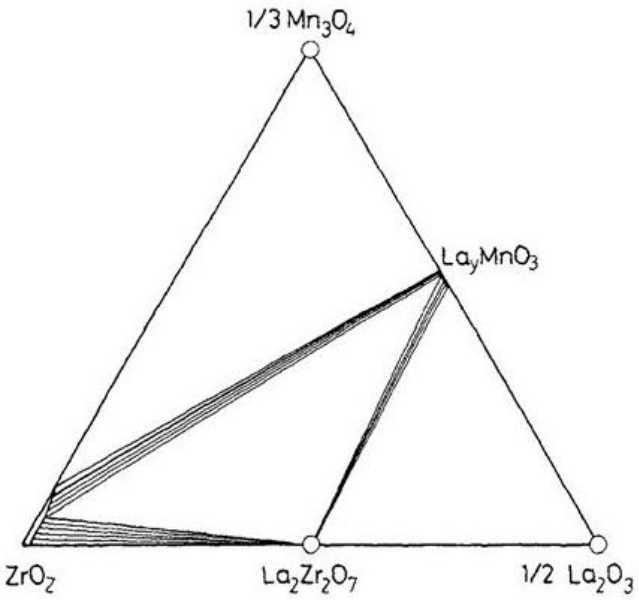

Figure 18 Compositional diagram for the La-Mn-Zr-O system

The specific electrical resistivity of $La_2Zr_2O_7$ is at least three orders of magnitude higher than LSM [81], which increases the cell internal resistivity losses. This would limit the potential applications of the LSM-based materials as the cathode of YSZ-based SOFCs. Badwal and Hughes [82] reported the diffusion of silica-based impurities from YSZ grain boundaries into the surface at SOFC working temperatures could influence SOFC long term characteristics. Several recent studies presented that moisture in the cathode gas could have a significant impact on the performance and durability of LSM/YSZ composite cathode based SOFC [83], [84], [85]. Alireza Babaei, et al. [86] showed the performance and stability of $La_{0.8}Sr_{0.2}MnO_3$ cathode could be promoted with palladium based catalysts in solid oxide fuel cells. X Z Zhang et al. [87] reported a novel stable cathode made by $(La_{0.75}Sr_{0.25})_{0.95}Cr_{0.5}Mn_{0.5}O_{3-\delta}$_$Sm_{0.2}Ce_{0.8}O_{1.9}$_YSZ (LSCMeSDCeYSZ) composite.

Lanthanum nickel ferrite (LNF) is a very promising SOFC material for intermediate temperature SOFCs. It has very good electronic conductivity, similar thermal expansion coefficient with YSZ electrolyte, and also high electrochemical oxygen reduction reaction. However, LNF cannot stand high temperatures. It degrades at temperatures above 1000°C (commonly used in sintering processes.). It was found that LNF shrinks above 1000°C; it also reacts with the ZrO_2 based electrolyte at

sintering temperature. And then LNF forms a highly resistant $La_2Zr_2O_7$ layer at the interface. [88] The LNF is actually a good cathode material and maybe could be used in place of LSM if high temperature processing could be avoided. If a technique could avoid this high temperature processing, LNF would be very suitable for LNF cathode manufacture.

3.5.2 Anode

The advanced anode material for SOFCs is a Ni/YSZ cermet. It is an excellent catalyst for fuel oxidation, and also an effective current collector. The poor mechanical stability during oxidation and reduction cycles (redox stability) of the Ni/YSZ cermet has become the binding constraint of the development.

The air may come into the anode compartment, which should only allow fuel come in, when the SOFCs are working at high temperature. Unfortunately, the Ni-YSZ cermet, which is normally used as SOFC anode material, is strongly sensitive to oxidising atmosphere. The high operating temperature (around 800 °C), accelerate the Ni- YSZ oxidation process, which is significantly faster in comparison to Ni powder [89] [90]. The Ni phase in the cermet is rapidly transformed into its oxidised state nickel oxide after the system stops. The repeated starts and stops can be accompanied by cermet reduction and re-oxidation cycling. The phase change Ni→NiO involves 69% volumetric expansion. This may cause a dimensional expansion of the anode support. If this expansion exceeds the limits of the electrolyte, a fracture is created and the cell fails. There are some research presenting the redox instability mechanism and the thermo mechanical behaviour of Ni–YSZ composites under redox conditions [91], [92]. Furthermore, redox-stable anodes based on ceramic materials have been under consideration for several years, e.g. Ti-substituted yttria-stabilised ZrO2 [93], Sr- and Mn-substituted LaCrO3 [94], La or Y-substituted SrTiO3. [95], [96]

4. Experimental Theory

4. 1 Electroless

Electroless plating has been used for centuries. A lot of results and applications are achieved by this widely used technology [100], [101], [102]. There is only very few people using this technology in fuel cell industry. Wei Zhou et al. [103] prepared a silver-modified $Ba_{0.5}Sr_{0.5}Co_{0.8}Fe_{0.2O3-\delta}$ (BSCF) cathode by electroless plating. Baba Nor Bahiyah [104] fabricated a Ni-YSZ anode by electroless co-deposition method. Electroless plating is an autocatalytic or chemical reduction of aqueous metal ions plated onto a solid substrate to form a solid phase of continuous coating, without an external current source. Generally speaking, it does not require external current. The significant feature is that of the metal is autocatalytic and continuous. Electroless deposition is a purely chemical process. From the thermodynamic point of view, the electroless deposition can be considered as spontaneous, since ΔG° <0.

Van 't Hoff equation: $\Delta G = \Delta G^\circ + RT \ln J$ (1)

In a chemical equilibrium, ΔG=0, and use equilibrium constant K instead of J, so:

$\Delta G^\circ = -RT \ln K$ (2)

For a reaction like $\alpha A + \beta B ... = \rho R + \sigma S ...$ $K = \frac{(R)^\rho (S)^\sigma ...}{(A)^\alpha (B)^\beta ...}$ (3)

and in a cell, $\Delta G = W$, $W = -nFE$, so $\Delta G = -nFE$, (4) [105]

where F is the Faraday's constant, Eis the electrode potential, R is the universal gas constant, T is the temperature, n is the number of exchanged electrons, A and B are reactants, R and S are the products. So the Equation (4) gives the key of electroless that an electroless process takes place only if E> 0. There are mainly two kinds of electroless deposition, displacement deposition and autocatalytic deposition.

- Displacement deposition

The schema of displacement deposition is shown in figure 19. [106]

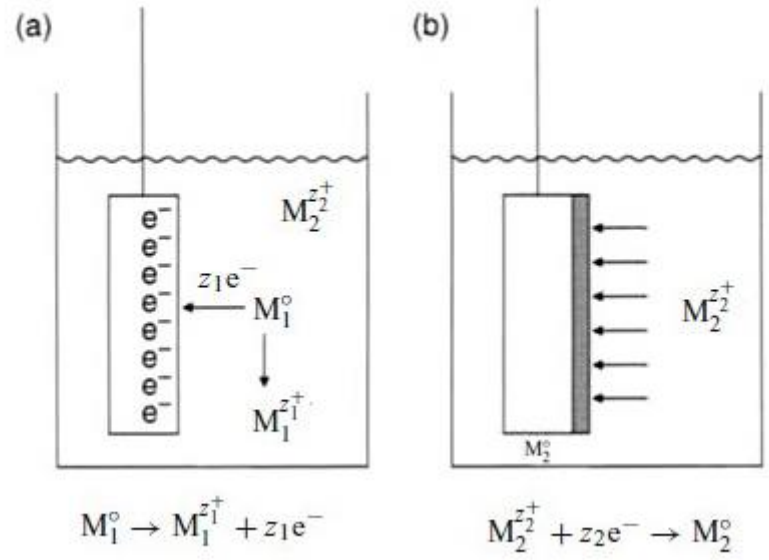

Figure 19 Schematic of principle of displacement electroless deposition

In this process, when a less noble metal (M_1) is placed into a solution, which has metallic ions (M_2^{z2+}); (M_2^{z2+}) is the ions of a more noble metal (M_2). There are reductions happening, according to these reactions:

$$M_2^{z_2^+} + z_2e^- \rightarrow M_2^0$$

$$M_1^0 \rightarrow M_1^{z_1^+} + z_1e^-$$

The combined galvanic deposition can be described as:

$$M_2^{z_2^+} + \frac{z_2}{z_1} M_1^0 \rightarrow M_2^0 + \frac{z_2}{z_1} M_1^{z_1^+}$$

The less noble metal, is the reducing agent in solution M_1°. The more noble metal M_2 acts like an oxidizing agent. The metal ions, which react with chemical reducing

agents, are reduced to metal (in the form of a powder or a continuous film) by accepting electron at the noble metal surface. The reaction keeps going as long as the substrate remains in contact with the solution. Generally, there is an order for common metals from less noble to more noble:

Mg, Al, Zn, Fe, Sn, Pb, (H), Cu, Hg, Ag, Pt, Au

When the left side less noble metal is immersed into a solution with right side more noble metal, the deposition of the noble metal will start. And some systems are commonly used, such as Ag/Zn, Au/Ni, Au/Ag, Cu/Zn, Cu/Fe, Cu/Al, Pd/Ni, Pt/Fe, Pt/Co, and similar.

- Autocatalytic deposition

The less noble metal in the displacement deposition acts like a reducing agent. In autocatalytic deposition, there are plenty of reducing agents, such as formaldehyde, hydrazine, hypophosphite, ascorbic acid, polyhydroxy, alcohols, and hydrogen, etc. The chemical reductant in solution, R^{n+}, could discharge of metal ions in the solution. The metal ions, which react with chemical reducing agents, are reduced to metal by accepting electron. The catalyst could be the work piece or metallic surface; it could accelerate the electroless chemical reaction. Once the reaction is initiated, it keeps going as long as the substrate remains in contact with the solution. The following equations are the reactions of electroless deposition of a metal Me, using a reducing agent R^{n+}. The reducing agent could be negative too, like R^{n-}, shown as well

$$Me^{z+} + z \bullet e^{-} \rightarrow Me$$

$$R^{n+} \rightarrow R^{(n+z)+} + z \bullet e^{-} \qquad R^{n-} \rightarrow R^{z-n} + z \bullet e^{-}$$

Combining the above two equations gives equations below:

$$R^{n+} + Me^{z+} \rightarrow R^{(n+z)+} + Me \qquad R^{n-} + Me^{z+} \rightarrow R^{z-n} + Me$$

As shown above, the metallic ions Me^{+} will be reduced to metal Me, while the reducing agent ions R^{n+} (R^{n-}) will be oxidized to $R^{(n+z)+}$ (R^{z-n}).

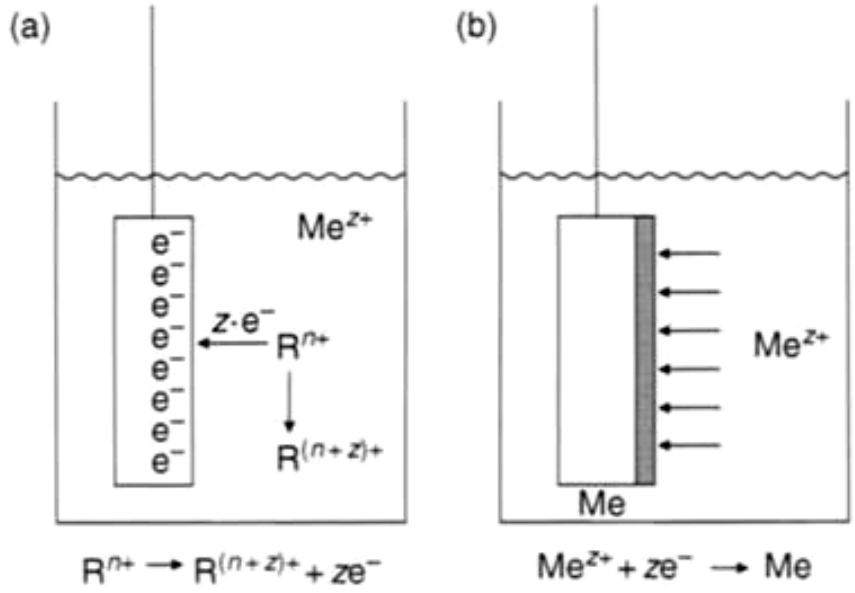

Figure 20 Schema of principle of autocatalytic electroless deposition

(a) Oxidation of the reductant;

(b) Reduction of the metal ion, leading to formation of the metal layer

4.1.1 Electroless nickel plating (nickel deposition)

Electroless nickel (EN) plating has been the most widely used since the discovery by Brenner and Riddel in 1941. Electroless nickel baths may consist of four types:

- Acid / nickel-phosphorus, which has three types:
  - 1-4% P (low phosphorus)
  - 5-9% P (medium phosphorus)
  - 10-13% P (high phosphorus)
- Alkaline / nickel-phosphorus,
- Acid / nickel-boron.
- Alkaline / nickel-boron,

There is an example bath:

Table 9 An Acid Hypophosphite-Reduced Electroless Nickel Bath

Nickel sulphate	28 g/L
Sodium acetate	17 g/L
Sodium pyrophosphate	24 g/L
Lead acetate	0.0015 g/L
pH	4.4-4.6
Temperature	82-88°C(180-190°F)

The chemical reducing agent normally is sodium hypophosphite (NaH_2PO_2), or sodium borohydride ($NaBH_4$), or an aminoborane such as n-dimethylamine borane (DMAB) [$(CH_3)_2NHBH_3$].

The electroless nickel plating used in this research is the acid / nickel-phosphorus, which has a reaction equation as followed:

$$NiSO_4 + NaH_2PO_2 + H_2O \xrightarrow[\text{Catalyst}]{\text{Heat}} Ni\ (\text{Plating}) + NaHPO_3 + H_2SO_4$$

The advantages of electroless nickel plating are:

- Does not use electrical power.
- Even coating on parts surface can be achieved.
- No sophisticated jigs or racks are required.
- There is flexibility in plating volume and thickness.
- The process can plate recesses and blind holes with stable thickness.
- Chemical replenishment can be monitored automatically.
- Complex filtration method is not required
- Matte, Semi Bright or Bright finishes can be obtained.

Disadvantages include:

- Lifespan of chemicals is limited.

- Waste treatment cost is high due to the speedy chemical renewal.

4.1.2 Electroless nickel co-deposition

The construct of this research is to deposit the LSM/YSZ and nickel at the same time, by electroless co-deposition technology, onto an alumina or YSZ substrate to form a practicable cathode for a SOFC, especially tubular. The reductant, sodium hypophosphite (NaH_2PO_2), loses two electrons and turns into $NaHPO_3$. The nickel ion, Ni^{2+} grasps two electrons, and forming nickel metal. When LSM/YSZ is added into the electroless nickel plating bath, the nickel ions will trap the LSM/YSZ powders like a fish net, and bring them onto the substrate. The schematic is shown in figure 21. This process could achieve several microns thickness coating, which contains nickel, YSZ, LSM, or LNF.

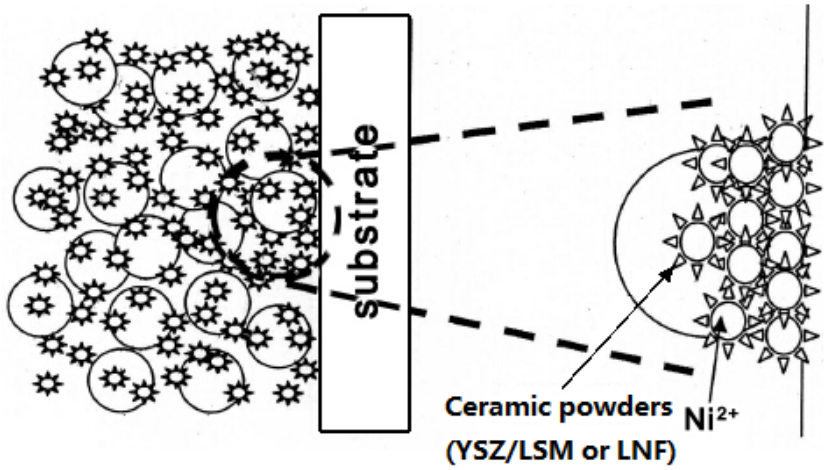

Figure 21 Schematic of electroless co-deposition of nickel and ceramic powders

4.2 Characterization techniques

4.2.1 Optical Microscope

The optical microscope is used in this research as general surface analysis of the samples, especially the cross-section. The Leitz Aristomet optical microscope has six variations of objective lenses, which are from 2 to 100 magnifications. Because the eye lens has 10 magnifications, so the true magnification is in a range from 20 to 1000.

The scale between the eye lens and the objective lens could measure the sample size, and then the true length could be calculated by the magnifications. The details are shown in table 10.

Table 10 Optical microscope magnification and scale

Objective magnification	True magnification	1 division of graticule (mm)
2	20	0.0625
5	50	0.02
10	100	0.01
20	200	0.005
50	500	0.002
100	1000	0.001

4.2.2 Scanning Electron Microscope (SEM)

A scanning electron microscope (SEM) [107] is a type of electron microscope, which could take images from a sample by scanning it with a high-energy beam of electrons in a raster scan pattern. The high energy beam comes from the electron gun; it is then gathered by the lenses before scan coils into a skein (with a diameter of 1-5nm, beam current of 10^{-11}-10^{-12}A). The skein of beam is controlled by the scan coils, and scans the surface of the samples, which are located in the vacuum chamber. The interaction of beam and samples gives secondary, backscattered electrons, X-rays, and so on, which are collected by the electron collector, and transferred into image signals for observation display or digital signals for further analysis, like topography, composition, and so on. SEM could magnify the samples surface image from 10 to million times, and also can investigate uneven samples with little effect to the samples. The schema of SEM is shown in figure 22.

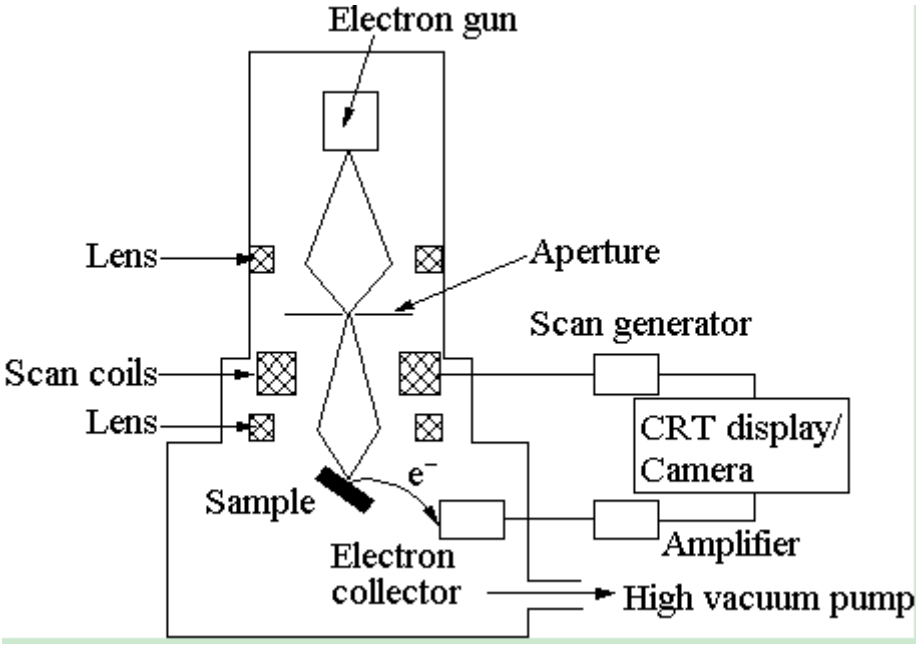

Figure 22 *Schema of SEM*

4.2.3 Energy Dispersive X-ray spectroscopy Analysis (EDXA)

Energy Dispersive X-ray spectroscopy Analysis (EDXA) [106] is also called Energy Dispersive x-ray Spectroscopy (EDS). It is normally part of SEM. It is a standard method for identifying and quantifying the elemental compositions in a tiny sample of even a few cubic microns. In principle, all elements from atomic number 4 to 92 can usually be detected. The schema of EDXA is shown in figure 23.

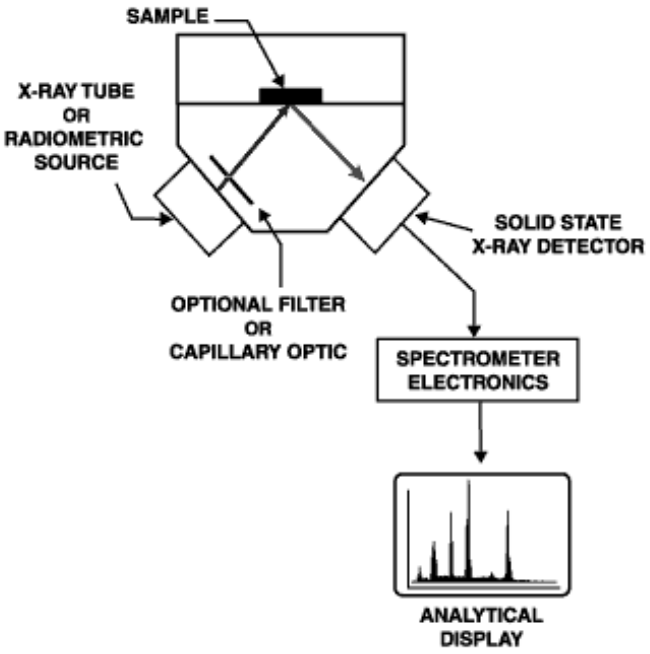

Figure 23 4.3 Schema of EDXA

4.2.3.1 Atomic structure

According to the Bohr model of the atom, the positive nucleus is surrounded by the electrons orbit; the number of electrons equals to the number of protons in the nucleus, which is also the atomic number, Z. The electron shells, which are also called principal energy levels, are named K shell, L shell, M shell, N shell…or 1shell, 2shell, 3shell, 4shell… from the closest to the nucleus to the outermost. Each shell consists of one or more subshells, and each subshell consists of one or more atomic orbitals. The subshells are named s, p, d, f…, and in the same shell, the energy of subshells increases in this order. The K shell has an s subshell, L shell has s and p subshell, M shell has s, p, and d subshell… Furthermore, the s subshell has 1 orbital, p has 3, and d has 5... According to the Pauli's exclusion principle, each orbital could have 2 electrons, which are in different spin directions. So K shell can have no more than 2 electrons, L shell can have no more than 8, M can have 18… Figure 24 shows the atomic structure.

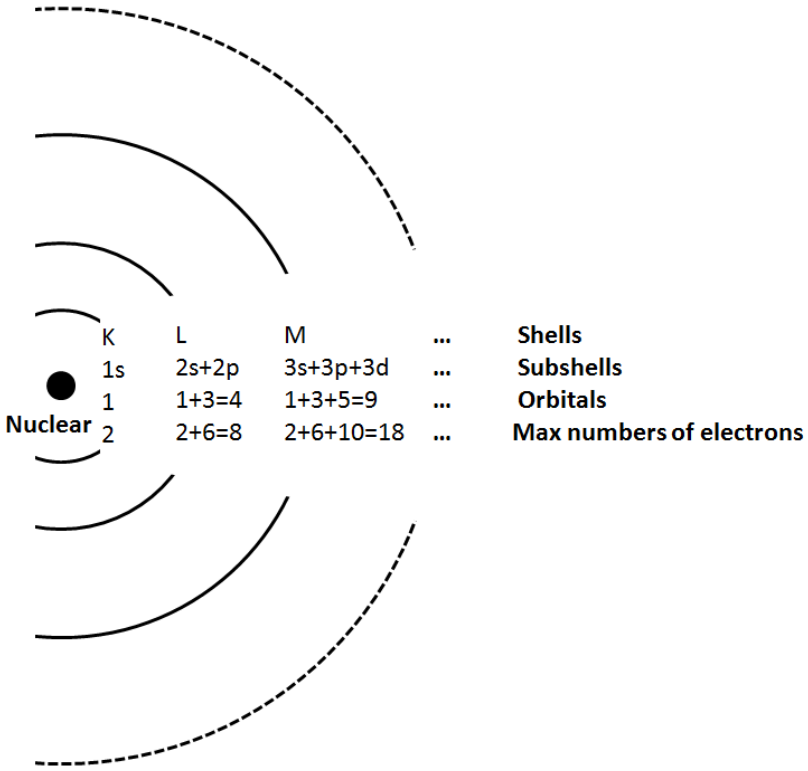

Figure 24 Schematic diagram of atomic structure and electron shells

An atom is always in the lowest energy level at ground state. When the electron shells are fulfilled with electrons, it does not follow the nearest shell first order; in fact, the order should be the level of the energy of the shells. Because in the same shell, the energy of the subshells is increasing in s, p, d, f… orders. Then, the higher subshell of a lower shell may have higher energy than a lower subshell of a high shell. For example, in most of the time, the energy of 4s is lower than 3d. So when the electron shells are fulfilled with electrons, it follows the energy level order shown below:

1s,2s,2p,3s,3p,4s,3d,4p,5s,4d,5p,6s,4f,5d,6p,7s,5f⋯

4.2.3.2 X-rays

Most of the time, Electrons occupying outer orbits does not directly produce X-ray spectra. X-rays come from electron transitions between inner orbits, but the inner orbits are normally fulfilled. In this case, a vacancy must be created by removing an electron in the inner orbits in order to let a outer orbit electron ‘jump’ or ‘fall’ into this

vacancy. The electron bombardment produces a vacancy, this is an extremely short time period; the atom will be at this unstable excited state for just 10^{-12}-10^{-14}s, and then it automatically turns into the stable ground state. Once the vacancy is created, a higher energy level electron may fall into the vacancy, resulting in a release of energy. The energy might be in different forms. It could be transferred to another electron, which is ejected from the atom as Auger electron; and also, it could be in the form of an X-ray. The energy of the X-ray equals to the difference between the higher-energy shell and the lower energy shell. For example the energy given by an electron jumping from L shell to K shell is shown below.

$$\Delta E = E_K - E_L$$

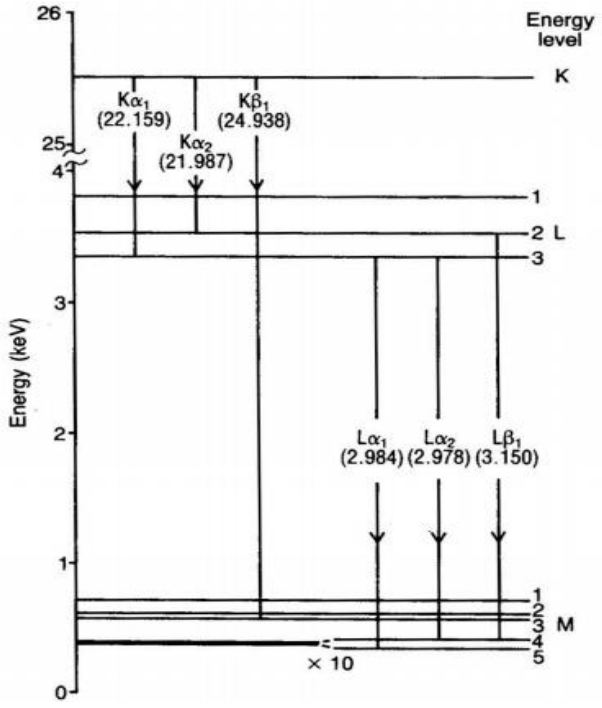

Figure 25 Energy level diagram for Ag showing Kα, and Lα emission lines, arrows show direction of vacancy movement, numbers are energy of emission

The K shell electron could be ejected and replaced by any electrons from higher energy shell. That gives a series of lines as the spectrum. For example, the electron jumps from L shell to K shell, gives the X-ray of Kα, with the energy of E_K-E_L. Kα is a group of lines of $K\alpha_1$ and $K\alpha_2$. Lα is the X-ray produced by an electron jumping from M shell to L shell, etc. The number and energy of the X-rays, which are relative to the

elements, could be measured by an energy-dispersive spectrometer. Figure25 shows the energy level diagram. [108]

4.2.3.3 Energy-dispersive spectrum

A solid state detector and a pulse height analyser are used to give output pulses proportional in height to the X-ray energy. The Energy-dispersive spectrum displays the X-ray energy in a digital form. X-axis represents the X-ray energy (normally in channels 10 or 20 eV wide), and the y-axis represents the numbers of counts of the channel. The X-ray line are analysed and given to a Gaussian profile.

4.2.3.4 Qualitative analysis

As mentioned above, the Energy of X-ray is equal to the difference between the higher-energy shell and the lower energy shell, and also

$$E=hv$$

Where, E is energy, h is the Planck constant, v is frequency,

Or $E=hc/\lambda$

Where, c is the speed of light, λ is wavelength.

So the energy of the X-ray is equal to the energy difference between the higher-energy shell and the lower energy shell. Because different elements give out different X-rays spectrums, which are related to different energy values. The elements could be determined by identifying the lines in the X-ray spectrum using the table of energy or wavelengths. Energy dispersive is normally used because a complete spectrum can be quickly received. A comparison with recorded spectrum will help the given element identify the correct position of the lines, which process could be done manually or by computer.

4.2.3.5 Quantitative analysis

The pulses generated in the detector by the X-ray photons emitted from samples will give the X-ray intensities. For a given time, the number of these counts could be recorded as a series of discrete measurement; and then form a Gaussian distribution with a standard deviation. It should be noticed that the accelerating voltage should at least double the highest excitation energy of any possible elements in the sample, in order to obtain adequate intensity.

According to Castaing (1951), the relative intensity of an X-ray line is approximately proportional to the mass concentration of the element concerned [108]. When the sample is penetrated by the incident electrons, the mass approximately remains the same. So the 'apparent concentration' (C') is introduced:

$$C' = \left(\frac{I_{sp}}{I_{st}}\right) C_{st}$$

Where I_{sp} is the intensities for the sample, I_{st} is the intensities for the standard, and C_{st} is the concentration of the element concerned in the standard. Also certain corrections could be introduced for the true concentration. ZAF corrections stand for atomic number effects (Z), absorption (A), and fluorescence (F); they are calculated separately using suitable physical models.

4.2.4 Electrochemical characterisation

4.2.4.1 Current and voltage measurement (IV)

An IV curve and power generation density calculation could measure the performance of a SOFC. The anode and cathode of the cell could be connected to an external circuit with wires, with no current drawing from the cell; an Open Circuit Voltage (OCV) could be tested by a voltmeter between the anode and cathode. Figure26 shows a schematic plot of voltage and current density of SOFC. OCV is normally lower than the theoretical voltage, which is provided by the Nernst equation. The different between U_{th} and U_{OCV} is called 'overpotential'. Compered to theoretic potentials, the anode is less negative, and the cathode is less positive; so the SOFC will supply less

energy than thermodynamically possible. The voltage drop quickly in the first stage at low current densities, this is mainly because of the activation polarisation, like electrodes charge transfers, so any electron leaks or other different parasitic losses will make voltage drop more sharply. The second stage then falls more linearly, which is the ohmic resistance part. In the last high current density part, the voltage falls rapidly mainly because of the diffusion polarisation, which is related to gas transporting through electrodes to the electrolyte/electrode interface, the increasing current density enlarges gases consumption. So, the ohmic and polarisation losses are responsible for the IV curve, and the polarisation loss concludes the activation polarisation and diffusion polarisation.

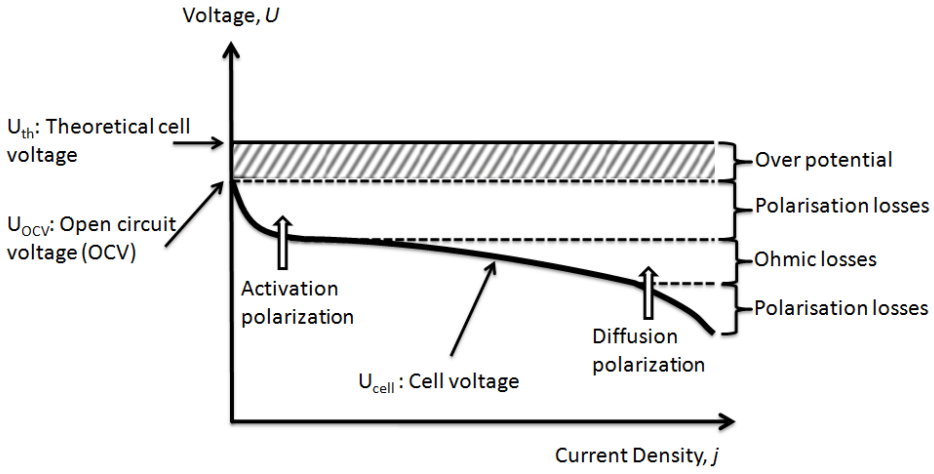

Figure 26 schematic plot of voltage and current density of SOFC

4.2.4.2 Electrochemical Impedance

The impedance of the SOFC is quite complex [97], [98]. The area specific resistance (ASR) of the cell is given by ohmic resistance (Rs) and the polarization resistance (Rp). [99] The Rs is mainly due to the resistance of the electrolyte (YSZ), the current collectors (mesh and wire); and the Rp is related to the activation polarization and the concentration polarization. The activation polarization is related to the electrode/electrolyte interface charge transfer; and the concentration polarization is related to the electrodes microstructure's ability of transporting the gases, which is diffusion. In fuel cells, the electrode/electrolyte would behave like double layer capacitance, because there are also polarisation and diffusion, the fuel cells would not

act like an ideal capacitance, so the imperfect capacitor - constant phase element (CPE) would be introduced, instead of a capacitance. A CPE has unclear physical significance; meanwhile, pure capacitance has two types, time constant and phase constant. In this case, the CPE, which behaving between capacitor and resistor, is more suitable for the simulation of the behaviour of a fuel cell, which is very complex. SOFC has electrodes/electrolyte double layer capacitance, but also has chemical capacitance.

For a full cell, the equivalent circuit (EC) below is used:

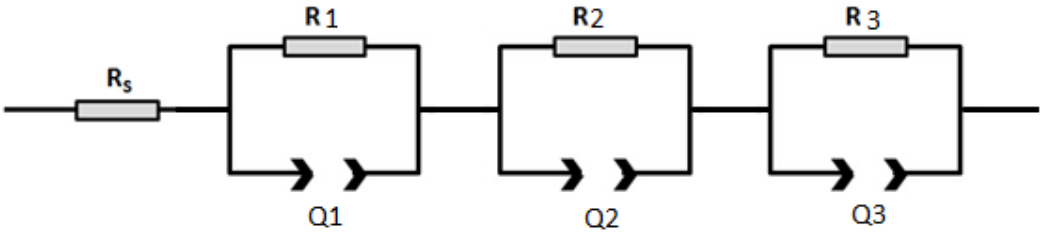

Figure 27 Equivalent circuit of cell (EC)

In this EC, the Rs is the ohmic resistance from electrolyte electrical resistance in electrodes, and current collectors; R1, R2, and R3 are considered as the total polarization resistance, Rp.

4.2.4.3 Electrochemical Impedance Spectroscopy (EIS)

Electrochemical Impedance Spectroscopy [109] [110] is also called Dielectric Spectroscopy, which involves measurements and analysis of materials in which ionic conduction strongly predominates. It is also valuable in the study of fuel cells, rechargeable batteries, and corrosion. The fuel cell EIS is shown in figure 28. In the impedance measurement, a frequency response analyzer (FRA) is used to impose a small amplitude AC signal to the fuel cell via the load. The AC voltage and current response of the fuel cell is analyzed by the FRA to determine the resistive, capacitive and inductive behavior, that's the impedance, of the cell at that particular frequency. When conducted over a broad range of frequencies, impedance spectroscopy can be used to identify and quantify the impedance associated with these various processes.

Figure29 shows Nyquist plot of a LSM/YSZ electrode impendence. There are two group of date showing in this figure, both of them are individual impedance test. The impedance is relative to the SOFC EC in figure 27. Take the lower curve as an example. There are generally three parts, part A is from Y-axis to the beginning of arc, which is the resistant of the electrolyte and wires; part B is the depressed capacitive arc (high- to media- frequency), which normally has a few phenomena overlapping, is related to the polarisation of the electrodes; and part C is lowest frequency part, which is related to gas diffusion on the electrodes. Also, part a of the X-axis shows the ohmic resistance, Rs, and part b shows the polarisation resistance, Rp.

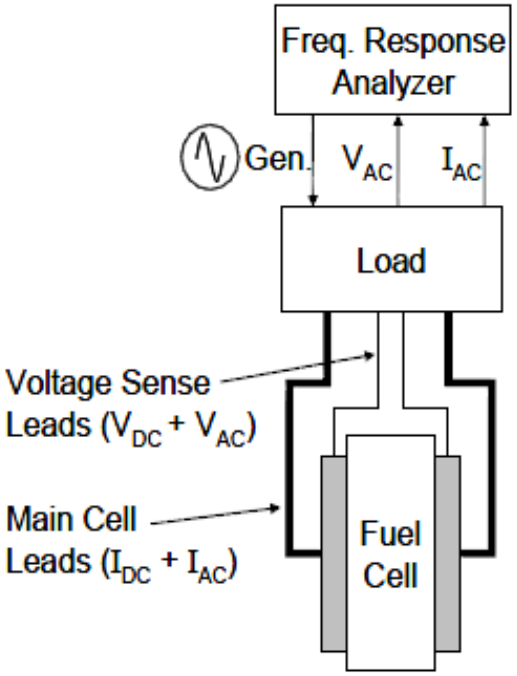

Figure 28 Instrumentation for EIS of fuel cells

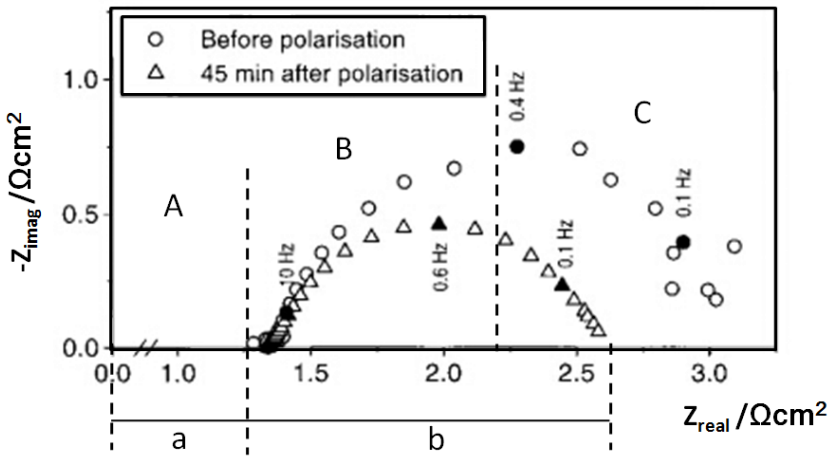

Figure 29 Impedance of a composite $(La_{0.85}Sr_{0.15})_{0.9}MnO_3$/YSZ electrode Sample geometry: pellet. Test conditions: 850°C, air [111]

5. Experimental Technique

5.1 Materials and solutions

5.1.1 Alumina Substrate

Alumina ceramics are a widely used ceramic material; they have high electrical insulation, high mechanical strength, high wear and chemical resistance, etc. The alumina used in this research is ordered from Ortech - the details are given in appendices. Alumina was used in the initial research mainly because of its low cost – the more expensive YSZ was used once the preliminary experimentation was proved successful.

5.1.2 YSZ

The YSZ powders were ordered from Unitec Ceramics. These were 13% yttria stabilised zirconia powders and had average particle sizes of 1, 2 and 5 microns.

5.1.3 LSM

LSM are very widely used in the SOFC's cathode. The LSM is ordered from Praxair, $(La_{0.8}Sr_{0.2})_{0.98}$Mn oxide, which has a part number PS-PLSM 304-3D4, Lot number is 03-P6510DM.

5.1.4 LNF

LNF has been considered as one of the most promising cathode materials in the intermediate temperature SOFC (ITSOFCs). However, it degrades at the high conventional processing temperatures so this current work investigated whether or not LNF could be deposited using the low temperature electroless technique

For the work carried out in this research, the LNF ($La_{0.99}Ni_{0.6}Fe_{0.4}$ Oxide) was ordered from Praxair; the part number was PS-PLANi301-3D70, the lot number was 03-P4585DM.

5.1.5 YSZ button substrate

The YSZ substrate of the button cell tested in the electrical test was ordered from Fuel-Cell Materials. The details were YSZ-sub-3.2d, (which means a diameter of 32mm); item number 211103, lot number 325-089 and the thickness was 250-300μm.

5.1.6 Pre-treatment solutions

Because the LSM/YSZ was going to be co-deposited with nickel by the electroless process, the substrate needed to be activated before the plating process. The pre-treatment solutions are given in Table 11. All of these solutions were made up and stored in flasks. To prolong their life, they were stored in tight flasks. In particular, once the dark Uniphase PHP Catalyst goes transparent, it should be remade. The catalyst was kept in a cool place away from direct light – it will expire quickly when exposed in air for a certain time. It is recommended that the container of catalyst should be small; the catalyst should be kept full, with as little air as possible in its container.

Table 11 Recipes of pre-treatment solutions for alumina substrate before electroless plating (SLOTONIP)

Trade name	Composition	
Cuprolite X96DP	Cuprolite X96DP A	50ml
	Cuprolite X96DP B	5ml
	Deionised water	To 1 litre
Uniphase PHP Pre-catalyst	Uniphase PHP A salt	200g
	37% Hydrocloric Acid RP	20ml
	Deionised water	To 1 litre
Uniphase PHP Catalyst	Uniphase PHP A salt	200g
	Uniphase PHP B	20ml
	37% Hydrocloric Acid RP	20ml
	Deionised water	To 1 litre
Niplast 78	Niplast AT 78	100ml
	Deionised water	To 1 litre

5.1.7 Acid Electroless nickel bath

The acid bath solution used in this research was SLOTONIP 1850, which is shown in Table 12. The pH of this SLOTONIP 1850 solution should be 4.9; if it is too high, sulphuric acid should be used to reduce its concentration while if it is too low, ammonium hydroxide can be used to increase it.

Table 12 Recipes of SLOTONIP 1850 solution

Trade name	Composition	
Electroless SLOTONIP 1850	SLOTONIP 1851	0.75 litre
	SLOTONIP 1853	3.95 litre
	Deionised water	3.95 litre

5.1.8 Alkaline Electroless nickel bath

For the alkaline bath, the following recipe was used.

Table 13 Recipe of alkaline electroless nickel solution

Nickel Chloride	30g/L
Sodium hypophosphite	25g/L
Sodium citrate	25g/L
Ammonium Chloride	50g/L

The pH of the alkaline bath used was 9.5 - the mixture of these powders dissolved in di-water along with ammonium hydroxide produced the correct pH.

5.2 Electroless co-deposition procedure

Generally speaking, the co-deposition procedure is shown in this flowchart:

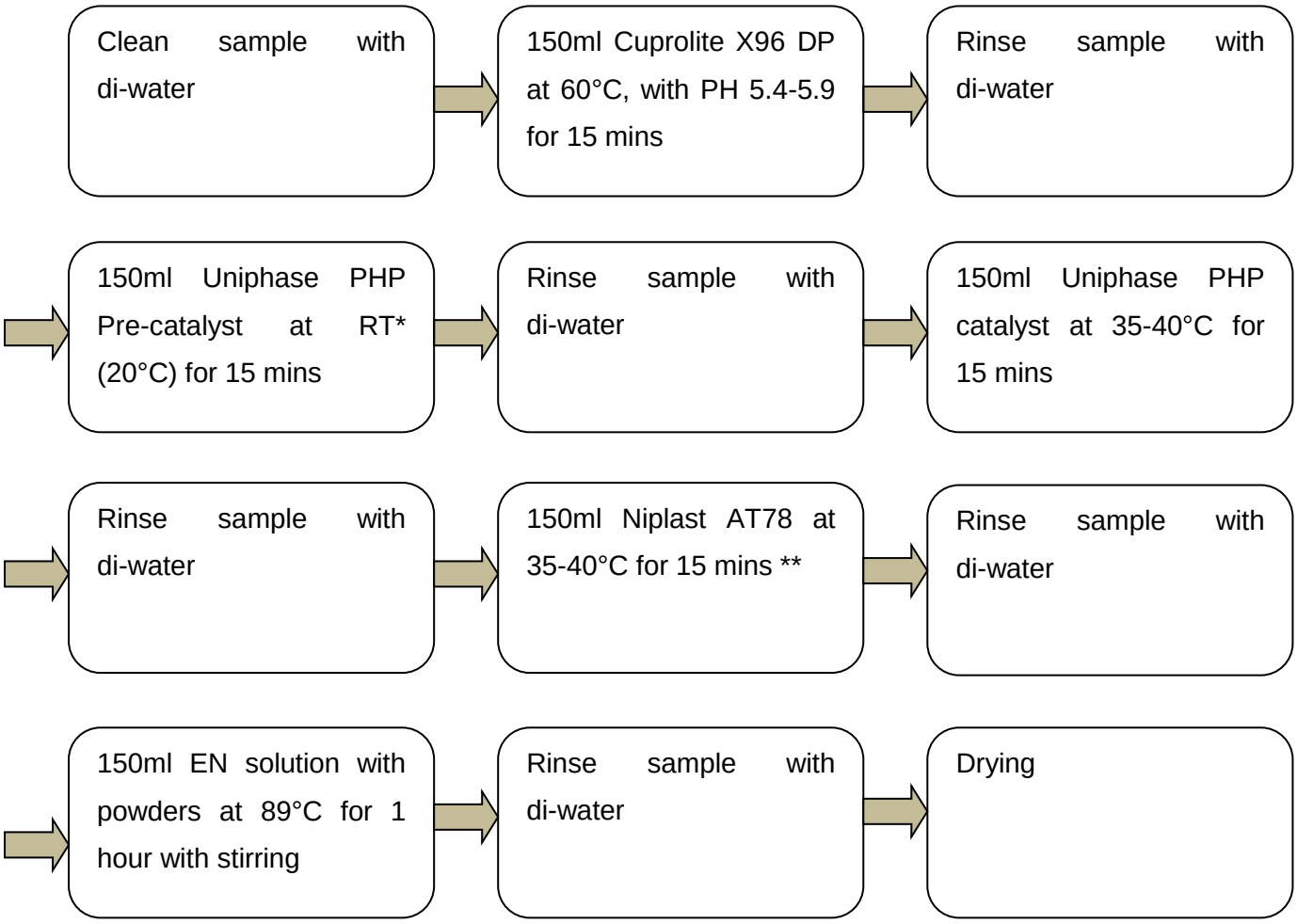

* Room Temperature..

** This step has been shorted or removed in most cases

Figure 30 Overall flowchart of electroless nickel LSM/YSZ co-deposition

The co-deposition used here followed the procedure in Figure 30. The Cuprolite X96 DP, Uniphase PHP Pre-catalyst, Uniphase PHP catalyst and Niplast AT78 (not SLOTONIP 1850) could be recycled for future use, but the expiry date should be noted and expired solutions should not be disposed of safely. The beaker should be cleaned very carefully between every step, and the pre-treating beaker is not suitable

for the electroless nickel LSM (or LNF)/YSZ co-deposition step, as the beaker might be activated and the nickel will be coated onto this beaker. All the waste should be kept in appropriate waste bottles.

5.3 Experiments

Few papers could be found on electroless nickel co-depositing LSM as a SOFC cathode. Theoretically, particles with smaller zeta potentials (absolute value) should be easier to be co-deposited because higher zeta potentials give higher repulsion between the particles. As shown in the table, the zeta potentials in EN solution is much smaller than di-water – that is why the co-deposition can happen in EN bath and not in di-water.

Table 14 Zeta potential of LSM and YSZ [112]

	YSZ	LSM
De-ionized water	29 mV	7 mV
EN solution	– 12mV	– 3 mV

LSM powder is very difficult to be co-deposited by electroless nickel co-deposition process even though LSM has a smaller zeta potential than YSZ, as shown in Table 14. As predicted by the equation mentioned in 4.1.1, some H_2SO_4 was produced which could bring the pH down after the co-deposition process. But in fact, the pH of the nickel solution after the co-deposition process increased. This is why the alkaline electroless nickel co-deposition was carried out to replace the acid process in the second stage.

5.3.1 Acid electroless co-deposition

Both planar and tubular Al_2O_3 substrates were plated by acid electroless co-deposition method.

Each sample was cleaned with di-water, pre-treated by Cuprolite then pre-catalysed, and catalysed respectively. Di-water was used to clean each sample and an air dryer was used to dry it out between every two steps. Then the sample was dipped in

Niplast, followed by rinsing and drying. 150ml of nickel solution in a 250ml beaker was heated up, and then the beaker was loaded with ceramic powders (YSZ, LSM). The YSZ powder was put into the beaker when the temperature met the requirement (89°C in most cases); the LSM, the sample was put in at last. This is very important because the sample will be coated by pure nickel if it is put in the solution without any powders. This will raise the content of nickel in the final de-position and would not help with coating process. It should be noticed that the LSM powder is magnetic so a mechanical stirrer should be used in this case rather than a magnetic stirrer.

Some factors influence a good coating – such as different stirrers (e.g. magnetic or mechanical), different hanging orientation (vertical or horizontal), size of particles, bath loading of particles, coating time, etc. The thickness of the coatings can be measured by Optical Microscopy; the chemical analysis is carried out by Energy Dispersive X-ray Analysis (EDXA) via a Scanning Electron Microscope (SEM).

5.3.2 Alkaline electroless co-deposition

LSM could be electroless nickel co-deposited onto alumina under an acid environment but it was found that after the acidic electroless coating process, the solution became more alkaline. Though some evaporation of acid content may exist, it is believed that LSM prefers an alkaline rather than acidic environment. [112] Therefore, the tubular Al_2O_3 substrates were also plated by an alkaline electroless co-deposition (the pH of the alkaline bath is 9.5). The procedure is similar to the acid electroless; the sample was pre-treated and was put in the alkaline electroless nickel solution at 80°C after the powders were added. Similar factors were researched to find the best coating method; in addition, a short time of nickel pre-coating was carried out. It has to be mentioned that the new batch of Al_2O_3 substrates were too smooth to get coated, so they had to be roughed using 120 grit sandpaper – this improved the adhesive ability. Samples were again tested by optical microscopy, SEM, and EDXA. The results were analysed for the best coating deposition.

5.3.2 Electrical test

Because of the scarcity of tubular electrical test equipment, a planar cell was built for the electrical testing. The circular planar cell used in this test is YSZ electrolyte supported. The NiO/YSZ anode was screen printed and the YSZ/LNF cathode was electroless nickel co-deposited.

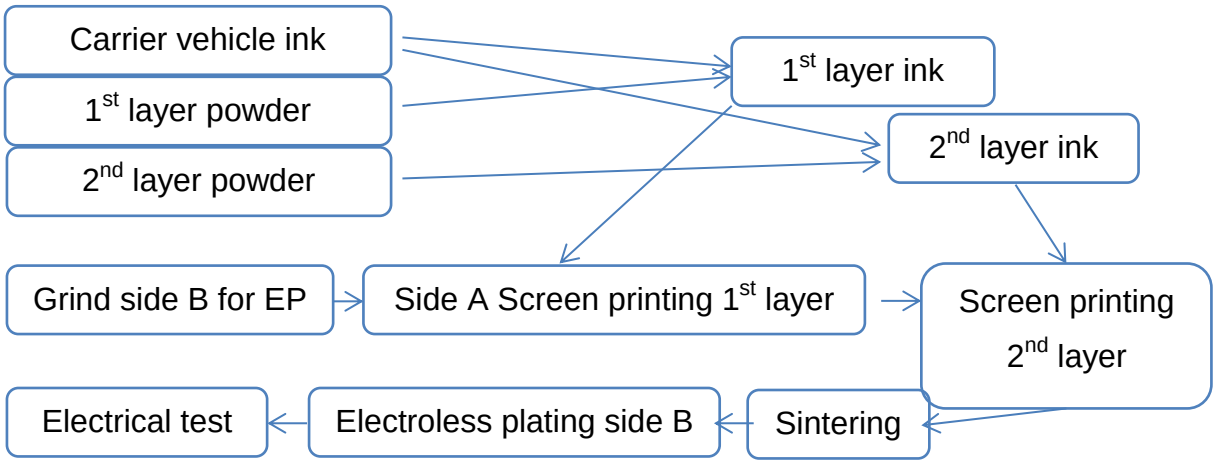

Figure 31 The flow chart of electrical test

Figure 31 shows the electrical test process. Side A represents the anode while Side B represents the cathode. First of all, side B was ground for a good roughness for the electroless nickel co-deposition process. Side A was screen printed with two layers of NiO/YSZ anode. After sintering, side A was masked by high temperature tape so that only side B would be electroless nickel co-deposited. Then the cell was ready to do the electrical test.

5.3.2.1 Anode

As mentioned above, the circular YSZ substrate was ground using 120 grit to improve the roughness in order to be available for the next electroless nickel plating process. This must be done before the screen printing and sintering process. Also, this must be done very gently with di-water because this may bring in some defect to the sample, which may cause cell cracking during the sintering or EIS testing process.

5.3.2.1.1 Ink make

The carrier vehicle in the ink was made by the mixture of 95g of Terpineol and 5g of Polyvinyl Butyral (PVB). The mixture was heated in a water bath at 50 °C for around 1 hour with stirring until full dissolution took place.

Two different layers in the anode needed to be screen printed onto the electrolyte. The first was the NiO/YSZ 50/50 ratio layer, and the second was pure YSZ layer. For the first one, 12.5g NiO powder and 12.5g 5μm YSZ powder were mixed with 0.5g Polyvinyl Pyrrolidone (PVP). Some acetone was used to make the mixed paste of the correct viscosity. The mixture was put in a zirconia milling cup with 7 zirconia milling balls. It was milled for 5 minutes at the speed level around 4 on the milling machine. Then the very thick paste was placed on a glass slide in an oven at 60°C to evaporate the remaining solvent. For the second layer, 25g of YSZ powder was mixed with 0.5g of PVP and a small amount of acetone; then, the same ball milling and oven drying process took place.

After the powder was fully dried, 7.25g of clear ink (the carrier vehicle) and 3g of the first layer powder were mixed in a zirconia milling cup with 4 milling balls at the speed level around 6 for 5 minutes. The same process was used in the second layer powder. The two kinds of paste were kept in jars.

5.3.2.1.2 Screen printing

The first layer ink (NiO/YSZ) was screen printed onto the YSZ substrate three times with the print set ‘alt’ on the screen printer. After each printing, the cell was put in an 80°C oven for 30 minutes until completely dry. Then the second layer ink (YSZ) was also printed three times use the same settings. It should be noted that the squeegee setup and frame height might needed to be slightly adjusted during the printing.

5.3.2.1.3 Sintering

The half-cell was placed in a furnace for sintering. It was heated at 3°C /min from room temperature to 1150°C, and then was held for 2hours; after that, it was cooled down to

room temperature at 3°C /min. The printing colour turned from dark green to light green after sintering.

The thickness of the anode was measured using optical microscopy - the thickness was between 30 and 40μm.

5.3.2.2 Cathode

The cathode was made by alkaline electroless nickel co-deposition. Before that, the half-cell was covered by a high temperature tape to make sure only the cathode side would be coated. Niplast was not used in the process, and the half-cell disk was hung vertically. 4g of LNF and 5.33g of YSZ with a particle size of 5μm were used in this co-deposition. The half-cell was coated for 1 hour at the temperature of 80°C in a 200ml solution. This was because the half-cell with tape was a good height in the 250ml beaker, so 200ml solution was used; the weight of LNF and YSZ was increased to keep the bath loading remaining the same as 3g/150ml LNF and 4g/150ml YSZ.

5.3.2.3 Electrical test

Nickel mesh and wire were used as the anode current collector; on the other side, gold mesh and nickel wire were used as cathode current collector. Some silver paste was used on the mesh to stick the mesh onto the electrodes. A single cell with screen printed anode and electroless co-deposited cathode was sealed on the top of an alumina double tube by fire cement. The cell was heated up to 700°C under the environment of nitrogen to avoid oxidation with heating rate of 3°C /min. At the meantime, nitrogen gas was supplied at a flow rate of 1.25L/min to protect the cell from oxidation. Then hydrogen gas was supplied at 1.25L/ml (sometimes 0.75L/min).

6. Experimental Results

6.1 Acid electroless nickel co-deposition

There are two most important aims for this case. The first one is to lower the nickel content to less than 50% in the co-deposition. That's because the thermal expansion coefficients of nickel is $16.9X10^{-6}$/°C, which is much larger than YSZ, $10.9X10^{-6}$/°C [113][114]. The high content of nickel would potentially cause cracking and break the cell. The second aim is to get a reasonably thick layer; 30-40μm is a reasonable thickness for a solid oxide fuel cell.

6.1.1 Nickel-LSM co-deposition

It has already been discussed that LSM is difficult to get electroless co-deposited onto an alumina substrate (see Section 5.3). Some factors were changed, like bath loading, magnetic or mechanical stirring, coating time, etc. in order to get some co-deposition on the substrate. But very disappointing results were obtained. Little LSM could be found on the SEM or in EDXA tests.

Table 15 EDXA results of electroless nickel coated alumina with YSZ

➢ Element	Weight%	Atomic%
O	30.38	48.66
Al	41.38	39.29
P	2.11	1.75
Ni	21.75	9.49
La	4.38	0.81
Totals	100.00	100.00

As seen in table 15, nickel was only 21.75% in weight percentage, and lanthanum was only 4.38% in weight percentage. At the same time, oxygen and aluminium were major elements detected (30.38% and 41.38% respectively in weight percentage), which indicated that the substrate, alumina Al_2O_3, was insufficiently covered by either

nickel or LSM. There was a little phosphorus in the coating, which probably came from the electroless nickel bath. Figure 32 shows the thickness of the LSM/Ni coating and it can be seen that the coating is not continuous and is not acceptable.

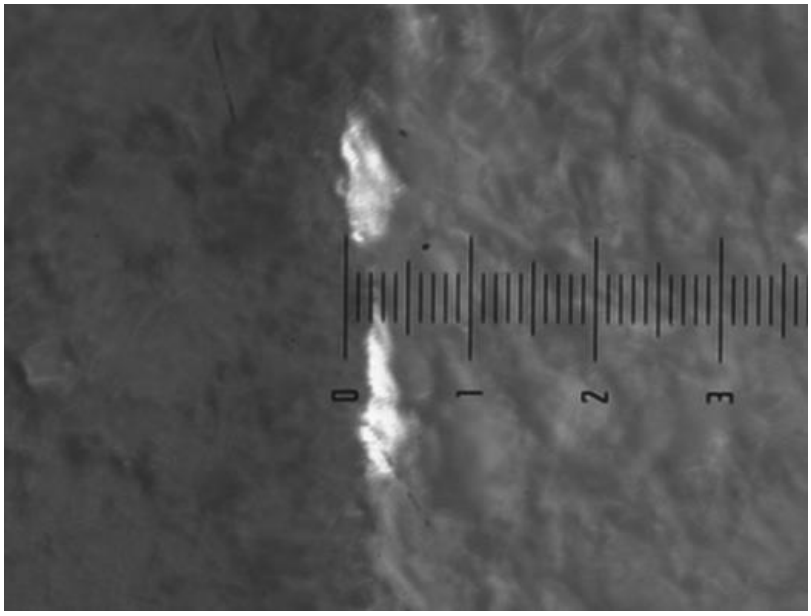

Figure 32 Image of nickel-LSM co-deposition
(magnification x1000, 1μm per division, roughly 3μm)

6.1.2 Nickel-YSZ co-deposition

It was relatively easy to co-deposit nickel and YSZ onto an alumina substrate by electroless nickel coating. A loading of 7g/150ml 5μm YSZ was used in the electroless nickel bath at 89°C for one hour and the result is given below.

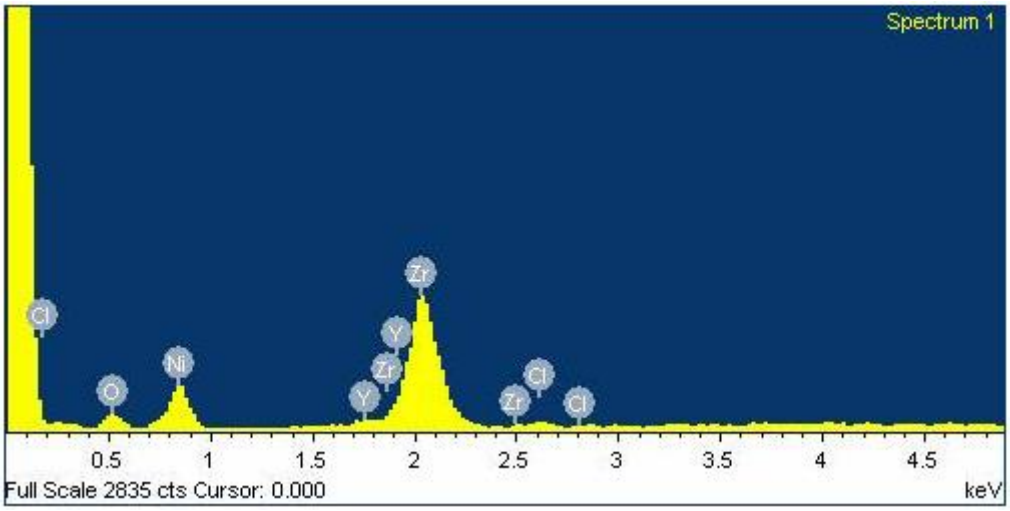

Figure 33 EDX spectrum of electroless nickel coated alumina with YSZ

Table 16 EDXA results of electroless nickel coated alumina with YSZ

➢ Element	Weight%	Atomic%
O	5.59	19.29
Cl	0.41	0.63
Ni	68.98	64.86
Y	4.48	2.78
Zr	20.54	12.43
Totals	100.00	100.00

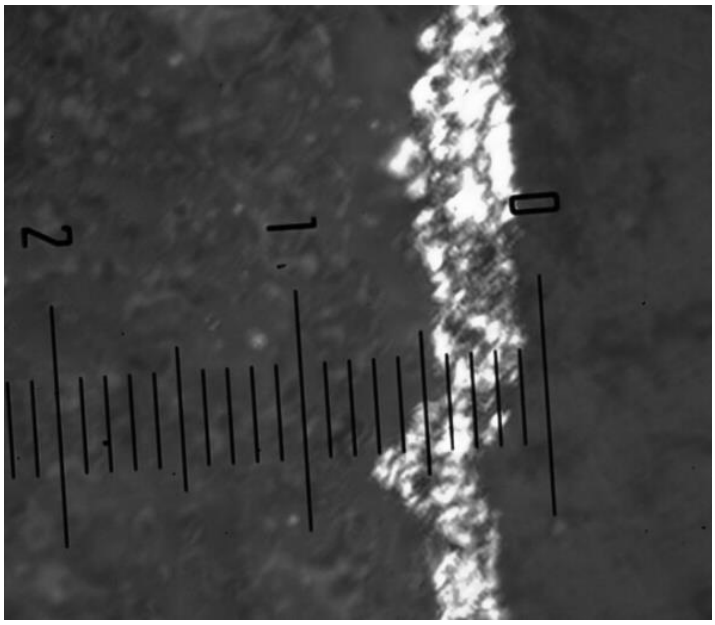

Figure 34 Image of nickel-YSZ co-deposition
(magnification x500, 2µm per division, roughly 10µm)

As can be seen from the images and Table 16, the Ni/YSZ coating is much more prominent than the Ni/LSM one. The coating has more coverage of the surface and has a lower nickel content. There is a significant amount of YSZ detected and the thickness is better too.

6.1.3 Nickel-LSM/YSZ co-deposition

LSM was then successfully co-deposited with the presence of YSZ so some tests were carried out to analyse the factors that could affect this improved coating performance.

6.1.3.1 YSZ particle size

Each particle size of YSZ (1µm, 2µm, and 5µm) was used along with the LSM while the other factors remained the same; these were: 15 minutes for each pre-treatment stage and a coating regime of 89°C, 3g/150ml LMS, 5g/150ml YSZ, 1hour coating time.

6.1.3.1.1 1µm YSZ

The very fine 1µm YSZ/nickel trial was able to cover the substrate completely as there was no aluminium shown in the EDXA result (Figure 35). But the nickel content was too high at 93.57% in weight percentage, which is totally unacceptable. It was almost a pure nickel coating onto the alumina substrate. Little lanthanum and zirconium could be found in the coating.

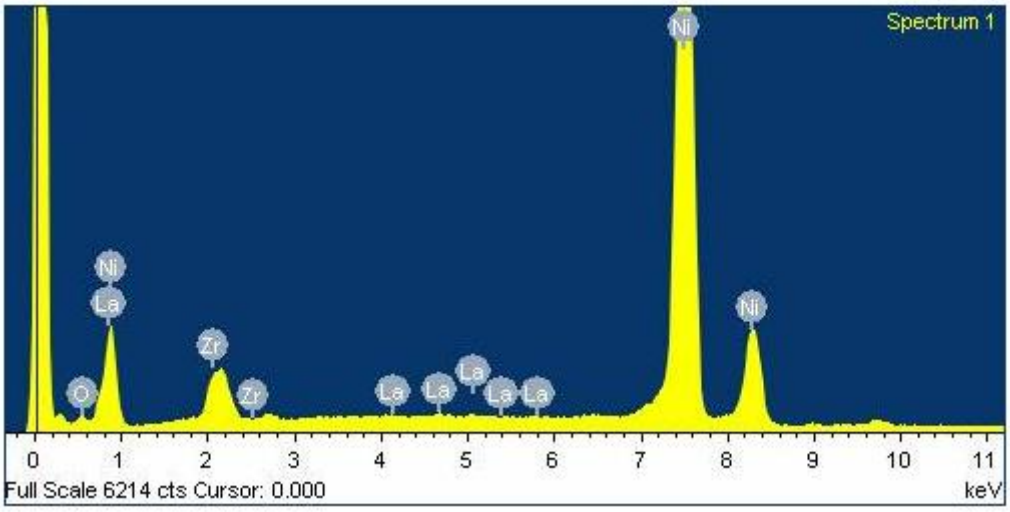

Figure 35 EDX spectrum of electroless nickel coated alumina with LSM and 1µm YSZ

Table 17 EDXA results of electroless nickel coated alumina with LSM and 1µm YSZ

Element	Weight%	Atomic%
O	1.39	5.00
Ni	93.57	91.98
Zr	4.47	2.83
La	0.47	0.20
Totals	100.00	100.00

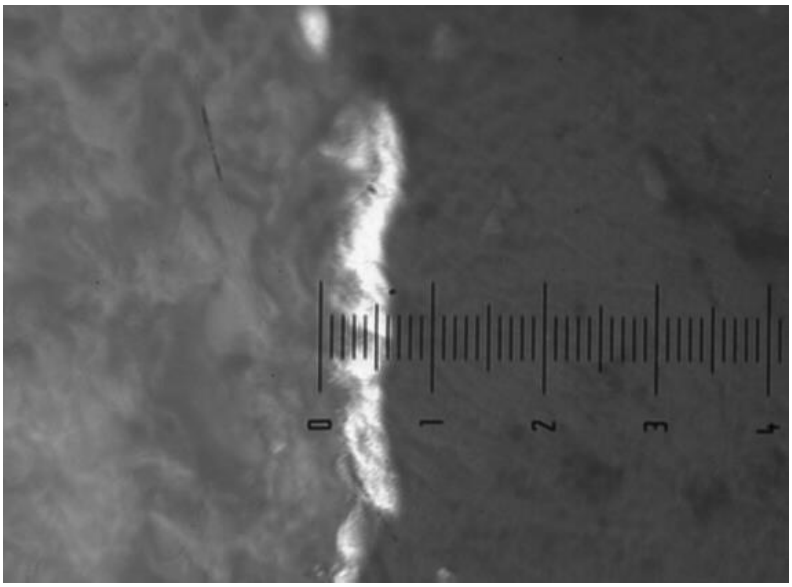

Figure 36 Image of nickel-LSM/YSZ co-deposition with 1µm YSZ powder (magnification x1000, 1µm per division, roughly 3µm)

6.1.3.1.2 2µm YSZ

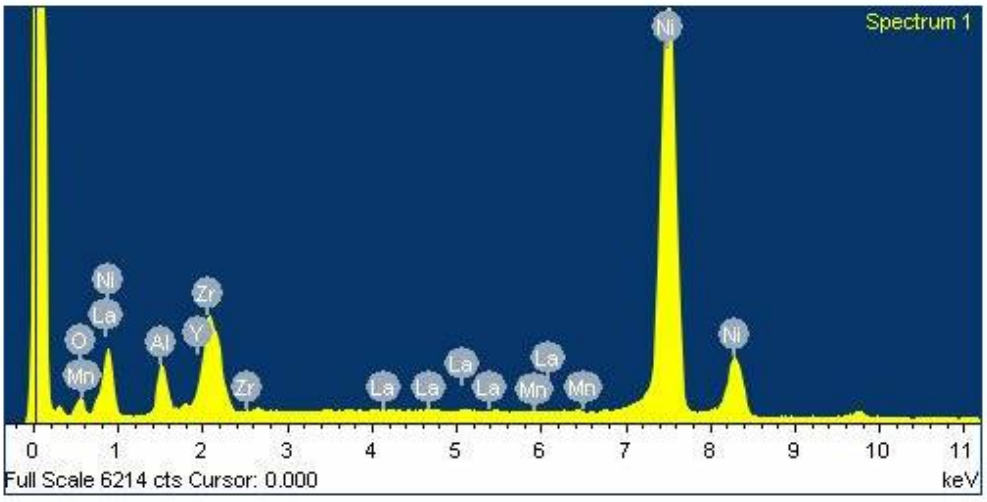

Figure 37 EDX spectrum of electroless nickel coated alumina with LSM and 2µm YSZ

The trials with 2µm and 5µm YSZ slightly brought down the nickel weight percentage - to around 75% - but there was a small amount of aluminium on the spectrum which meant the substrate had not been fully covered by a thick enough co-deposition. As

seen in Tables 18 and 19, the yttrium and lanthanum were still very low in their level of detection, and also the amount of yttrium was greater than lanthanum indicating that YSZ was easier to coat than LSM. The thicknesses of both coatings were around 5μm for the 1 hour coating time.

Table 18 EDXA results of electroless nickel coated alumina with LSM and 2μm YSZ

➢ Element	Weight%	Atomic%
O	5.56	17.70
Al	4.96	9.36
Mn	0.03	0.03
Ni	74.70	64.76
Y	1.27	0.72
Zr	13.01	7.26
La	0.48	0.17
Totals	100.00	100.00

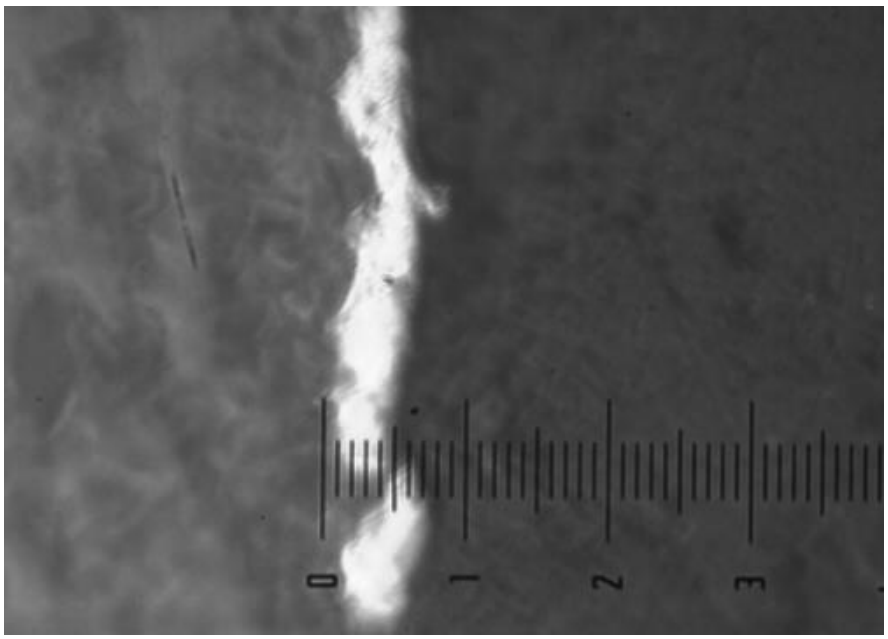

Figure 38 Image of nickel-LSM/YSZ co-deposition with 2μm YSZ powder (magnification x1000, 1μm per division, roughly 5μm)

6.1.3.1.3 5µm YSZ

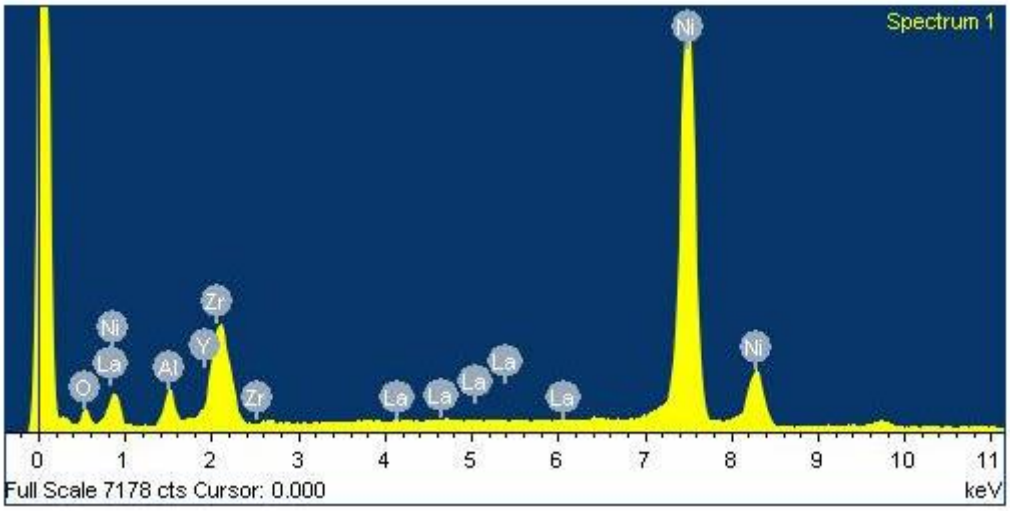

Figure 39 EDX spectrum of electroless nickel coated alumina with LSM and 5µm YSZ

Table 19 EDXA results of electroless nickel coated alumina with LSM and 5µm YSZ

Element	Weight%	Atomic%
O	5.15	16.71
Al	4.08	7.84
Ni	75.73	66.91
Y	0.83	0.49
Zr	14.06	7.99
La	0.16	0.06
Totals	100.00	100.00

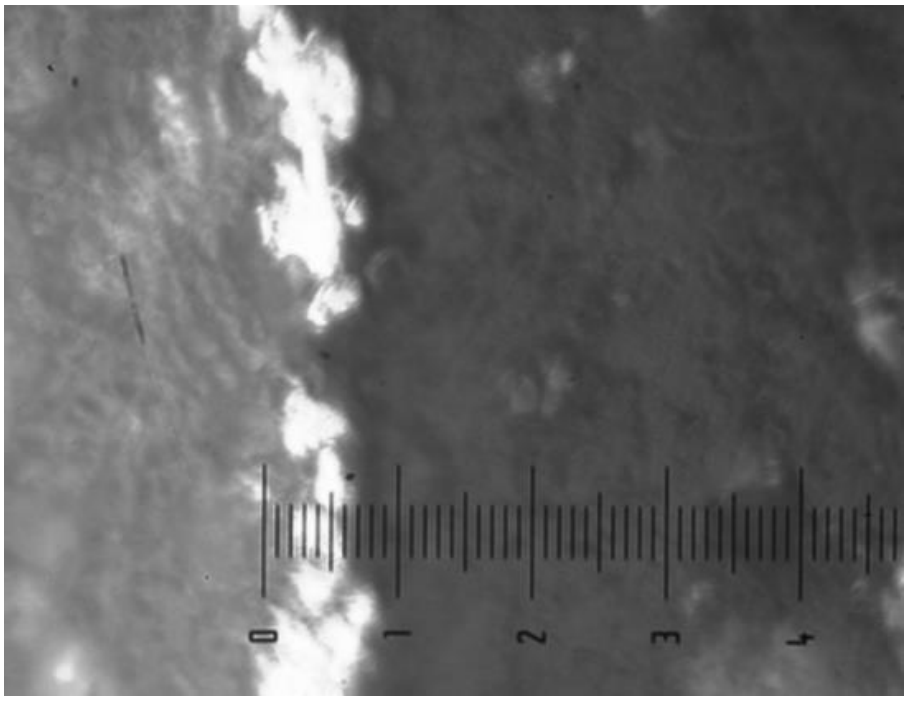

Figure 40 Image of nickel-LSM/YSZ co-deposition with 5μm YSZ powder (magnification x1000, 1μm per division, roughly 5-8μm)

6.1.3.2 Bath loading

Some plating was carried out using 1μm and 2μm YSZ powder with LSM, by using different bath loadings. Again, all other factors remained the same.

6.1.3.2.1 1μm YSZ

- *3g/150ml of LSM and 5g/150ml of YSZ*

Figure 41 and Table 20 shows the same situation mentioned in section 6.1.3.1.1 - the substrate was fully covered by this coating - there was no aluminium shown in the EDXA results. On the other hand, the LSM and YSZ elements were unfortunately very low in their concentrations - the coating was almost entirely nickel.

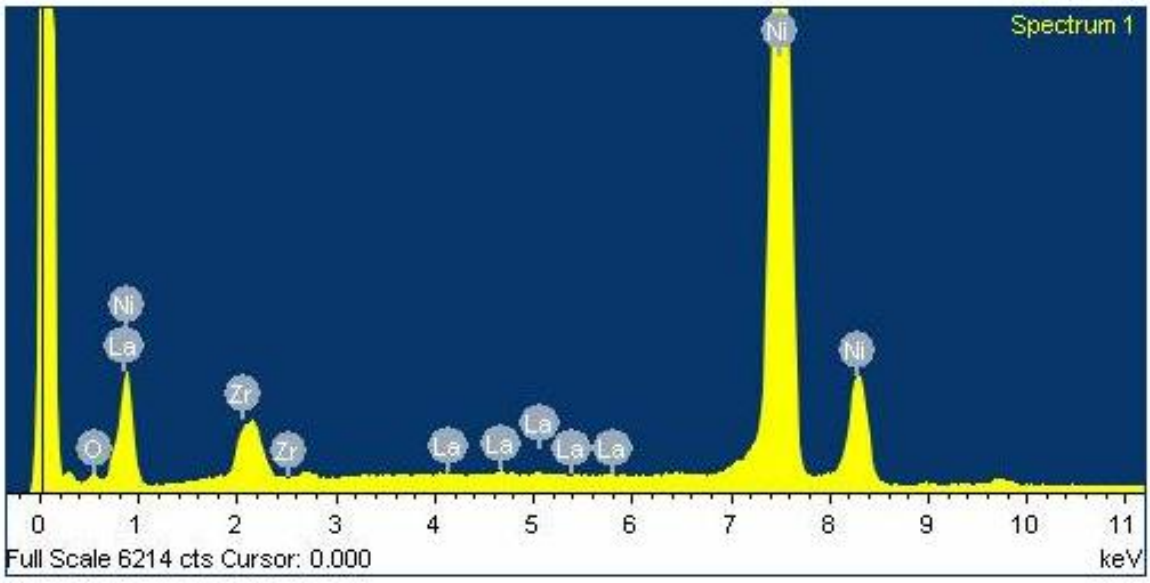

Figure 41 EDX spectrum of electroless nickel coated alumina with 3g/150ml of LSM and 5g/150ml of YSZ

Table 20 EDXA results of electroless nickel coated alumina with 3g/150ml of LSM and 5g/150ml of YSZ

Element	Weight%	Atomic%
O	1.39	5.00
Ni	93.57	91.98
Zr	4.47	2.83
La	0.47	0.20
Totals	100.00	100.00

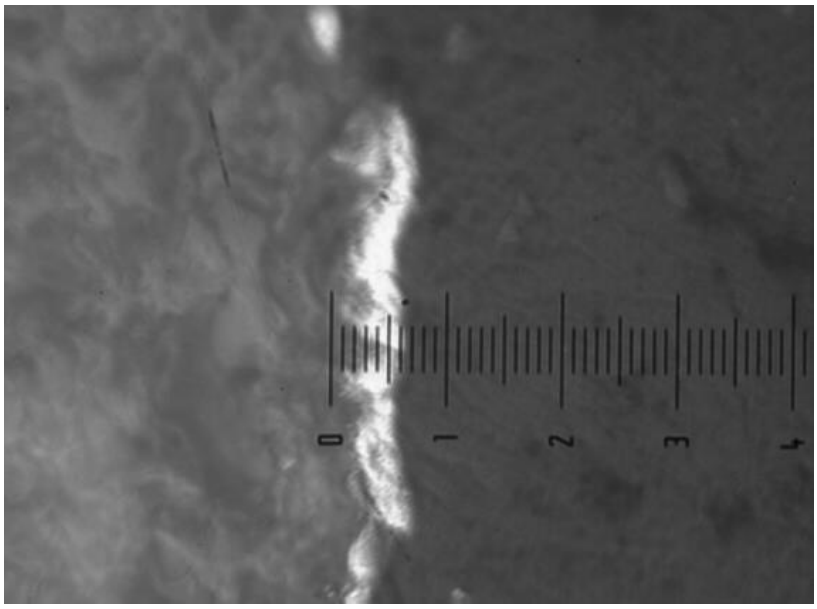

Figure 42 Image of nickel-LSM/YSZ co-deposition with 3g/150ml of LSM and 5g/150ml of YSZ (magnification x1000, 1μm per division, roughly 5μm)

- *3g/150ml of LSM and 4g/150ml of YSZ*

When 4g of 1μm YSZ powder was applied with LSM, reducing the usage of YSZ from 5g/150ml to 4g/150ml, the LSM and YSZ content in the coating slightly increased, but not significantly; the nickel content reduced slightly but was still dominant.

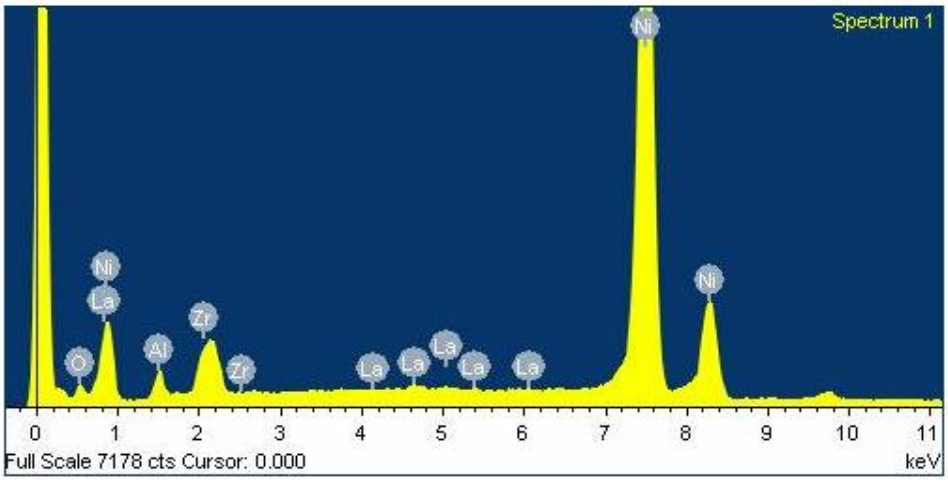

Figure 43 EDX spectrum of electroless nickel coated alumina with 3g/150ml of LSM and 4g/150ml of YSZ

Table 21 EDXA results of electroless nickel coated alumina with 3g/150ml of LSM and 4g/150ml of YSZ

Element	Weight%	Atomic%
O	2.22	7.62
Al	2.28	4.64
Ni	90.67	84.97
Zr	4.11	2.48
La	0.72	0.28
Totals	100.00	100.00

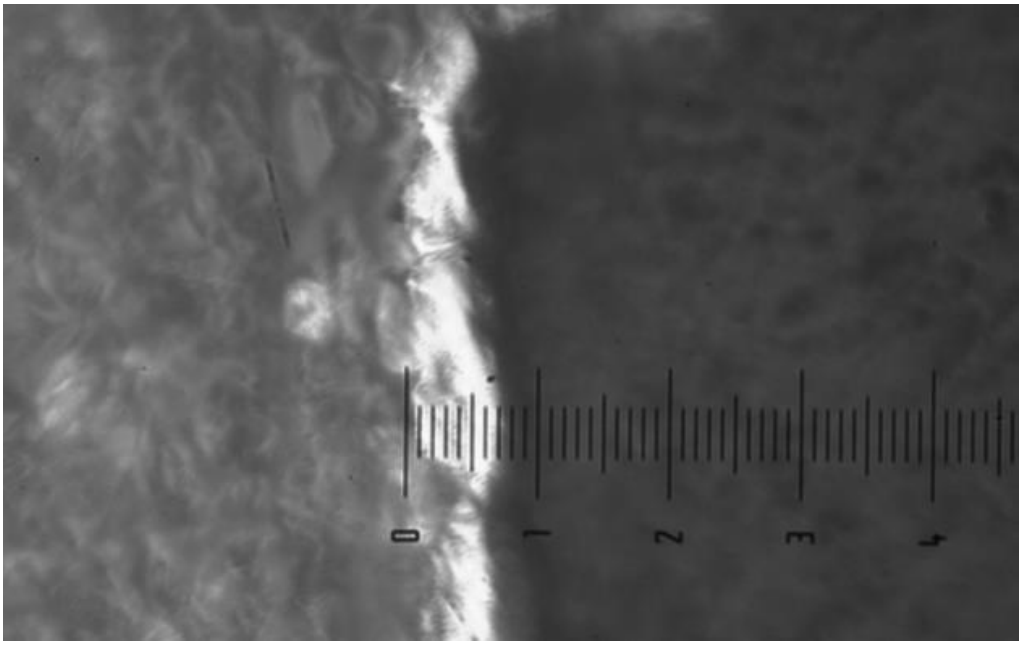

Figure 44 Image of nickel-LSM/YSZ co-deposition with 3g/150ml of LSM and 4g/150ml of YSZ (magnification x1000, 1µm per division, roughly 5-7µm)

6.1.3.2.2 2µm YSZ

- *3g/150ml of LSM and 5g/150ml of YSZ*

Usage of 5g of 2µm YSZ powder in acid electroless nickel co-deposition resulted in the alumina substrate not be covered fully by the coating or being too thin a coating. This was similar to the 1µm results.

As can be seen from Tables 22 and 23, LSM and YSZ increased slightly and the nickel content reduced slightly when 4g/150ml YSZ was used instead of 5g/150ml YSZ.

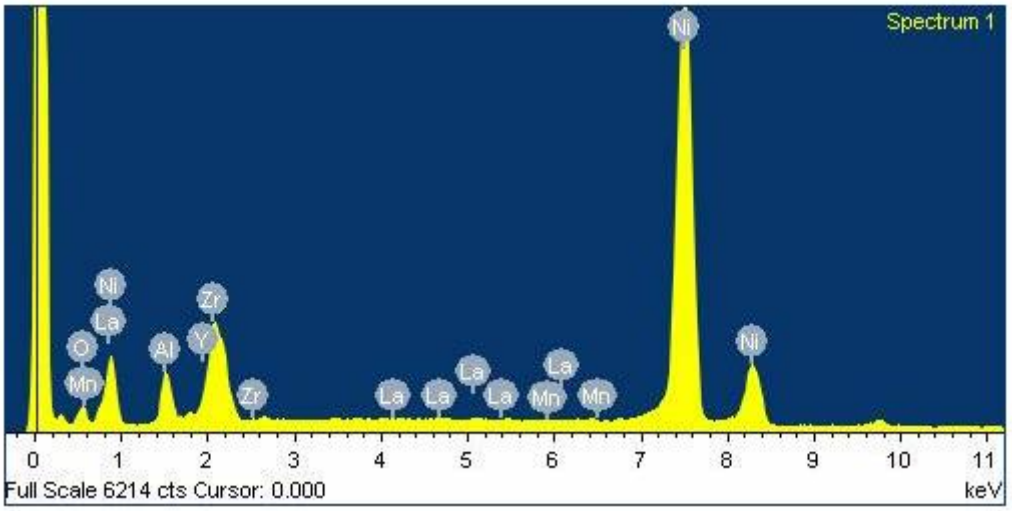

Figure 45 EDX spectrum of electroless nickel coated alumina with 3g/150ml of LSM and 5g/150ml of YSZ

Table 22 EDXA results of electroless nickel coated alumina with 3g/150ml of LSM and 5g/150ml of YSZ

Element	Weight%	Atomic%
O	5.56	17.70
Al	4.96	9.36
Mn	0.03	0.03
Ni	74.70	64.76
Y	1.27	0.72
Zr	13.01	7.26
La	0.48	0.17
Totals	100.00	100.00

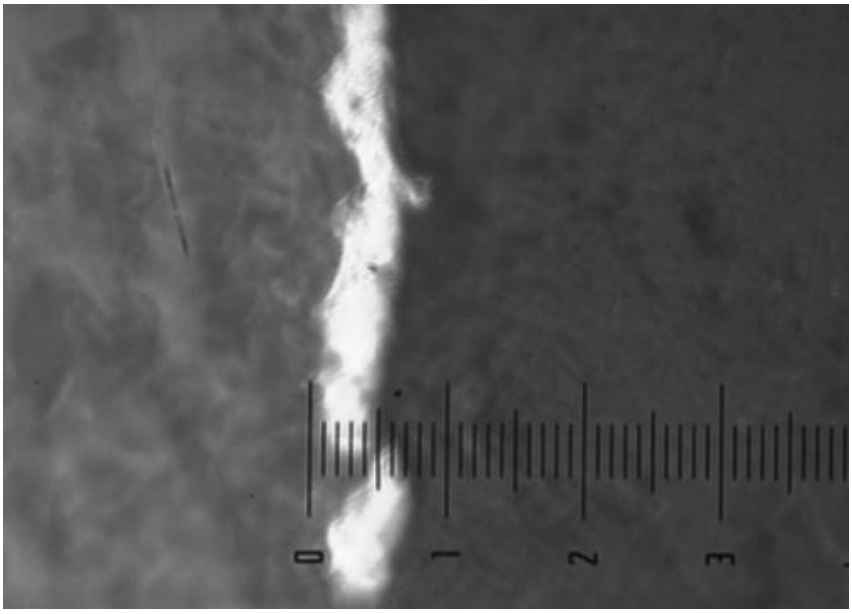

Figure 46 Image of nickel-LSM/YSZ co-deposition with 3g/150ml of LSM and 5g/150ml of YSZ (magnification x1000, 1µm per division, roughly 5-7µm)

- *3g/150ml of LSM and 4g/150ml of YSZ*

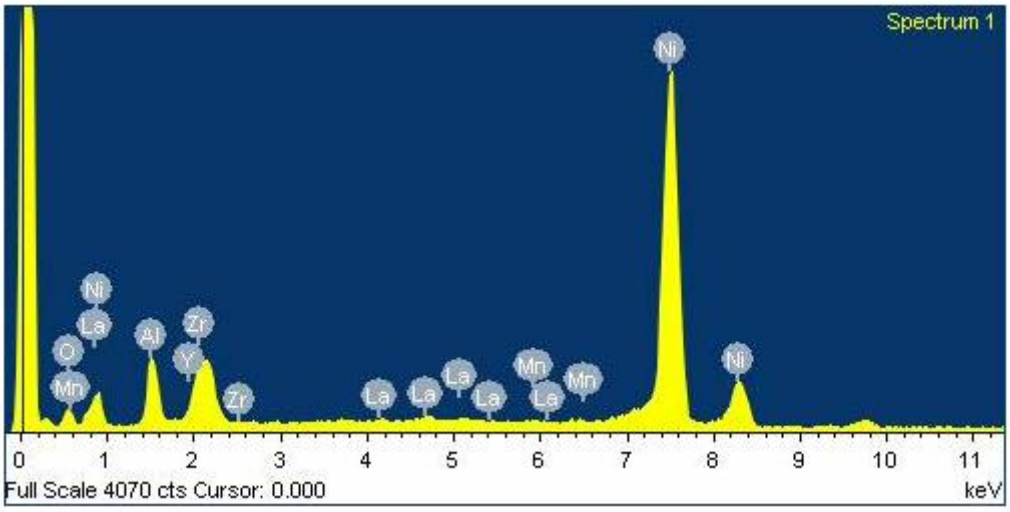

Figure 47 EDX spectrum of electroless nickel coated alumina with 3g/150ml of LSM and 4g/150ml of YSZ

Table 23 EDXA results of electroless nickel coated alumina with 3g/150ml of LSM and 4g/150ml of YSZ

Element	Weight%	Atomic%
O	5.95	18.05
Al	8.39	15.08
Mn	0.14	0.12
Ni	72.82	60.18
Y	1.16	0.63
Zr	10.38	5.52
La	1.16	0.41
Totals	100.00	100.00

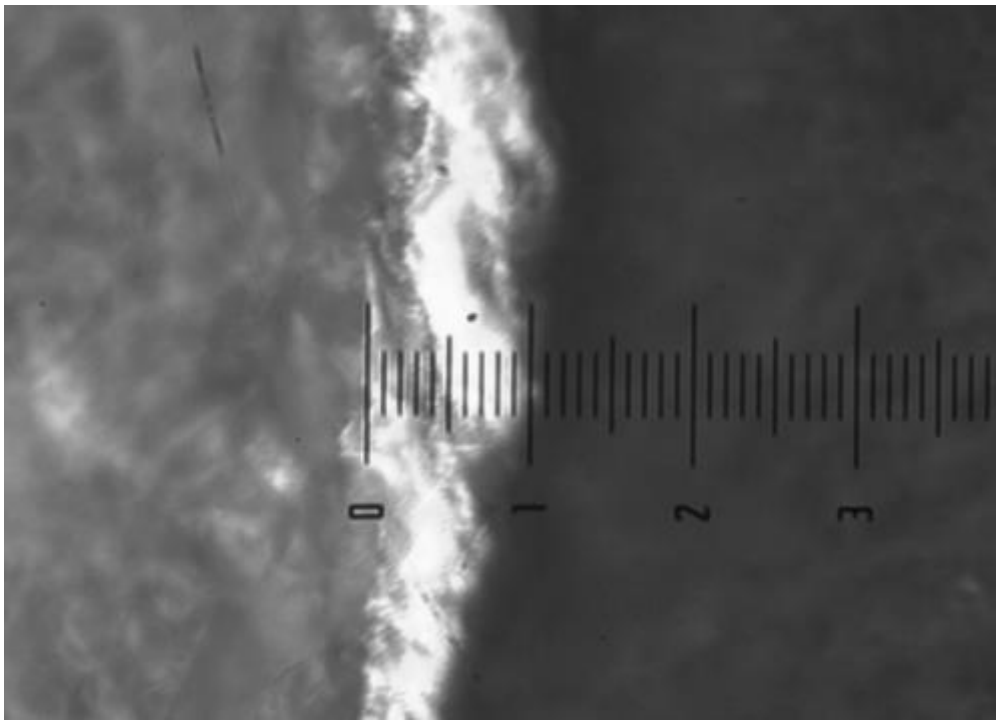

Figure 48 Image of nickel-LSM/YSZ co-deposition with 3g/150ml of LSM and 4g/150ml of YSZ (magnification x1000, 1μm per division, roughly 10μm)

6.1.5 Conclusion of acid electroless nickel co-deposition

The results above show that the LSM was very difficult to be co-deposited with nickel without the presence of YSZ using the acid electroless nickel plating process. However, the presence of YSZ helped LSM to be co-deposited with it. The 5μm YSZ gave the best thickness result of all three YSZ particle sizes; also, a bath loading of 3g/150ml LSM and 4g/150ml YSZ gave better results than 3g/150ml LSM and 5g/150ml YSZ.

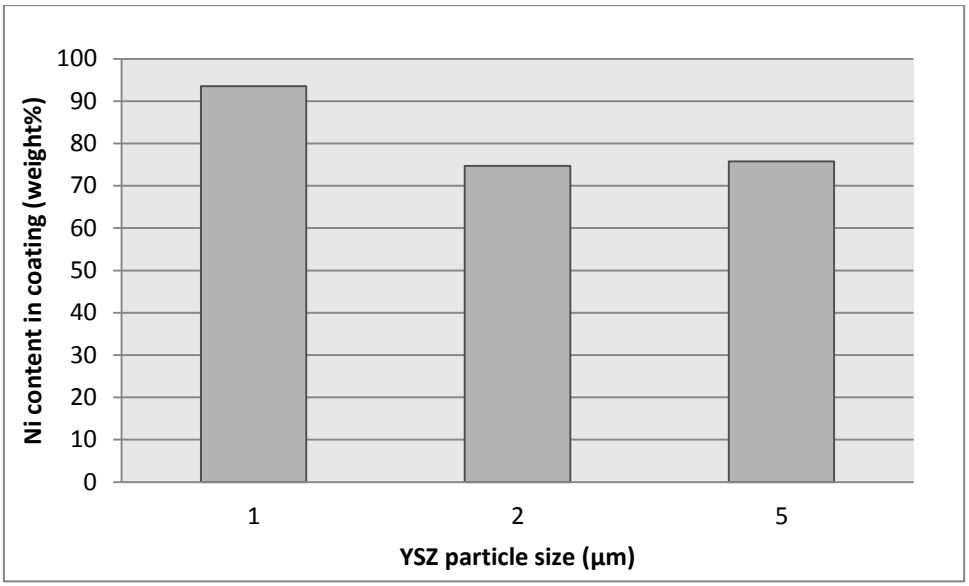

Figure 49 Relationship between Ni content and YSZ particle size in acid nickel bath

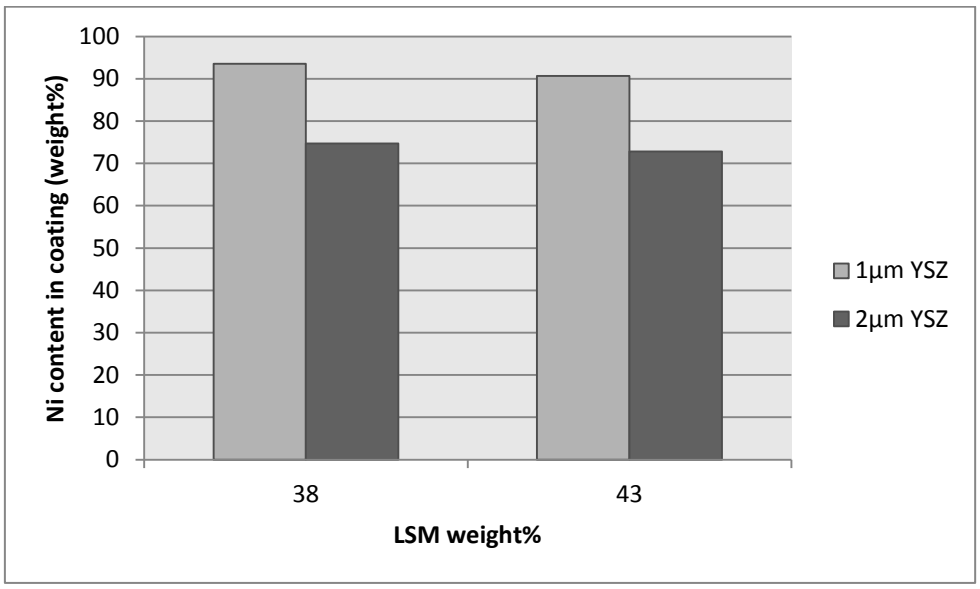

Figure 50 Relationship between Ni content and LSM weigh% in acid nickel bath

Figure49 shows that the 2µm and 5µm YSZ gave better nickel content in the coating, but all of those are high than 70%. Figure 50 shows the nickel content in the coating by using different bath load of LSM and YSZ under 1µm and 2µm YSZ. The nickel content of the sample using 1µm YSZ was all higher than 90%; also 2µm one was higher than 70%.

6.2 Alkaline electroless co-deposition

6.2.1 Nickel-LSM/YSZ co-deposition

6.2.1.1 YSZ particle size

As in the acidic process, YSZ particle sizes of 1µm, 2µm and 5µm were used with the LSM. They were again electroless nickel plated onto alumina substrates. The other factors remained the same, which were: 15 minutes of each pre-treatment each, 2g/150ml LMS, 3g/150ml YSZ and a 1hour coating time. The temperature of the alkaline bath was 80^{o}C and the results are shown below.

6.2.1.1.1 1µm YSZ

In a similar result to the acid electroless nickel/YSZ/LSM co-deposition, the 1µm YSZ powder covered the substrate very well, with no aluminium being found in the EDXA spectrum. The lanthanum content was slightly better than acid result (0.94% to 0.47%); also, the manganese was detectable with a weight percentage of 0.24%; and the nickel content dropped from 93.57% in acid to 87.35% in this alkaline bath. However, the nickel content is still too high for a use in an SOFC cathode.

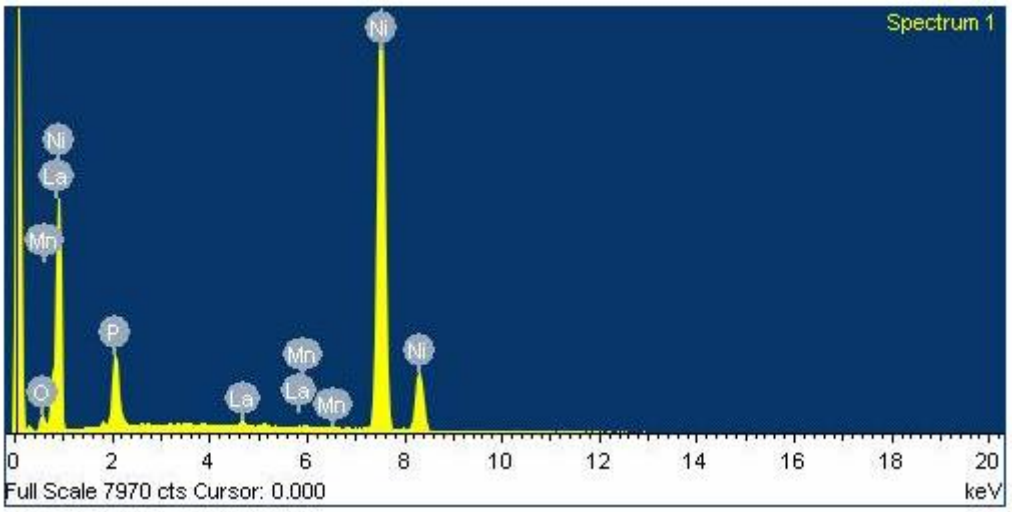

Figure 51 EDX spectrum of electroless nickel coated alumina with LSM and 1µm YSZ

Table 24 EDXA results of electroless nickel coated alumina with LSM and 1μm YSZ

Element	Weight%	Atomic%
O	4.48	13.97
P	6.99	11.25
Mn	0.24	0.22
Ni	87.35	74.22
La	0.94	0.34
Totals	100.00	100.00

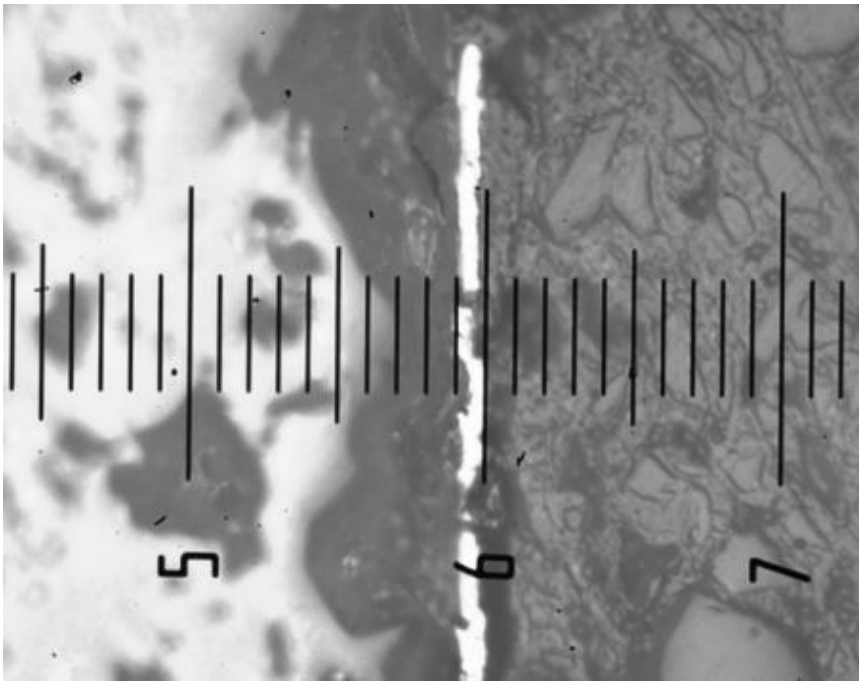

Figure 52 Image of nickel-LSM/YSZ co-deposition with 1μm YSZ (magnification x200, 5μm per division, roughly 5μm)

6.2.1.1.2 2μm YSZ

The usage of 2μm YSZ powder brought down the nickel content slightly, but without any increasing of the LSM content. But compare with figure 52, the thickness with 2μm YSZ (Figure 54) is much better than the 1μm one.

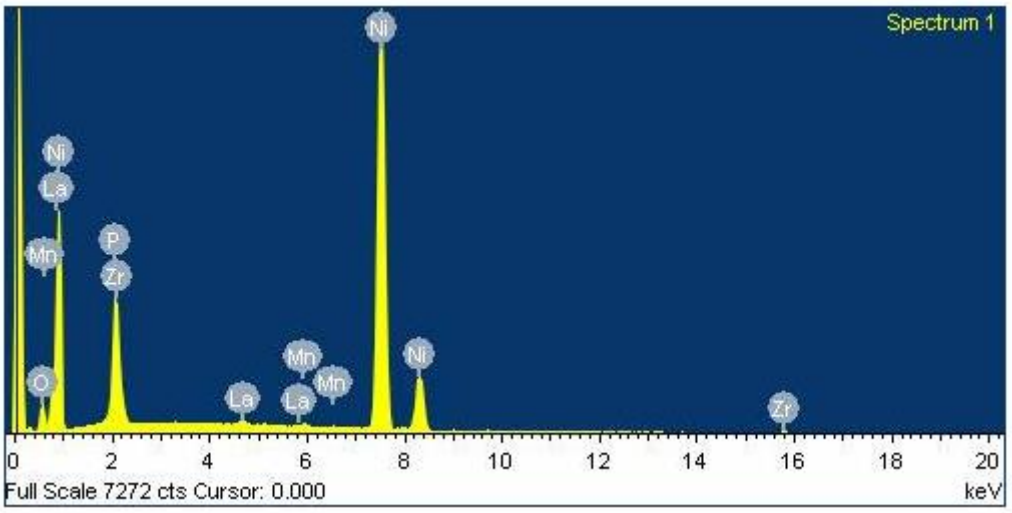

Figure 53 EDX spectrum of electroless nickel coated alumina with LSM and 2μm YSZ

Table 25 *EDXA results of electroless nickel coated alumina with LSM and 2μm YSZ*

Element	Weight%	Atomic%
O	7.64	22.88
P	6.69	10.34
Mn	0.31	0.27
Ni	75.08	61.25
Zr	9.47	4.97
La	0.81	0.28
Totals	100.00	100.00

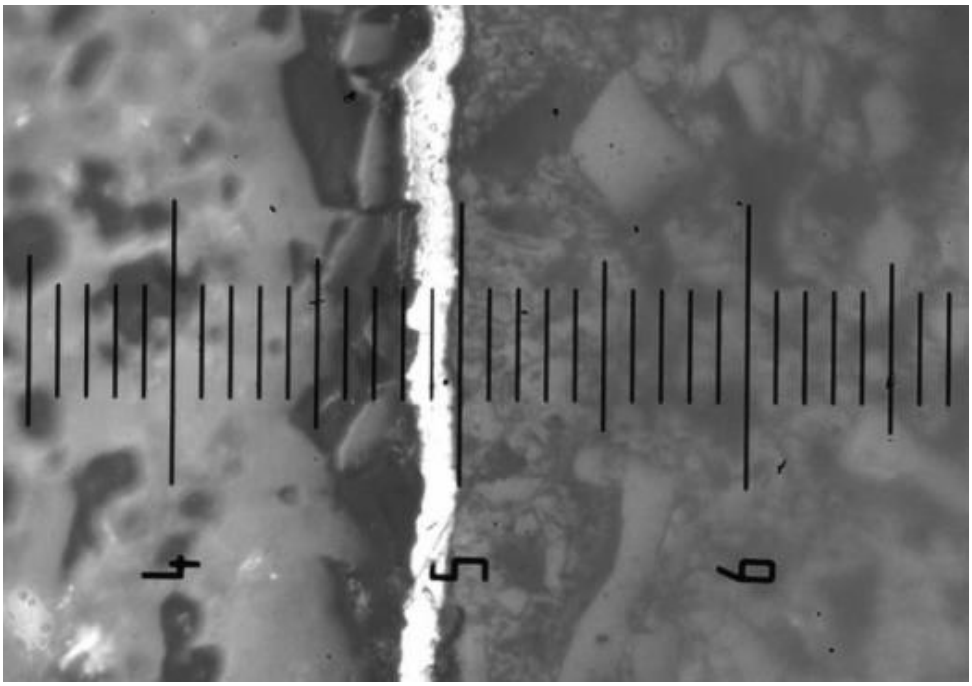

Figure 54 Image of nickel-LSM/YSZ co-deposition with 2μm YSZ (magnification x200, 5μm per division, roughly 5-10μm)

6.2.1.1.3 5μm YSZ

Compared to the 1μm and 2μm YSZ, the 5μm YSZ had a similar lanthanum content; but the zirconium content increased slightly, from 9.47% to 12.72%. Encouragingly, the thickness of the 5μm YSZ samples was about 5-10μm.

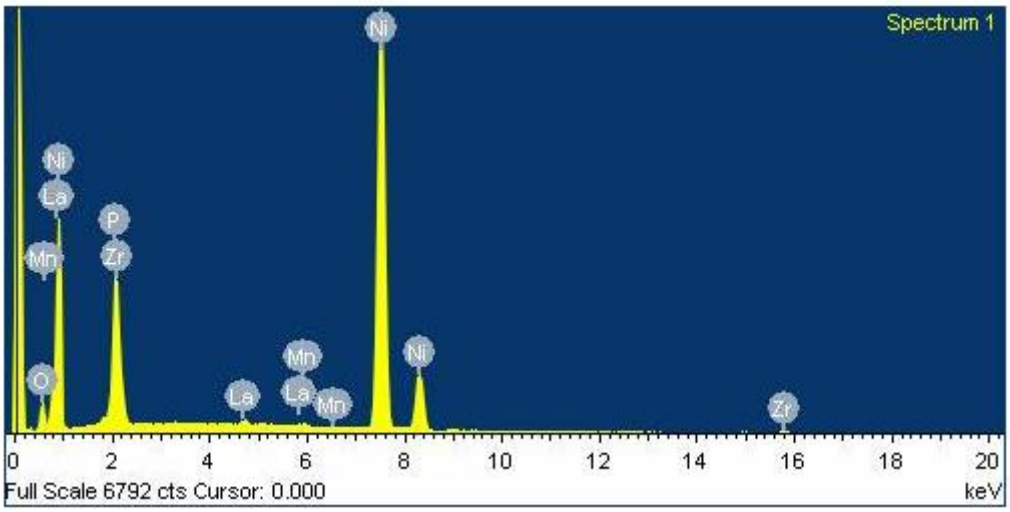

Figure 55 EDX spectrum of electroless nickel coated alumina with LSM and 5μm YSZ

Table 26 EDXA results of electroless nickel coated alumina with LSM and 5μm YSZ

Element	Weight%	Atomic%
O	8.17	24.50
P	6.28	9.73
Mn	0.22	0.19
Ni	71.64	58.55
Zr	12.72	6.69
La	0.97	0.34
Totals	100.00	100.00

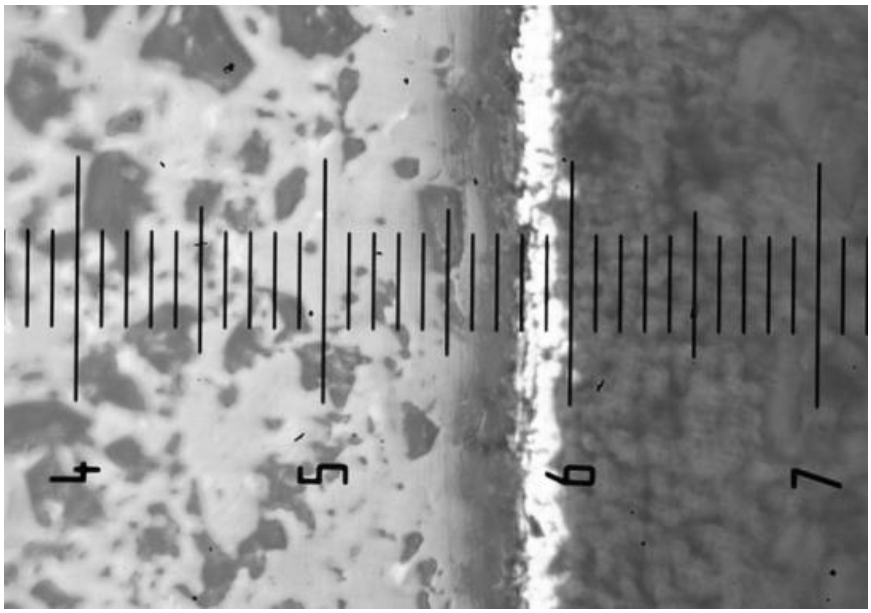

Figure 56 Image of nickel-LSM/YSZ co-deposition with 5µm YSZ (magnification x200, 5µm per division, roughly 10µm)

6.2.1.2 Bath loading

Some plating was carried out using 5µm YSZ powder and LSM, but with different bath loadings. Again, all other factors remained unchanged.

6.2.1.2.1 1g/150ml LSM and 3g/150ml YSZ

This combination resulted in LSM not being detected by the EDXA - the spectrum only showed zirconium. The nickel content was still too high (about 80%) but there was no aluminium detected which was encouraging – as was the coating thickness.

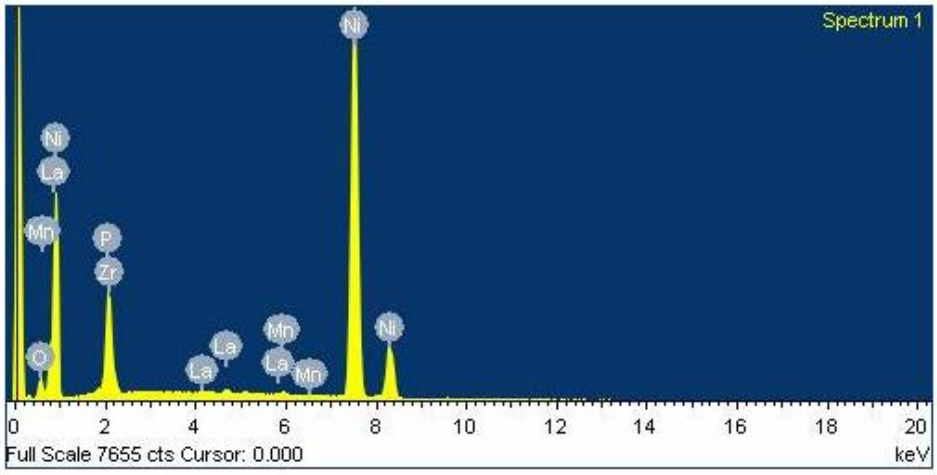

Figure 57 EDX spectrum of electroless nickel coated alumina with 1g/150ml LSM and 3g/150ml YSZ

Table 27 *EDXA results of electroless nickel coated alumina with 1g/150ml LSM and 3g/150ml YSZ*

Element	Weight%	Atomic%
O	5.68	17.43
P	7.59	12.03
Ni	79.86	66.83
Zr	6.88	3.70
Totals	100.00	100.00

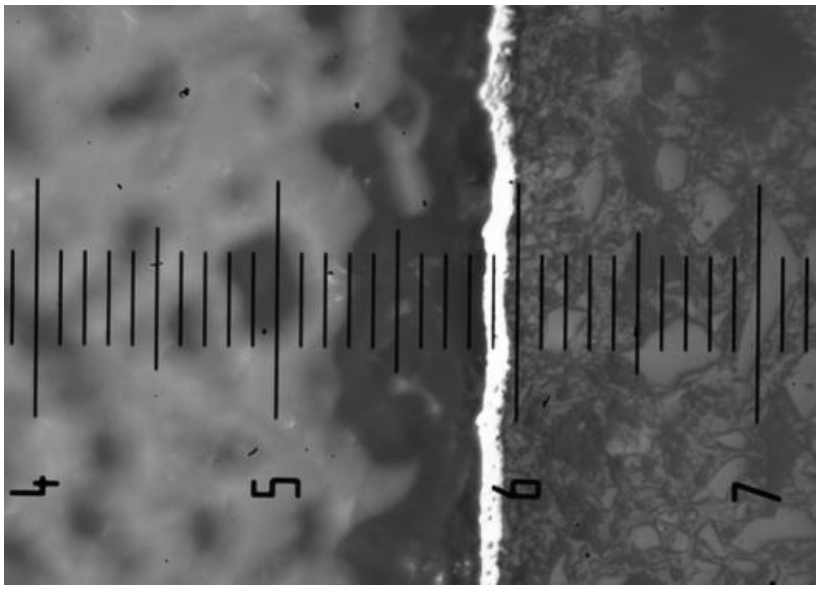

Figure 58 Image of nickel-LSM/YSZ co-deposition with bath load of 1g/150ml LSM and 3g/150ml YSZ (magnification x200, 5µm per division, roughly 5µm)

6.2.1.2.2 2g/150ml LSM and 3g/150ml YSZ

An increased proportion of LSM was used in this co-deposition trial. Lanthanum could be found in the EDXA results, showing as 0.97%. There was no aluminium detected, so the substrate appeared to be fully covered and of an appropriate thickness. The nickel content was slightly lower than the 1g/150ml LSM sample, but was still too high.

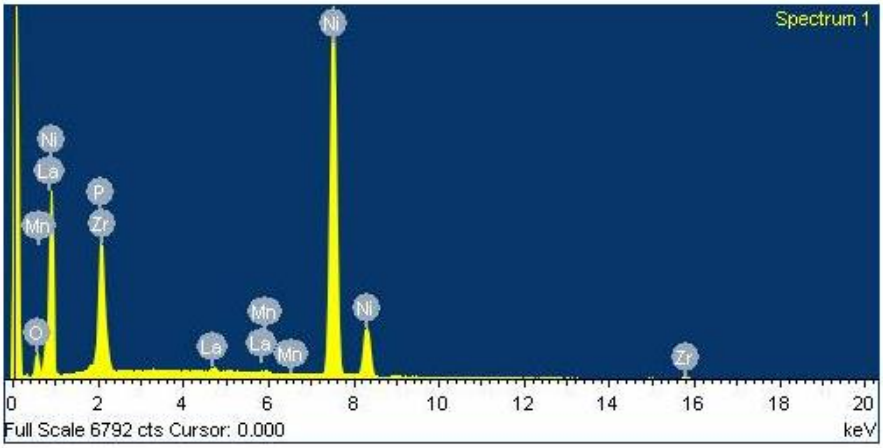

Figure 59 EDX spectrum of electroless nickel coated alumina with 2g/150ml LSM and 3g/150ml YSZ

Table 28 *EDXA results of electroless nickel coated alumina with 2g/150ml LSM and 3g/150ml YSZ*

Element	Weight%	Atomic%
O	8.17	24.50
P	6.28	9.73
Mn	0.22	0.19
Ni	71.64	58.55
Zr	12.72	6.69
La	0.97	0.34
Totals	100.00	100.00

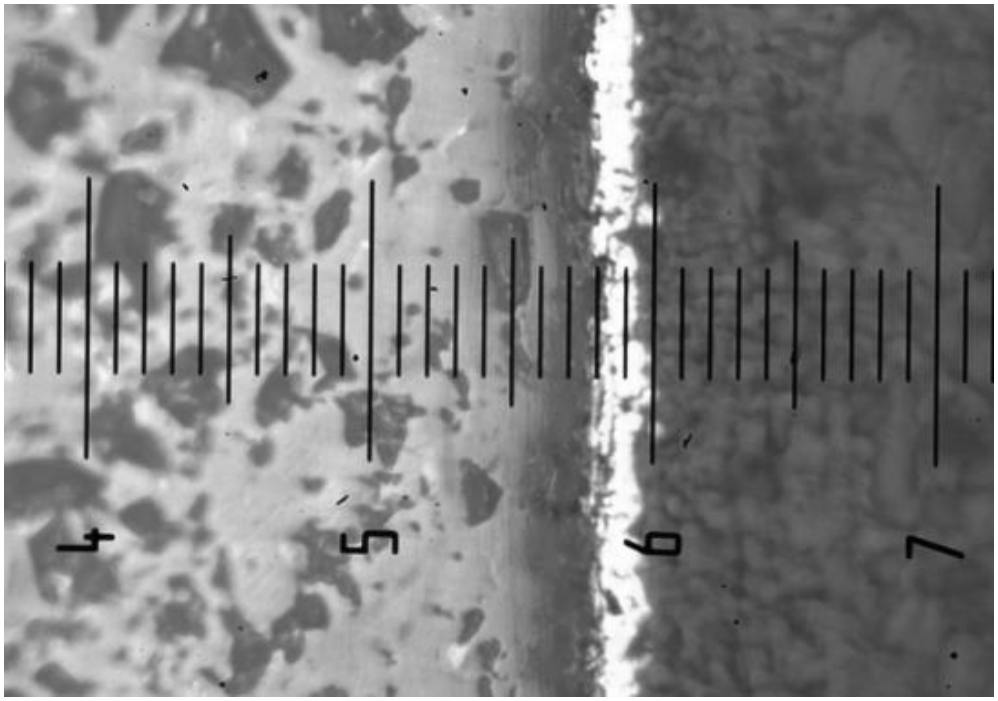

Figure 60 Image of nickel-LSM/YSZ co-deposition with bath load of 2g/150ml LSM and 3g/150ml YSZ (magnification x200, 5μm per division, roughly 5μm)

6.2.1.2.3 1g/150ml LSM and 4g/150ml YSZ

The combination of 1g/150ml LSM and 4g/150ml YSZ makes the coating more like a YSZ/Ni coating. The EDXA spectrum again revealed too high a nickel content for an SOFC cathode although the absence of aluminium indicated a satisfactory coverage of the alumina substrate.

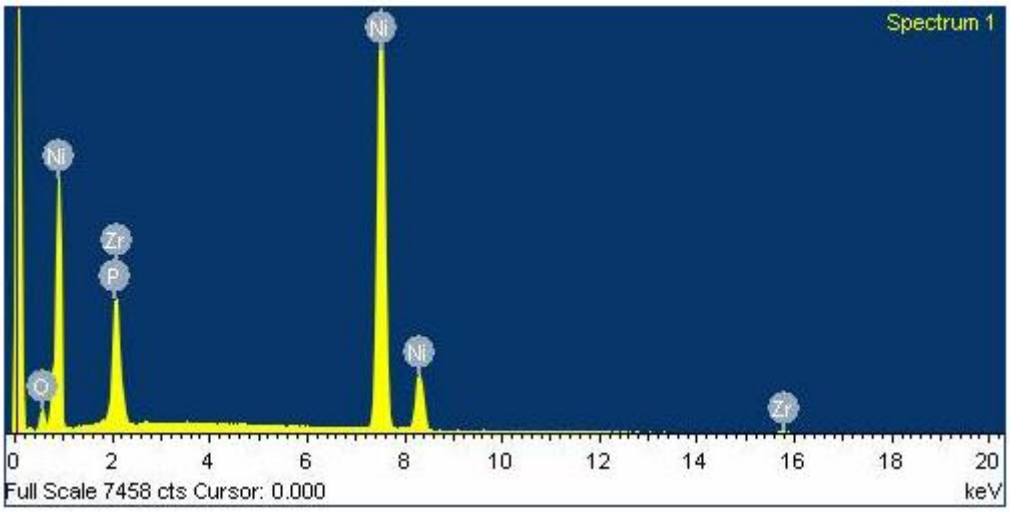

Figure 61 EDX spectrum of electroless nickel coated alumina with 1g/150ml LSM and 4g/150ml YSZ

Table 29 *EDXA results of electroless nickel coated alumina with 1g/150ml LSM and 4g/150ml YSZ*

Element	Weight%	Atomic%
O	6.13	19.18
P	5.73	9.26
Ni	76.32	65.07
Zr	11.81	6.48
Totals	100.00	100.00

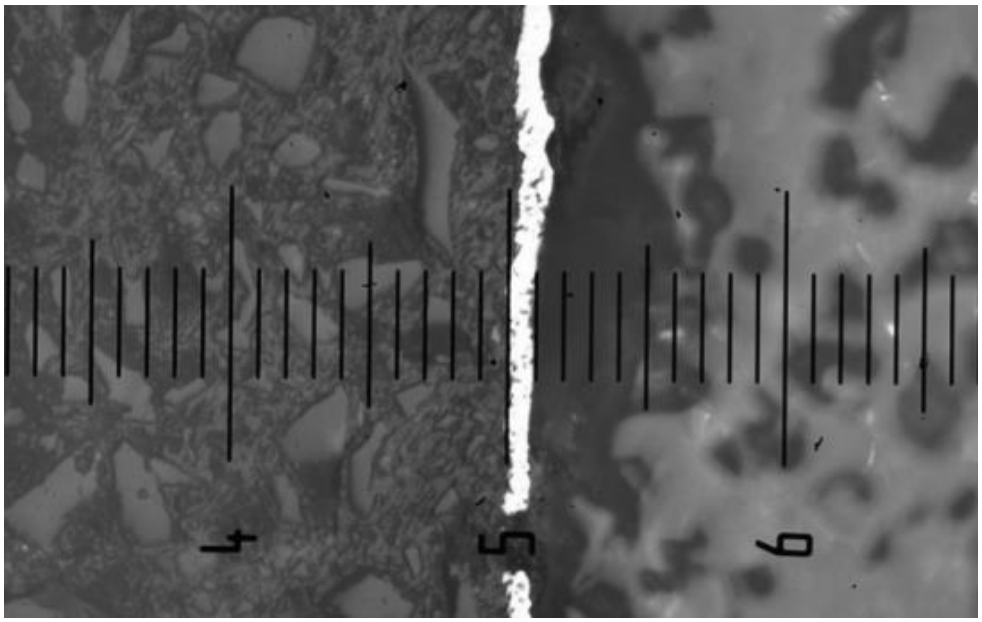

Figure 62 Image of nickel-LSM/YSZ co-deposition with bath load of 1g/150ml LSM and 4g/150ml YSZ (magnification x200, 5µm per division, roughly 5µm)

6.2.1.2.4 2g/150ml LSM and 4g/150ml YSZ

The combination of 2g/150ml LSM and 4g/150ml YSZ again failed to give results good enough for an SOFC cathode – the nickel content was still too high.

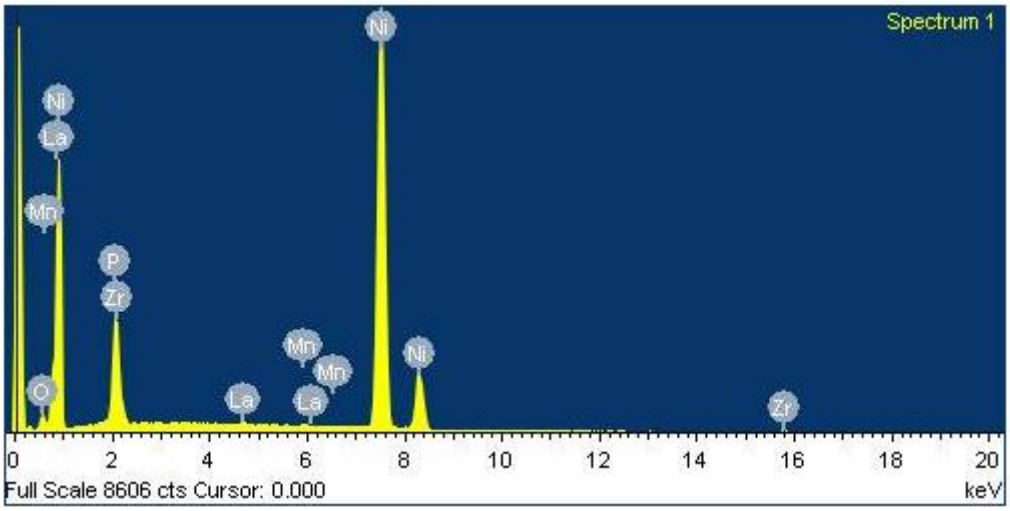

Figure 63 EDX spectrum of electroless nickel coated alumina with 2g/150ml LSM and 4g/150ml YSZ

Table 30 *EDXA results of electroless nickel coated alumina with 2g/150ml LSM and 4g/150ml YSZ*

Element	Weight%	Atomic%
O	4.33	13.86
P	6.88	11.37
Mn	0.19	0.18
Ni	80.26	69.99
Zr	7.93	4.45
La	0.41	0.15
Totals	100.00	100.00

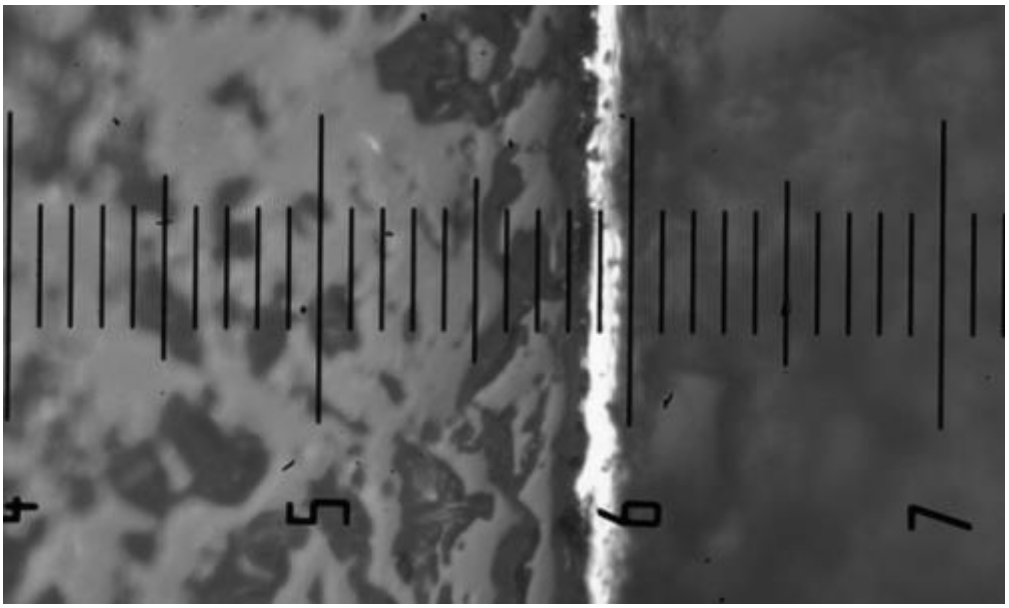

Figure 64 Image of nickel-LSM/YSZ co-deposition with bath load of 2g/150ml LSM and 4g/150ml YSZ
(magnification x200, 5μm per division, roughly 5-8μm)

6.2.1.2.5 3g/150ml LSM and 4g/150ml YSZ

The combination of 3g/150ml LSM and 4g/150ml YSZ resulted in a slightly better coating in terms of reduced nickel content and coating thickness.

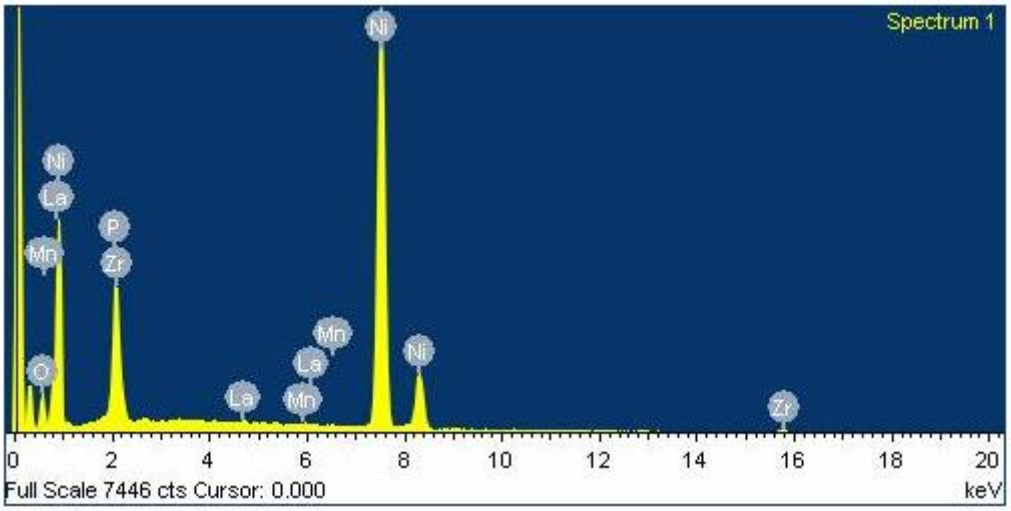

Figure 65 EDX spectrum of electroless nickel coated alumina with 3g/150ml LSM and 4g/150ml YSZ

Table 31 *EDXA results of electroless nickel coated alumina with 3g/150ml LSM and 4g/150ml YSZ*

Element	Weight%	Atomic%
O	10.76	30.41
P	6.09	8.89
Mn	0.15	0.13
Ni	71.21	54.83
Zr	11.24	5.57
La	0.54	0.18
Totals	100.00	100.00

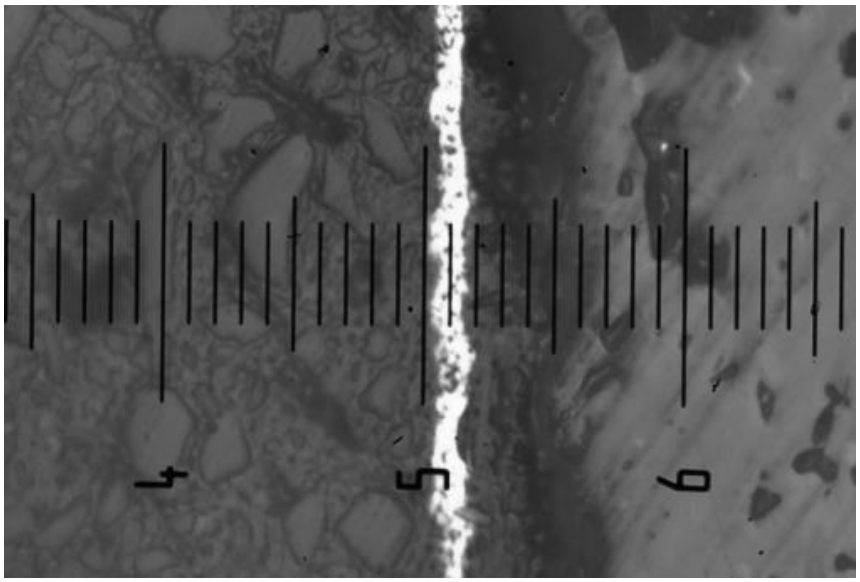

Figure 66 Image of nickel-LSM/YSZ co-deposition with bath load of 3g/150ml LSM and 4g/150ml YSZ (magnification x200, 5µm per division, roughly 5-10µm)

6.2.1.2.6 2g/150ml LSM and 2g/150ml YSZ

When equal amounts of 2g/150ml of both LSM and YSZ, the resulting coating was similar in composition and thickness to the 3g/150ml LSM and 4g/150ml YSZ combination.

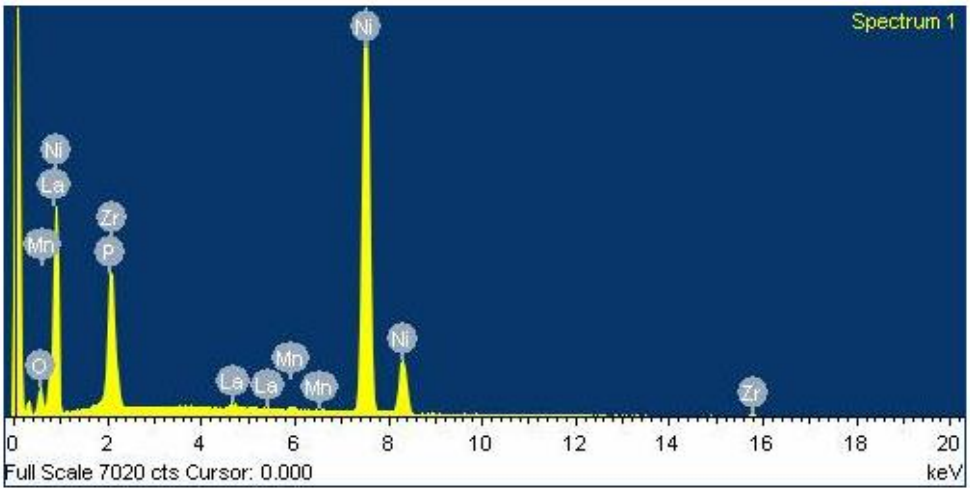

Figure 67 EDX spectrum of electroless nickel coated alumina with 2g/150ml LSM and 2g/150ml YSZ

Table 32 *EDXA results of electroless nickel coated alumina with 2g/150ml LSM and 2g/150ml YSZ*

Element	Weight%	Atomic%
O	7.96	24.01
P	5.90	9.20
Mn	0.32	0.28
Ni	72.57	59.65
Zr	12.44	6.58
La	0.81	0.28
Totals	100.00	100.00

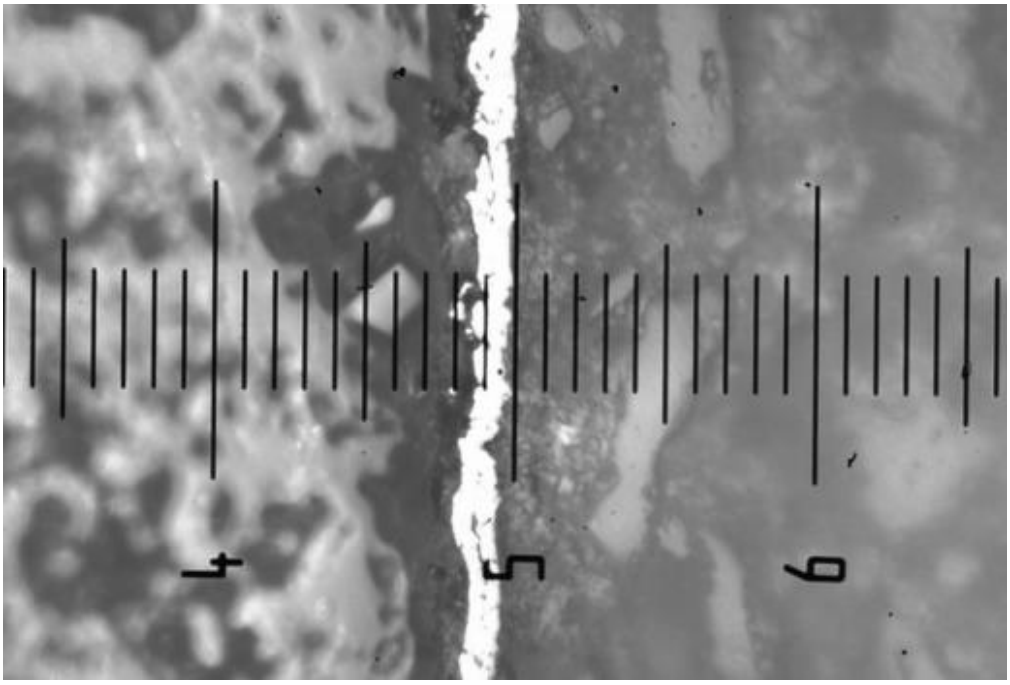

Figure 68 Image of nickel-LSM/YSZ co-deposition with bath load of 2g/150ml LSM and 2g/150ml YSZ (magnification x200, 5μm per division, roughly 5-8μm)

6.2.1.2.7 3g/150ml LSM and 2g/150ml YSZ

When the LSM proportion was greater than the YSZ, it raised the lanthanum content in the coating to 1.21% and decreased the zirconium content to 7.74; the nickel content was 77.72%. More importantly, the high usage of LSM brought back the problem in 6.1.1, namely that the coating was not continuous (Figure 70).

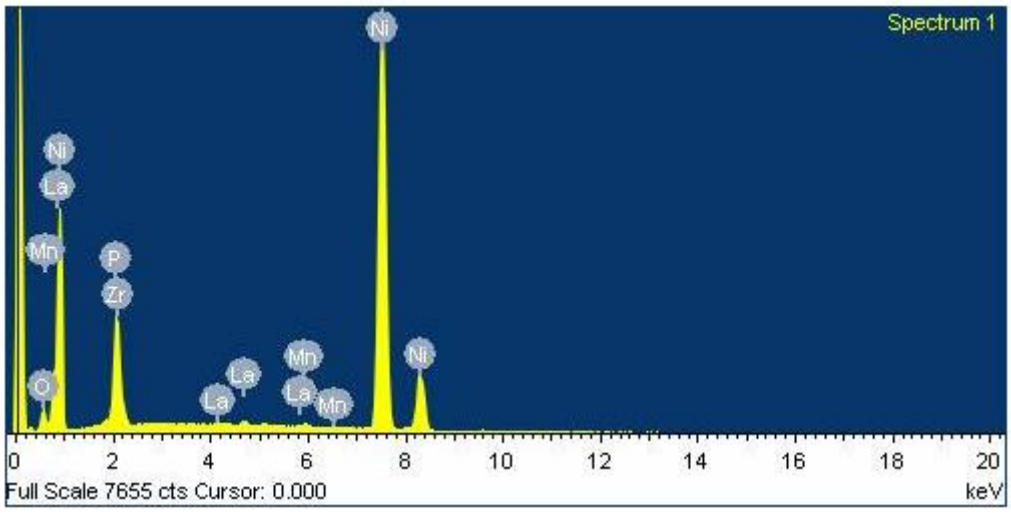

Figure 69 EDX spectrum of electroless nickel coated alumina with 3g/150ml LSM and 2g/150ml YSZ

Table 33 *EDXA results of electroless nickel coated alumina with 3g/150ml LSM and 2g/150ml YSZ*

Element	Weight%	Atomic%
O	6.10	18.82
P	6.89	10.97
Mn	0.34	0.30
Ni	77.72	65.29
Zr	7.74	4.19
La	1.21	0.43
Totals	100.00	100.00

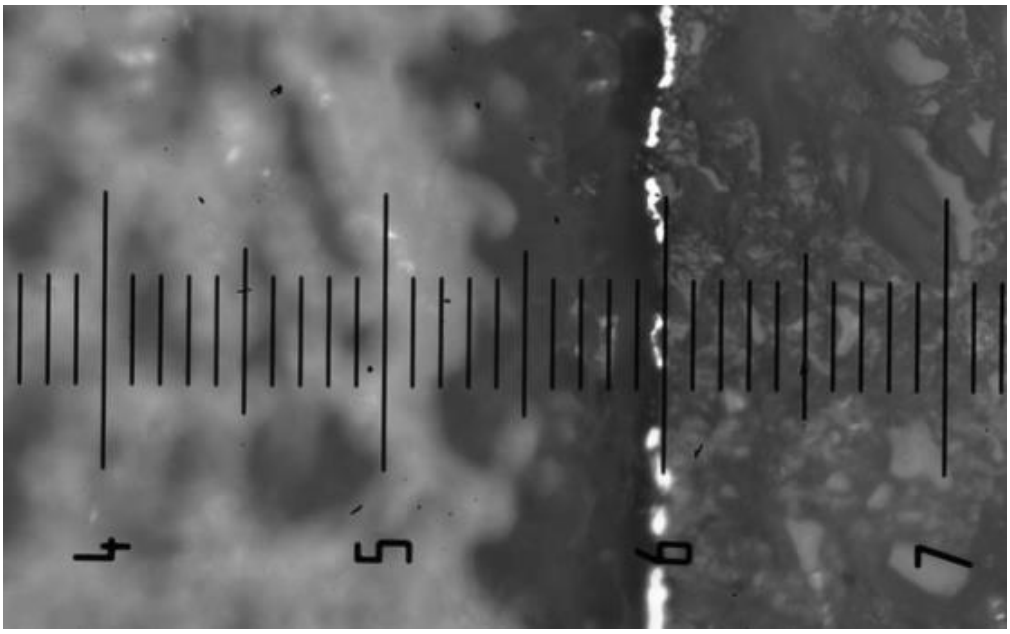

Figure 70 Image of nickel-LSM/YSZ co-deposition with bath load of 3g/150ml LSM and 2g/150ml YSZ (magnification x200, 5µm per division, less than 5µm)

6.2.2 Nickel-LNF/YSZ co-deposition

6.2.2.1 Thickness

When the thickness levels of LNF/YSZ samples were tested, the results showed that they were about 5µm after 1hour of coating – see Figures 71 and 72.

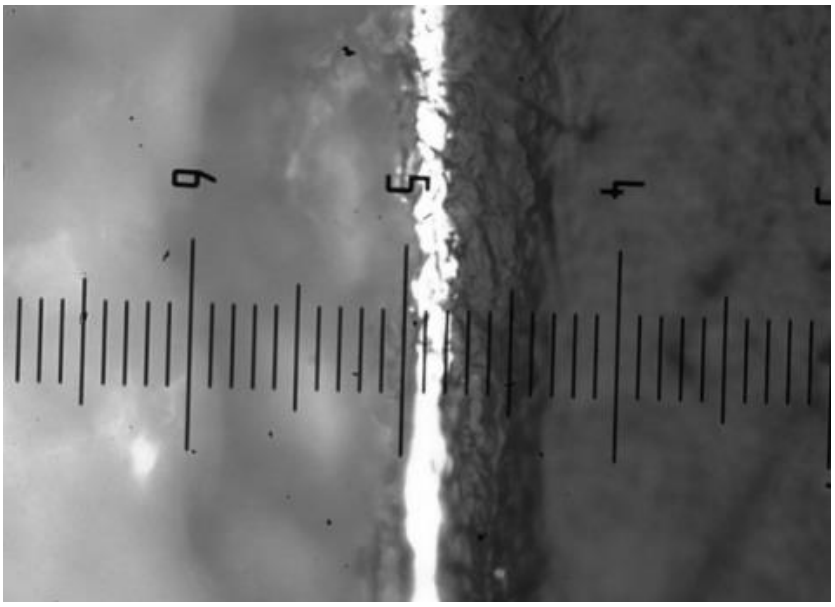

Figure 71 Image of nickel-LNF/YSZ co-deposition with a bath load of 2g/150ml LNF and 3g/150ml 5µm YSZ with 30sec Ni pre-coating (magnification x500, 2µm per division, about 5µm)

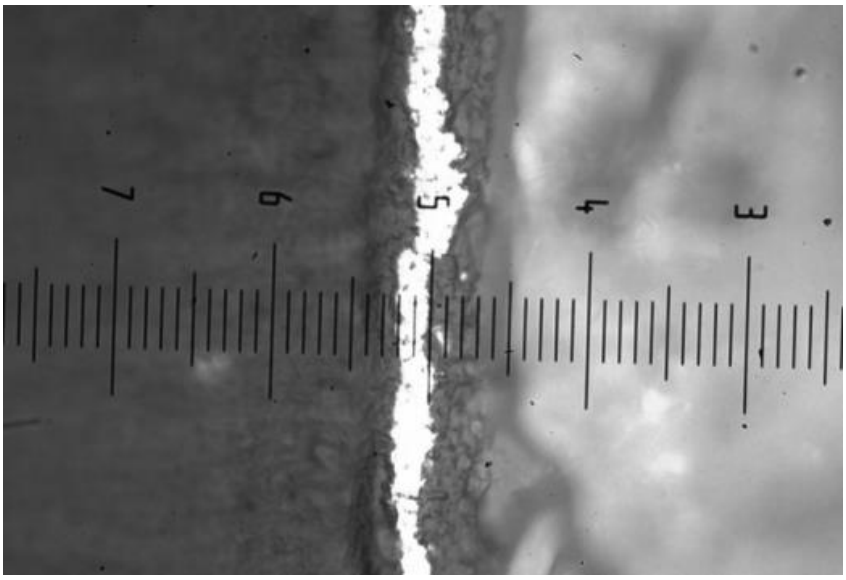

Figure 72 Image of nickel-LNF/YSZ co-deposition with bath load of 3g/150ml LNF and 4g/150ml 5µm YSZ (magnification x500, 2µm per division, about 5µm)

6.2.2.2 YSZ particle size

As with previous experiments, YSZ particle sizes of 1µm, 2µm and 5µm were used in the two sets of tests with LNF. The first set used a bath loading of 3g/150ml LNF and 4g/150ml YSZ while the second used 2g/150ml LNF and 3g/150ml YSZ. The results are shown below.

6.2.2.2.1 1µm YSZ

- *2g/150ml LNF, 3g/150ml YSZ*

Comparing Tables 34 and 24, using the same bath loading (LNF instead of LSM), slightly more lanthanum (1.62% to 0.94%) was found in the former co-deposition; encouragingly, the nickel content was less (62.44% to 87.35%); however, aluminium was found as well indicating that the sample's surface was not fully covered by the coating, with some alumina exposed.

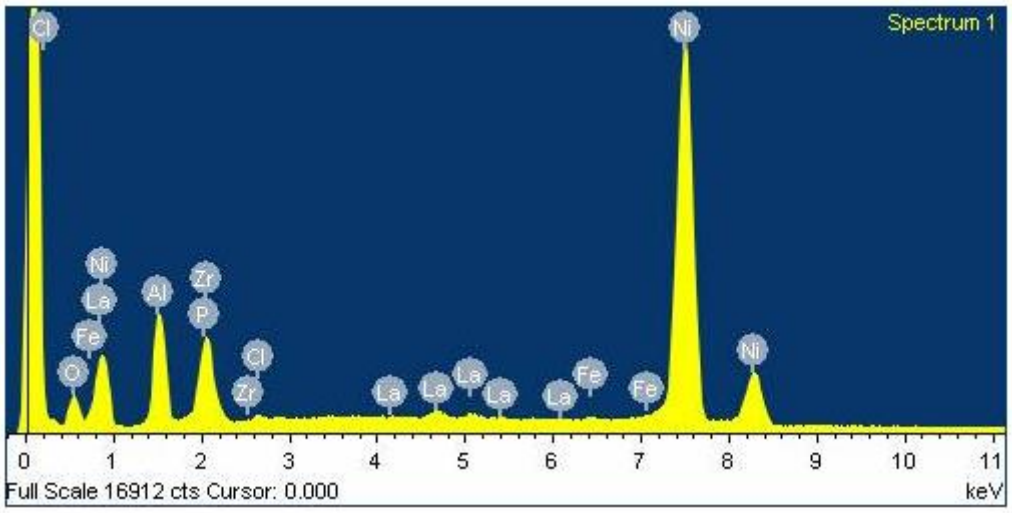

Figure 73 EDX spectrum of electroless nickel coated alumina with LNF and 1µm YSZ bath loading: 2g/150ml LNF, 3g/150ml YSZ

Table 34 *EDXA results of electroless nickel coated alumina with LNF and 1μm YSZ bath loading: 2g/150ml LNF, 3g/150ml YSZ*

Element	Weight%	Atomic%
O	11.18	27.75
Al	13.49	19.85
P	5.26	6.74
Cl	0.41	0.46
Fe	0.23	0.16
Ni	62.44	42.23
Zr	5.38	2.34
La	1.62	0.46
Totals	100.00	100.00

- *3g/150ml LNF, 4g/150ml YSZ*

When the usage of LNF increased from 2g/150ml to 3g/150ml, aluminium was not detected, which meant the surface was adequately covered by the coating. The lanthanum and zirconium contents also increased slightly but the nickel content was still on the high side.

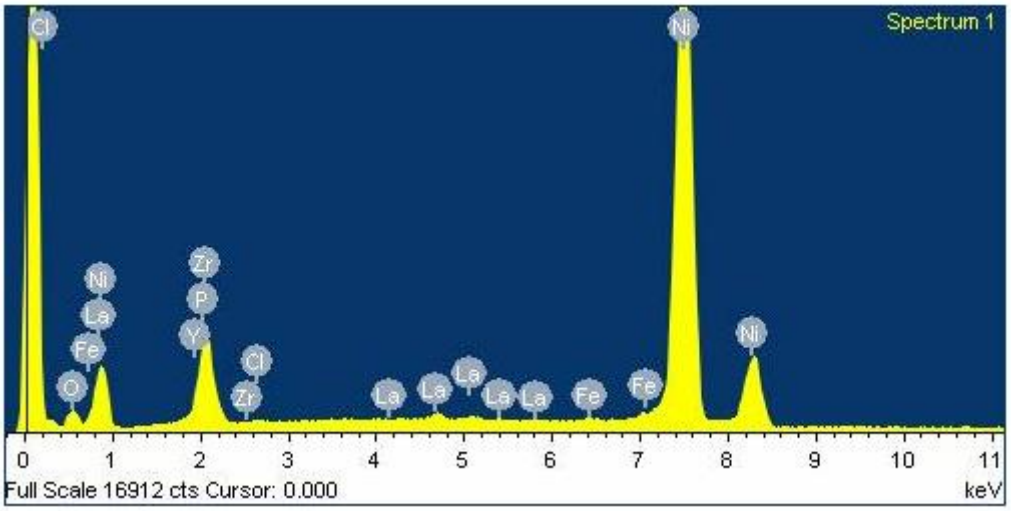

Figure 74 EDX spectrum of electroless nickel coated alumina with LNF and 1µm YSZ bath loading: 3g/150ml LNF, 4g/150ml YSZ

Table 35 EDXA results of electroless nickel coated alumina with LNF and 1µm YSZ bath loading: 3g/150ml LNF, 4g/150ml YSZ

Element	Weight%	Atomic%
O	6.38	20.21
P	3.24	5.30
Cl	0.20	0.28
Fe	0.25	0.23
Ni	78.74	67.99
Y	1.46	0.83
Zr	8.44	4.69
La	1.30	0.47
Totals	100.00	100.00

6.2.2.2.2 2µm YSZ

- *2g/150ml LNF, 3g/150ml YSZ*

Using 2µm YSZ instead of 1µm YSZ, the content of aluminium reduced from 13.49% to only 3.25%. The content of lanthanum and nickel was similar but the zirconium content was doubled.

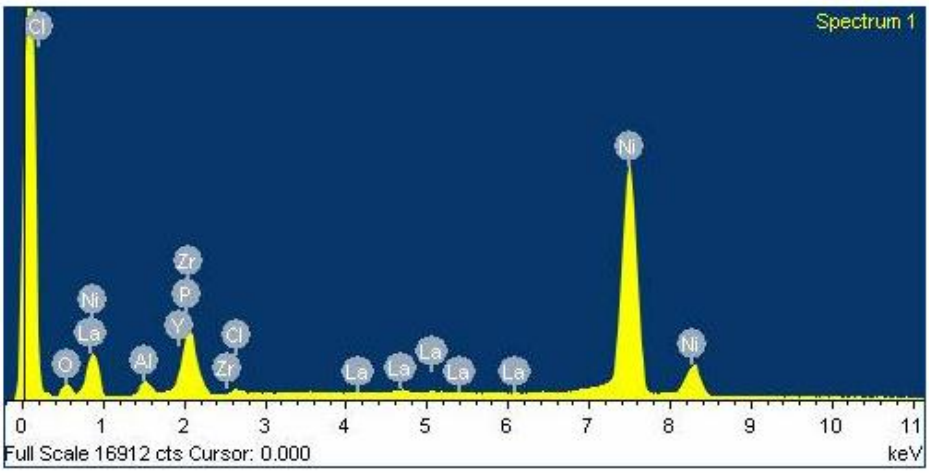

Figure 75 EDX spectrum of electroless nickel coated alumina with LNF and 2µm YSZ bath loading: 2g/150ml LNF, 3g/150ml YSZ

Table 36 EDXA results of electroless nickel coated alumina with LNF and 2µm YSZ bath loading: 2g/150ml LNF, 3g/150ml YSZ

Element	Weight%	Atomic%
O	9.57	27.60
Al	3.25	5.56
P	3.76	5.61
Cl	0.69	0.90
Ni	66.84	52.50
Y	2.46	1.28
Zr	12.11	6.12
La	1.31	0.43
Totals	100.00	100.00

- *3g/150ml LNF, 4g/150ml YSZ*

In this combination, the aluminium content was similarly low compared to the previous bath loading result, which means that the surface was covered pretty well too. Furthermore, the lanthanum content increased from 1.31% to 3.66% and the zirconium content increased greatly from 12.11% to 22.20%; also, the nickel content dropped from 66.84% to 51.65%. Overall, this is a very encouraging co-deposition combination.

Comparing Tables 37 and 35, usage of 2μm YSZ instead 1μm (with the same bath loading) resulted in the lanthanum content increasing from 1.30% to 3.66%, zirconium increasing from 8.44% to 22.20% and the nickel content decreasing from 78.74% to 51.65%. It is clear that the 2μm YSZ does gave much better co-deposition results than the 1μm YSZ.

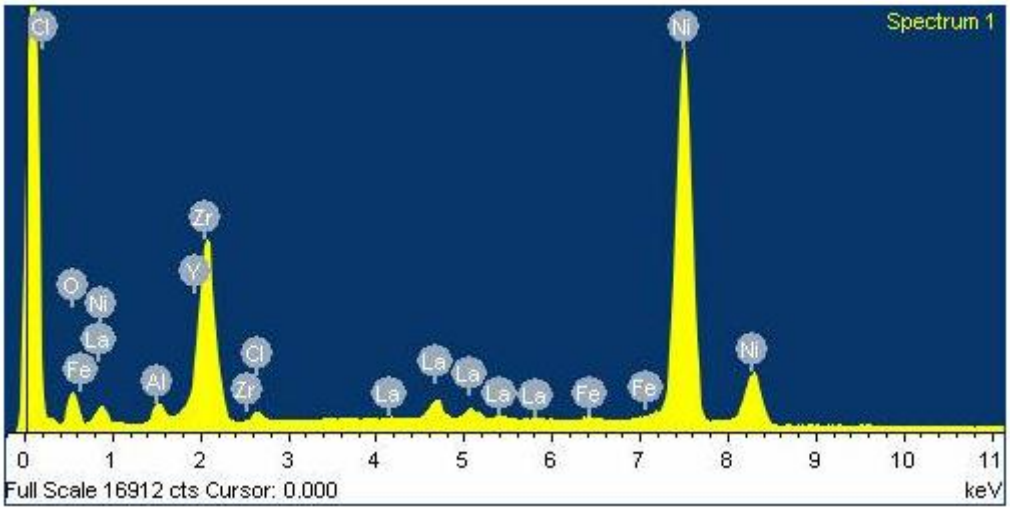

Figure 76 EDX spectrum of electroless nickel coated alumina with LNF and 2μm YSZ bath loading: 3g/150ml LNF, 4g/150ml YSZ

Table 37 EDXA results of electroless nickel coated alumina with LNF and 2μm YSZ bath loading: 3g/150ml LNF, 4g/150ml YSZ

Element	Weight%	Atomic%
O	13.58	39.32
Al	1.71	2.94
Cl	0.81	1.06
Fe	0.31	0.26
Ni	51.65	40.76
Y	6.07	3.16
Zr	22.20	11.28
La	3.66	1.22
Totals	100.00	100.00

6.2.2.2.3 5μm YSZ

- *2g/150ml LNF, 3g/150ml YSZ*

Compared to the 1μm and 2μm YSZ, the 5μm YSZ coating EDXA spectrum revealed similar lanthanum and nickel contents; but the zirconium content increased greatly - from 5.38% and 12.11% to 18.93%.

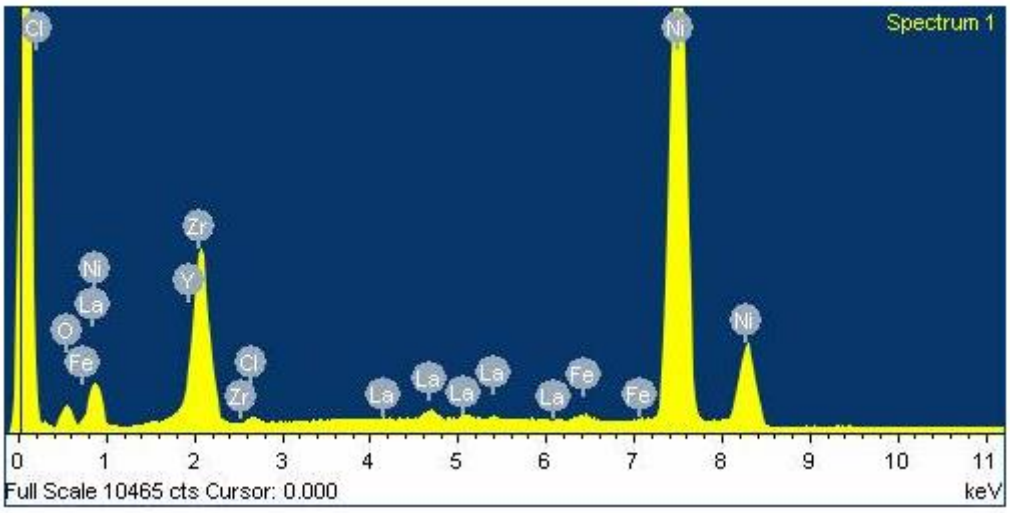

Figure 77 EDX spectrum of electroless nickel coated alumina with LNF and 5µm YSZ bath loading: 2g/150ml LNF, 3g/150ml YSZ

Table 38 EDXA results of electroless nickel coated alumina with LNF and 5µm YSZ bath loading: 2g/150ml LNF, 3g/150ml YSZ

Element	Weight%	Atomic%
O	7.31	24.24
Cl	0.44	0.66
Fe	0.40	0.38
Ni	66.64	60.25
Y	4.91	2.93
Zr	18.93	11.01
La	1.38	0.53
Totals	100.00	100.00

- *3g/150ml LNF, 4g/150ml YSZ*

With this combination, the 5µm YSZ gave an impressive 6.73% lanthanum content, and a very impressive 30.03% zirconium content. In addition, a nickel content of 40.64% revealed that this LNF/YSZ/nickel co-deposition combination is very good.

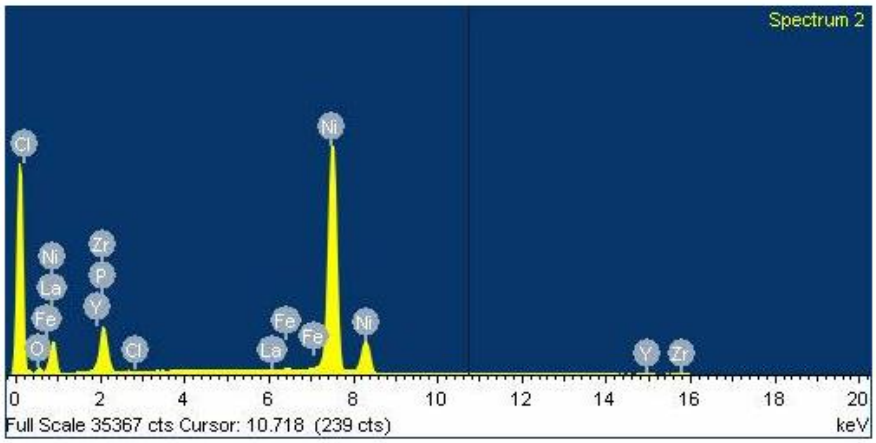

Figure 78 EDX spectrum of electroless nickel coated alumina with LNF and 5µm YSZ bath loading: 3g/150ml LNF, 4g/150ml YSZ

Table 39 *EDXA results of electroless nickel coated alumina with LNF and 5µm YSZ bath loading: 3g/150ml LNF, 4g/150ml YSZ*

Element	Weight%	Atomic%
O	5.99	20.39
Al	7.87	13.83
Cl	0.81	1.24
Fe	3.95	3.85
Ni	40.64	37.69
Y	3.98	2.44
Zr	30.03	17.93
La	6.73	2.64
Totals	100.00	100.00

6.2.2.3 Bath loading

Some plating was carried out using 5µm YSZ powder with LNF using different bath loadings. Again, the other factors remained the same.

6.2.2.3.1 2g/150ml LNF and 3g/150ml YSZ

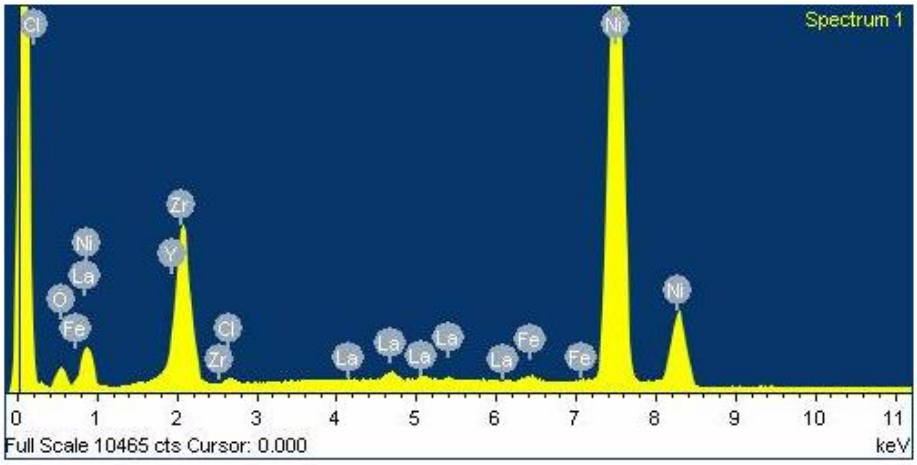

Figure 79 EDX spectrum of electroless nickel coated alumina with 2g/150ml LNF and 3g/150ml YSZ

Table 40EDXA results of electroless nickel coated alumina with 2g/150ml LNF and 3g/150ml YSZ

Element	Weight%	Atomic%
O	7.31	24.24
Cl	0.44	0.66
Fe	0.40	0.38
Ni	66.64	60.25
Y	4.91	2.93
Zr	18.93	11.01
La	1.38	0.53
Totals	100.00	100.00

6.2.2.3.2 3g/150ml LNF and 4g/150ml YSZ

Although there is a little aluminium detected in this sample, the lanthanum, zirconium, and nickel contents were far better than the 2g/150ml LNF and 2g/150ml YSZ sample.

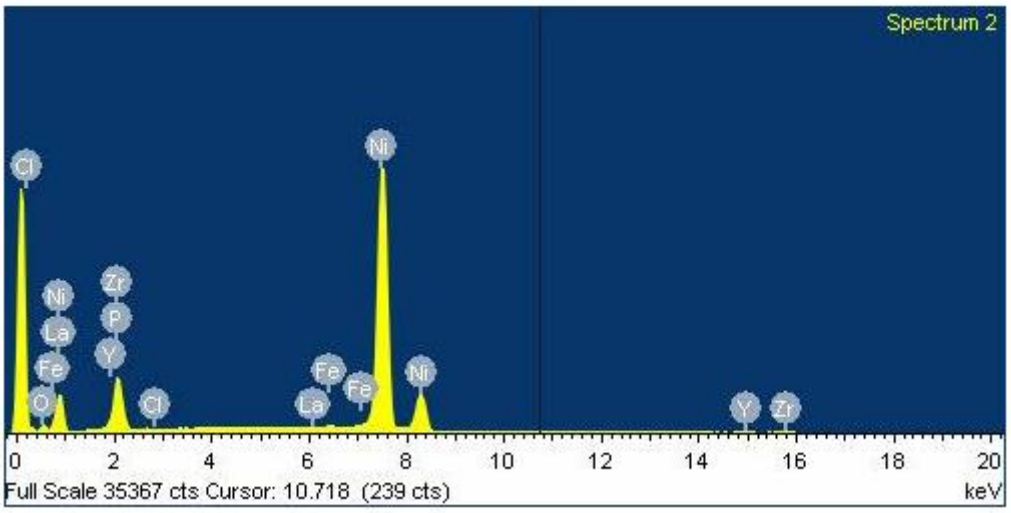

Figure 80 EDX spectrum of electroless nickel coated alumina with 3g/150ml LNF, 4g/150ml YSZ

Table 41 EDXA results of electroless nickel coated alumina with 3g/150ml LNF and 4g/150ml YSZ

Element	Weight%	Atomic%
O	5.99	20.39
Al	7.87	13.83
Cl	0.81	1.24
Fe	3.95	3.85
Ni	40.64	37.69
Y	3.98	2.44
Zr	30.03	17.93
La	6.73	2.64
Totals	100.00	100.00

6.2.2.3.3 4g/150ml LNF and 5g/150ml YSZ

When the bath loading increased from 3g LNF and 4g YSZ per 150ml to 4g LNF and 5g YSZ, the extra ceramic was not reflected in the EDXA components. The lanthanum and zirconium contents were less than before (2.28% to 6.73%, and 16.72% to 30.03% respectively) and the nickel content increased from 40.64% to 58.77%.

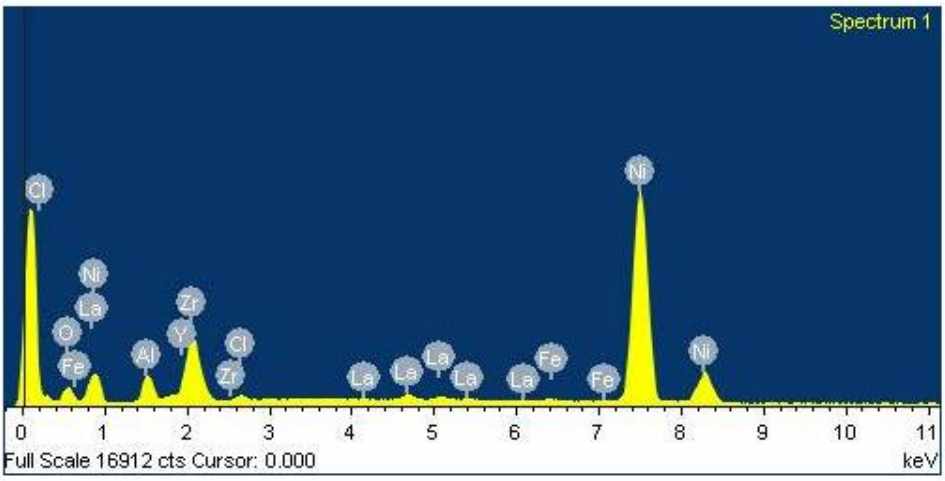

Figure 81 EDX spectrum of electroless nickel coated alumina with 4g/150ml LNF, 5g/150ml YSZ

Table 42 *EDXA results of electroless nickel coated alumina with 4g/150ml LNF and 5g/150ml YSZ*

Element	Weight%	Atomic%
O	11.92	33.77
Al	5.03	8.45
Cl	0.74	0.95
Fe	0.29	0.24
Ni	58.77	45.37
Y	4.25	2.16
Zr	16.72	8.31
La	2.28	0.74
Totals	100.00	100.00

6.2.2.3.4 4g/150ml LNF and 3g/150ml YSZ

This bath loading gave very similar results to the 2g LNF and 3g YSZ one - both were not as good as the 3g LNF and 4g YSZ bath loading result.

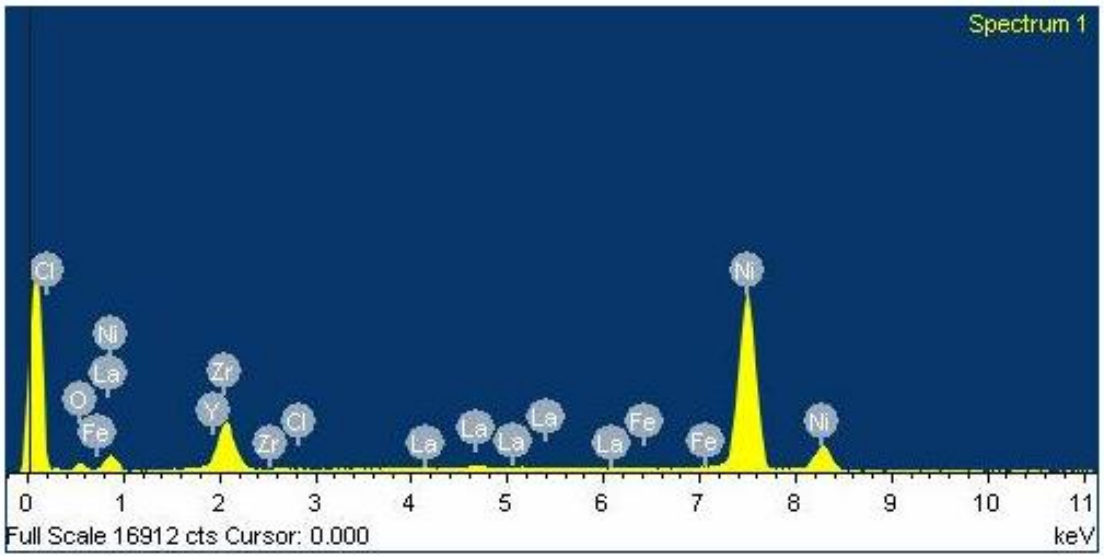

Figure 82 EDX spectrum of electroless nickel coated alumina with 4g/150ml LNF, 3g/150ml YSZ

Table 43 EDXA results of electroless nickel coated alumina with 4g/150ml LNF and 3g/150ml YSZ

Element	Weight%	Atomic%
O	8.43	27.16
Cl	0.33	0.48
Fe	0.32	0.30
Ni	66.83	58.69
Y	5.03	2.92
Zr	17.43	9.85
La	1.63	0.61
Totals	100.00	100.00

6.2.2.3.5 2µm YSZ bath loading tests result

These results can be found in Section 6.2.2.2.2. Some tests with a bath loading of 3g/150ml LNF, 4g/150ml YSZ, and 2g/150ml LNF, 3g/150ml YSZ were carried out separately. The first coating resulted in better elemental components than the second one.

6.2.2.4 Ni pre-coating

In this case, the alumina substrate was pre-coated in the electroless nickel bath for a short time (about 30 seconds) without inclusion of any ceramic powders. A thin layer of pure nickel was thus plated on the alumina, and the LNF/YSZ nickel co-deposition was then coated on to the top of the nickel layer.

6.2.2.4.1 Ni pre-coating with bath loading 3g/150ml LNF and 4g/150ml YSZ

Compared to the same combination but without the nickel pre-coating, the Ni pre-coated sample had much more lanthanum - 18.39% compared to 6.73%. But the content of aluminium was high at 38.75% which made the low nickel content of 18.97% meaningless.

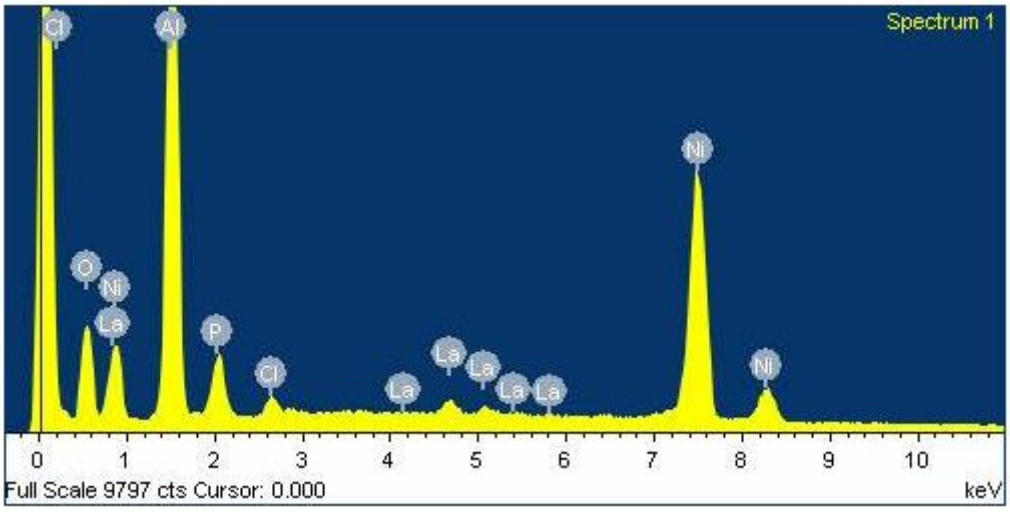

Figure 83 EDX spectrum of electroless nickel coated alumina with LNF and 5µm YSZ bath loading: 3g/150ml LNF, 4g/150ml YSZ (30sec Ni pre-coated)

Table 44 EDXA results of electroless nickel coated alumina with LNF and 5μm YSZ bath loading: 3g/150ml LNF, 4g/150ml YSZ (30sec Ni pre-coated)

Element	Weight%	Atomic%
O	14.44	29.22
Al	38.75	46.49
P	6.89	7.20
Cl	2.57	2.34
Ni	18.97	10.46
La	18.39	4.29
Totals	100.00	100.00

6.2.2.4.2 Ni pre-coating with bath loading 2g/150ml LNF and 3g/150ml YSZ

As above, the nickel pre-coating had a larger lanthanum content (10.94% to 1.38%), a similar zirconium content (17.40% to 18.93%) and the aluminium content was still too high at 15.65%; the Ni content was 31.07%. This coating is not suitable for a SOFC cathode either.

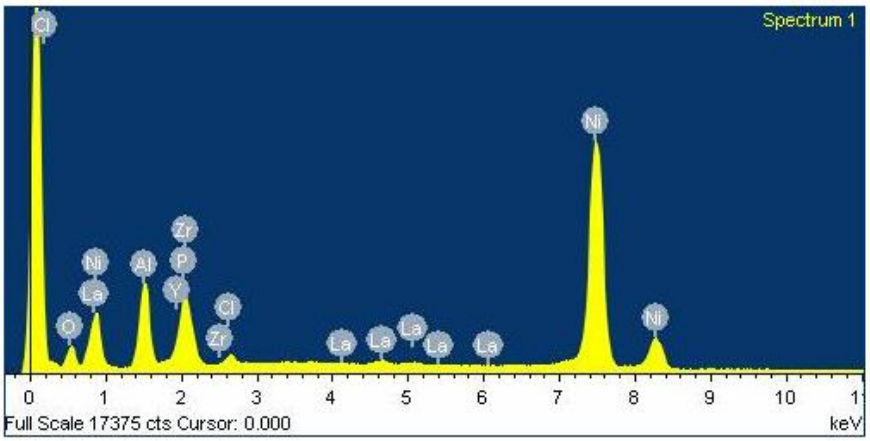

Figure 84 EDX spectrum of electroless nickel coated alumina with LNF and 5μm YSZ bath loading: 2g/150ml LNF, 3g/150ml YSZ (30sec Ni pre-coated)

Table 45 EDXA results of electroless nickel coated alumina with LNF and 5μm YSZ bath loading: 2g/150ml LNF, 3g/150ml YSZ (30sec Ni pre-coated)

Element	Weight%	Atomic%
O	10.02	25.85
Al	15.65	23.93
P	9.18	12.23
Cl	3.40	3.96
Ni	31.07	21.84
Zr	17.40	7.87
La	10.94	3.25
Totals	100.00	100.00

6.2.3 Conclusion of alkaline electroless nickel co-deposition

6.2.3.1 Ni-LSM/YSZ

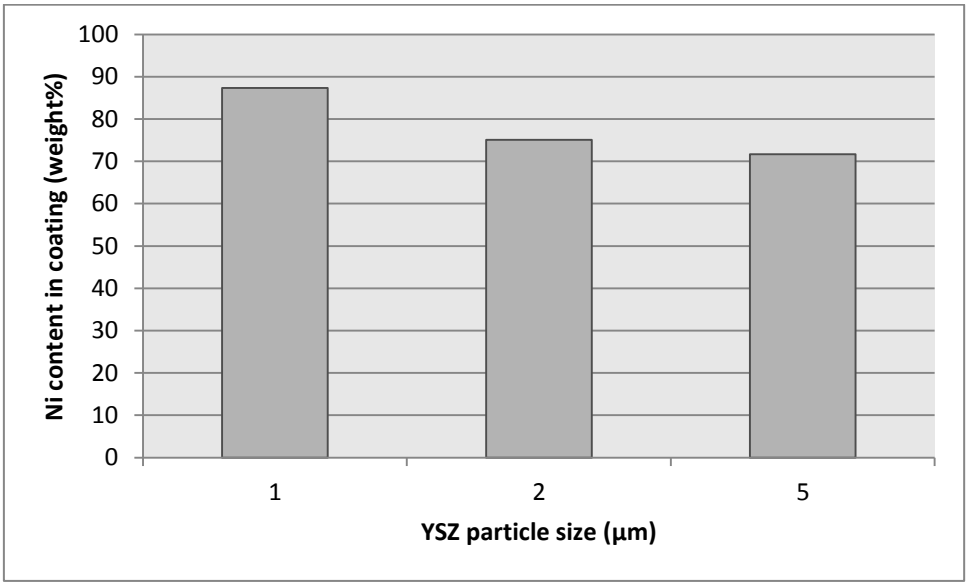

Figure 85 Relationship between Ni content and YSZ particle size (LSM and YSZ in alkaline nickel bath)

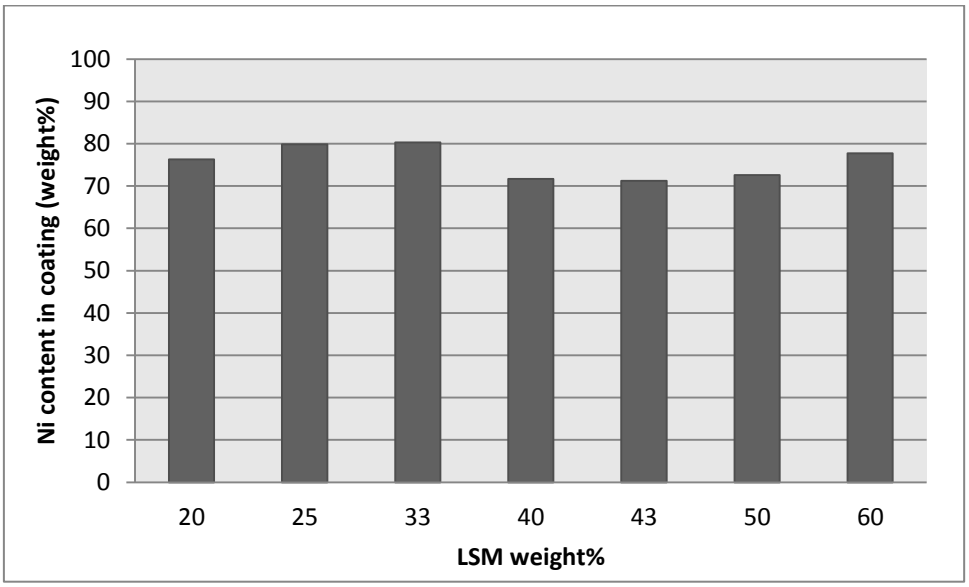

Figure 86 Relationship between Ni content and LSM weigh% in alkaline nickel bath

The results in section 6.2.1 show that, LSM was co-deposited better in an alkaline bath rather than an acidic one. It can be seen that the coating thickness slightly increased with the larger particle size of YSZ used (Figure 85). The bath loading did not seem to affect the thickness too much (Figure 86). But it is clearly shown that the increased LSM content (6.2.1.2.7) coincided with a poor coating surface.

A 5μm YSZ particle size gave a lower nickel content in the co-deposited plating than the other two smaller YSZ particle sizes. Figure 81 shows the nickel content of the EDXA results in the different co-deposition conditions discussed above with 40-50% of the 40-50% of LSM/(LSM+YSZ) ratio giving the best (lowest) nickel content. This corresponds to 2g/150ml LSM / 3g/150ml YSZ and 3g/150ml LSM / 4g/150ml YSZ.

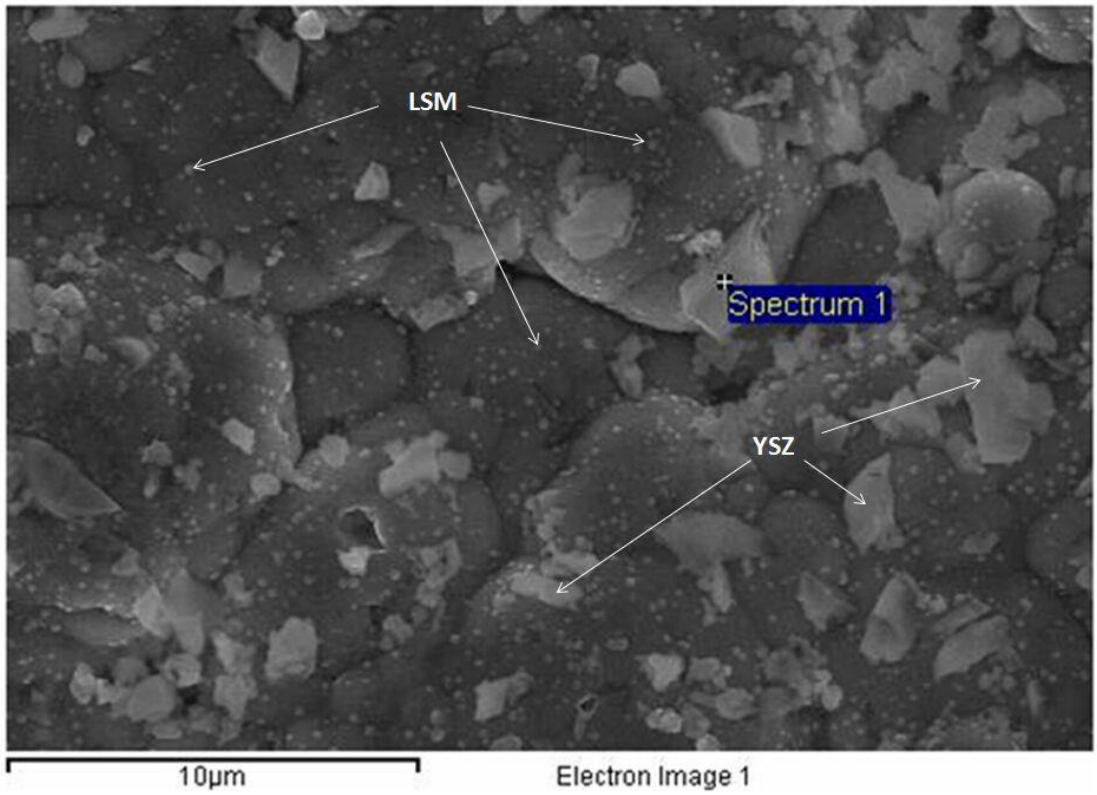

Figure 87 SEM image of alkaline electroless LSM/YSZ co-deposition with LSM and 5μm YSZ bath loading: 2g/150ml LSM, 3g/150ml YSZ

The surface of the LSM/YSZ co-deposition is shown in Figure 87. It clearly can be seen that the LSM and YSZ particles are successfully co-deposited onto the substrate. Because the nickel content is more than 70% in this alkaline electroless nickel

co-deposition with LSM/YSZ ceramic powders, the particles in Figure 82 are not copious; the most part of the surface is covered by nickel. The larger particles are 5μm YSZs and much smaller particles are the 1μm LSMs.

6.2.3.2 Ni-LNF/YSZ

The 6.2.2 results showed that the LNF could be co-deposited with YSZ in an alkaline environment. The thickness tests showed that the thickness for this deposit was about 5μm in a 1 hour plating time and that thickness was hardly affected by other factors.

The results in section 6.2.2.2 showed that, the nickel content of 5μm YSZ coating was much better than the other two smaller particle sizes (Figure 88). Furthermore, the bath loading results showed that the best combination was 3g/150ml LNF and 4g/150ml YSZ (43% LNF weigh percent). The results are shown in Figure 89 (based on 5μm YSZ). At the same time, the 2μm YSZ results support the 5μm YSZ results (by 51.65% of 3g/150ml LNF and 4g/150ml YSZ vs. 66.84% of 2g/150ml LNF and 3g/150ml YSZ).

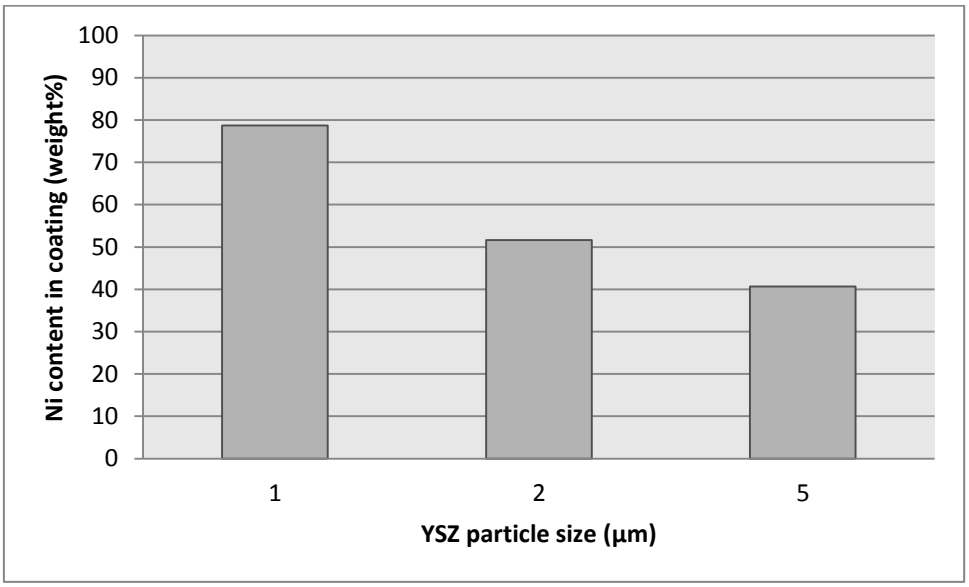

Figure 88 Relationship between Ni content and YSZ particle size (LNF and YSZ in alkaline nickel bath)

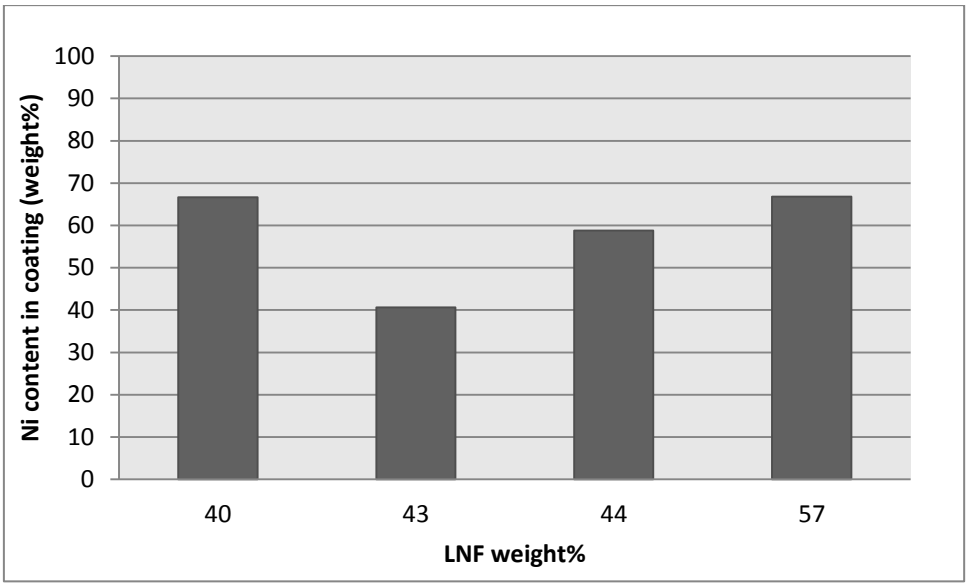

Figure 89 The relationship between the content of nickel and the LNF ratio

The nickel pre-coating tests showed that it did not help with the nickel content in the final coating; instead, it revealed an aluminium content – bad because the substrate was not fully covered by the co-deposition and the alumina was exposed at the surface.

Figure 90 shows an SEM image of the LNF/YSZ co-deposition surface. With the nickel content in the co-deposition of 40%-50%, it can be seen that the surface is covered by the LNF/YSZ ceramic powders very well (compared to figure87) and again the larger particles are YSZs and the smaller ones are LNFs.

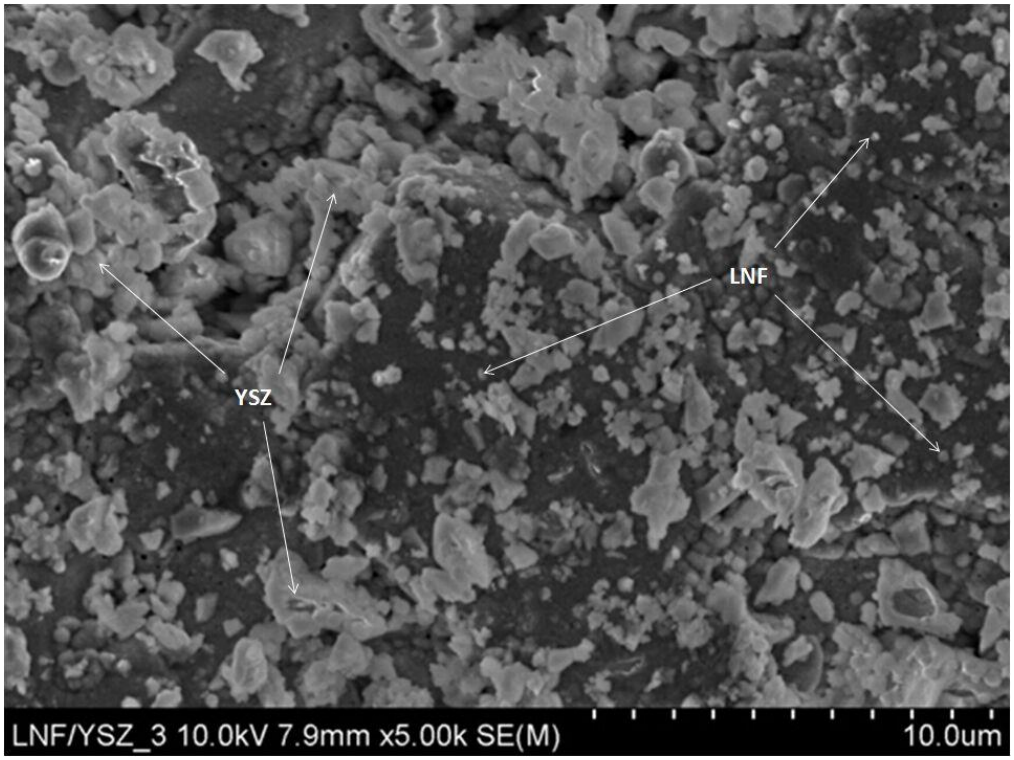

Figure 90 SEM image of alkaline electroless LNF/YSZ co-deposition with LNF and 5μm YSZ bath loading: 3g/150ml LNF, 4g/150ml YSZ

6.3 Electrical testing

6.3.1 Open circuit voltage (OCV) test

As mentioned in the experimental section, a single solid oxide fuel cell was manufactured by conventional screen printing and sintering (anode) and novel electroless co-deposited (cathode) onto an YSZ electrolyte in a button cell configuration. When the cell was heated up to 600°C, the open circuit voltage (OCV) increased from 0.4V to 0.7V. After the cell was heated up to 700°C, OCV was stable, and the highest OCV being tested was 0.856V (with 1.5L/min dry hydrogen flow rate). It was found that the OCV increased with the operation time in this test. This is because the NiO in the anode and current collector was reduced to Ni, by the H_2. This creates some porosity in the cathode, which helps the oxygen through. And some particle agglomeration may happen at the same time [116]. So some preliminary time should be carried out on the cell before the performance was tested. It is well known that the preliminary loading could reduce the internal resistance of cell, and bring

voltage recovery, and increase the cell performance [117]. Weber et al. [118] also reported that the cathode microstructure at the cathode electrolyte interface was altered at the preliminary loading process by using a LSM/YSZ/Ni-YSZ cell. The preliminary time for LNF cathode can take up to a week, and the current density can be in the range of 0.3-1 A/cm^2 [88]. The figure below shows the fuel cell having an increasing OCV from the beginning of 0.818 to 0.826 in one minute. These increasing OCVs show the same situation and performance of the cell might well improve after more than a hundred hours operation time

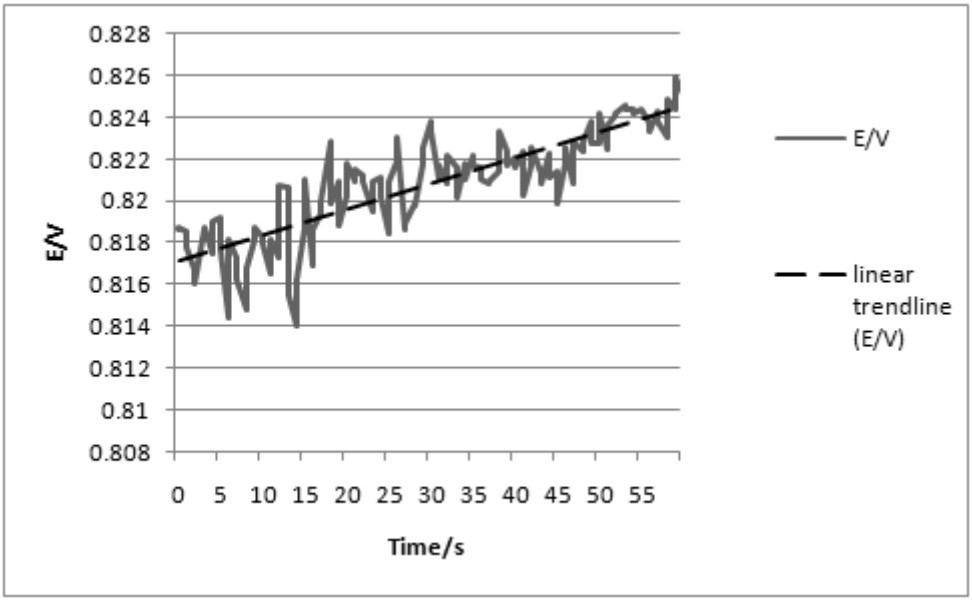

Figure 91 Results of open circuit voltage vs time

6.3.2 IV test

The IV test of the cell was carried out at 700°C - each step of the current was held for 5 mins, and then the average value was taken. With a high hydrogen flow rate of 1.5L/min, the cell gave an OCV of 0.856V, which should decrease as the current increases. In figure 92, square dots are voltage values to the left axis and triangle dots are current density to the right axis. As can be seen, the voltage has a slight trend of decrease with the increase of current density. At the largest current density in this test, 200mA • cm^{-2}, the power density is about 170 mW • cm^{-2}. The power density should increase to a maximum and then fall away along with decreasing voltage. In this case, the results show only the first stage of the whole process, and the maximum power

density is beyond this graph. The impedance analyser could not load a large enough current density to yield the power density to a maximum value. Also in this case, the voltage decreased very slowly beside the first stage reason, this is partly affected by the voltage coverage brought by increasing operation time, which was discussed before.

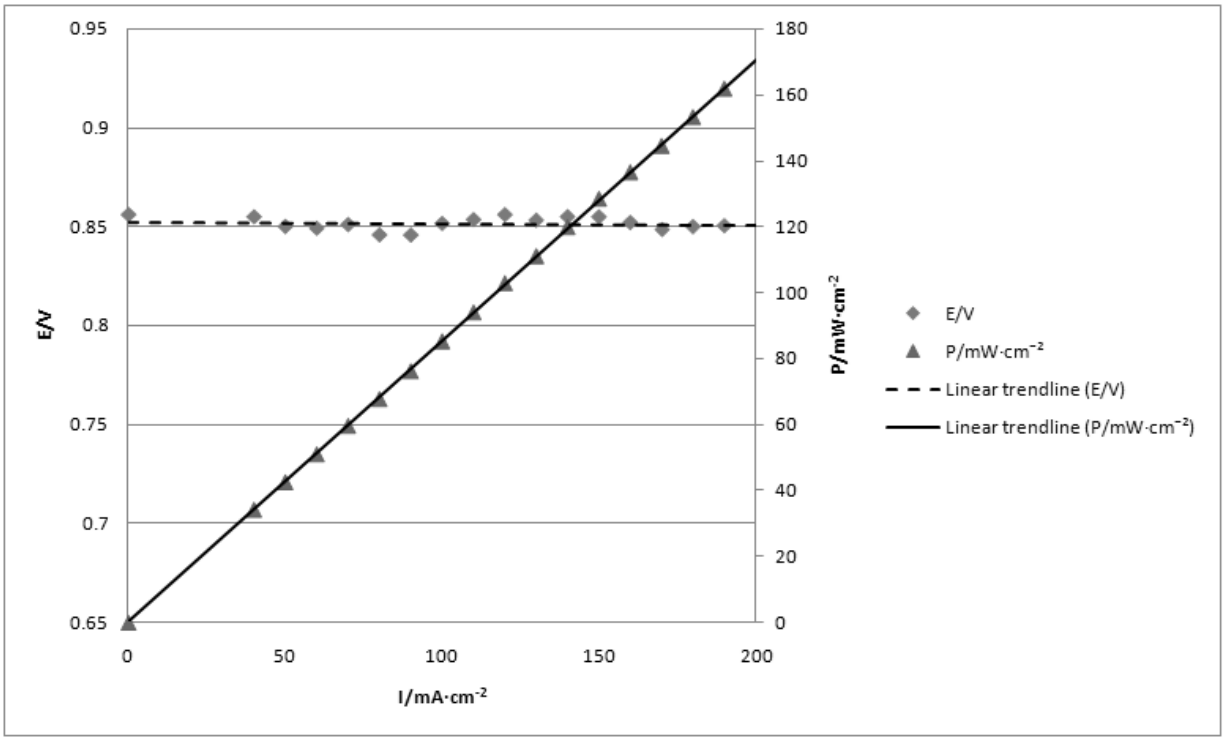

Figure 92 The IV curve of test with 1.5L/min hydrogen flow rate at 700°C

6.3.3 Conclusion of Electrical testing

The results show that the OCV increases as long as the SOFC operation time, and the highest OCV being tested was 0.856V (with 1.5L/min dry hydrogen flow rate at 700°C, which is reasonable for an intermediate temperature SOFC.

The IV test shows that the voltage decreased very slowly since the OCV of 0.856V. It is because the voltage was still increasing during the stabilisation period. With the capable maximum current density 200mA • cm^{-2}, the power density was about 170

mW • cm^{-2}, the power density is very linear because of the slowing linearly decreasing voltage.

Impedance testing of the cell was not a fundamental aim of this thesis. It was to demonstrate whether or not cathodes for tubular SOFCs could be manufactured, using LNF, by the novel electroless co-deposition process. However, it is strongly recommended that future work be carried out in this area.

7. Conclusions

High temperature traditional SOFC manufacturing techniques are expensive and limited the SOFC commercialisation, but more importantly, some material (for example LNF) is not suitable for any high temperature manufacturing process due to its degradation. In this research, a low temperature, low cost manufacturing technique, nickel co-deposition with ceramic powders, which are solid oxide fuel cell materials, has been successfully carried out. In addition, electroless nickel co-deposition with ceramic powder to make an SOFC cell was found to produce electrical power.

Pure LSM could not be co-deposited in the acid electroless nickel bath as easy as YSZ. However, it was found that YSZ particles could apply good bonding between the coating and the substrate. So with the present of YSZ, an LSM/YSZ powder combination was successfully deposited onto a ceramic substrate. In the acid condition, co-deposition with LSM and 2μm YSZ or 5μm YSZ powder onto the ceramic electrolyte gave lower nickel content in the co-deposition than the 1μm YSZ. Also the 5μm YSZ gave the best thickness. But all three particle size YSZ could not get a usable co-deposition with reasonable nickel content.

It was clear that LSM was more efficiently co-deposited in the alkaline electroless nickel solution. Similar to the acid condition, the 5μm YSZ gave good nickel content and thickness in the all three YSZ particles. The increasing usage of LSM in the bath load made the coating discontinuous and increased the nickel content. The best combination was found that 40%-50% LSM weigh percent will provide the best co-deposition component; though the nickel content was still too high for a SOFC cathode use.

After the best combination of coating conditions was established, the highly promising material - lanthanum nickel ferrite (LNF) - was brought in and replaced the conventional LSM. The alkaline electroless nickel co-deposition tests with LNF/YSZ proved to be very promising. A good co-deposition with less than 50% of nickel was achieved with 5μm YSZ and bath load of 3g/150ml LNF and 4g/150ml YSZ. Though the thickness was only 5μm, which is too thin for an anode-supported SOFC but

adequate for an electrolyte-supported cell. The SEM image shows that the ceramic substrate was well covered by the LNF/YSZ nickel co-deposition.

Some electrical tests were carried out to test the cell with a screen printed YSZ/NiO anode and electroless nickel co-deposited LNF/YSZ cathode onto an YSZ electrolyte. The cell exhibited a satisfactory performance as a working SOFC device. IV tests and OCVs tests were carried out successfully. The OCV was tested as 0.856V at 700°C, and the highest power density was about 170 mW • cm^{-2} when the current density was 200mA • cm^{-2}

This important success shows that the lanthanum nickel ferrite (LNF) – which degrades using conventional high temperature processing – can be deposited using a low temperature technique without degradation. The SOFC with an electroless nickel co-deposited LNF/YSZ cathode works good.

8. Future Work

Although the cell is shown to work, there is some future work needed to be carried out. For an anode-supported cell, the thickness of the cathode should be no less than 30μm. But the thickness achieved in this research with LNF was only 5μm. For example, a surfactant could be an option to help with the co-deposition rate. Furthermore, because the 5μm YSZ is the largest size in this research, and it gives the best thickness, some larger size combinations of YSZ and LNF powder may be helpful. An increase of the thickness might improve the properties of the deposition. Some impedance test could be carried out to the cell, and the half-cell. Also according to LNF cathode SOFCs needing a preliminary stabilisation period to get good performance, some electrical test and impedance test could be carried out after a long operation time of the LNF cathode SOFC.

9. Contribution to Knowledge

In the tubular solid oxide fuel cell (SOFC) manufacturing field, electroless nickel co-deposition of cathodes with ceramic powders in both acid and alkaline solutions is a novel technology. This co-deposition concept was presented by William Waugh in 2009 and Nor Bahiyah Babaa in 2010, but these investigations were on planar SOFCs. Similarly Nkem Nwosu (2013) co-deposited planar cathodes using lanthanum strontium manganite (LSM). But there have been no studies working on co-deposited cathode and lanthanum nickel ferrite (LNF).

The LNF is a promising material for SOFC cathode in intermediate temperature SOFC (IT-SOFC). To the candidate's knowledge, no research has been found using LNF cathodes and manufactured by electroless nickel co-deposition technology. In this research, LNF was electroless nickel co-deposited onto both alumina and yttria-stabilised zirconia (YSZ) substrates in an alkaline nickel bath with the presence of YSZ ceramic powder. The EDXA tests proved a layer of LNF/YSZ and nickel co-deposition has been successfully produced. The content of nickel is at a very good level; in terms of having enough to provide electronic conductivity yet not too much that would cause an excessive mis-match of coefficient of thermal expansion. The electrical tests demonstrated that a working cell was built with co-deposited LNF/YSZ cathode.

The success achieved in this thesis suggests that this low-cost electroless nickel co-deposition technique may be widely applied in SOFC manufacturing once the technique is refined.

10. References

1. United States. (2002) *Annual energy review 2001*, Washington, D.C.: U.S. Department of Energy.
2. Jay, L., Dimitri, C. and Scott, S. (2002) *Climate of 2001 - Annual Review Significant U.S. and Global Events,* Asheville, NC: NOAA's National Climatic Data Center.
3. Energy Information Agency (EIA), [online]October 2001
4. Grove,W.R. (1839) 'On Voltaic Series and the Combination of Gases by Platinum'. The London and Edinburgh Philosophical Magazine and Journal of Science v.14(86), pp. 127-130
5. Grove, W. R. (1837) 'Experiments on the Gas Voltaic Battery, with a View of Ascertaining the Rationale of Its Action, and on Its Application to Eudiometry'. Proceedings of the Royal Society of London v.4, pp.463-463.
6. Nerst W. Z. (1899). Über die elektrolytische Leitung fester Körper bei sehr hohen Temperaturen. Zeitschrift Für Elektrochemieb v. 6 (2), pp.41-43.
7. Mond, L. and Langer, C. (1889) 'A new form of gas battery'. Proc. R. Soc. London v.46, pp.296-304
8. Sopian, K. and Daud, W. (2006) 'Challenges and future developments in proton exchange membrane fuel cells'. Renewable Energy 31 (5), pp.719-727
9. Stambouli,A.B. and Traversa,E. (2002) 'Solid oxide fuel cells (SOFCs): a review of an environmentally clean and efficient source of energy'. Renewable and Sustainable Energy Reviews 6, pp433–455
10. Möbius, H.-H. (1997) 'On the history of solid electrolyte fuel cells'. Journal of Solid State Electrochemistry: Current Research and Development in Science and Technology 1(1), pp.2-16.
11. Baur, E. and Preis, H. Z. (1937) 'Fuel cells with rigid conductors'. Z. Elektrochem v.43, pp. 727–732.
12. Gerven, van. R. J. F., and van der Veer, J.H.C. (1998) *Fuel Cell Seminar*, USA: Palm Springs..
13. Yamamoto, O. (2000) 'Solid oxide fuel cells: fundamental aspects and prospects'. Electrochimica Acta v. 45, pp. 2423–2435

14. Li, J. (2007) ‘Solid oxide fuel cells: development status and key technologies’, Journal of functional materials and devices *v.*13 (6), pp. 683-687.
15. Tietz, F., Buchkremer, H.-P. and Stover, D. (2002) ‘Components manufacturing for solid oxide fuel cells’. Solid State Ionics v.152 (1), pp. 373-381
16. Minh, N. Q. (2004) ‘Solid oxide fuel cell technology — features and applications’. Solid State Ionics v. 174, pp. 271-277.
17. Kendall, K., Minh, N. Q. and Singhal, S.C. (2003) ‘Cell and stack designs’, in Singhal, S.C. and Kendall, K. (Ed.), *High Temperature Solid Oxide Fuel Cells: Fundamentals, Design and Applications,* Burlington: Elsevier
18. Singhal,S.C. (2000) ‘Science and Technology of Solid-Oxide Fuel Cells’. MRS Bulletin V.25(3), pp. 16-21.
19. Pal, U. B. and Singhal, S. C. (1990) ‘Electrochemical Vapour Deposition of Yttria‐Stabilized Zirconia Films’. J. Electrochem. Soc. 137(9), pp. 2937-2941
20. KUO, L. J. H., VORA, S. D. and SINGHAL, S. C. (1997), ‘ChemInform Abstract: Plasma Spraying of Lanthanum Chromite Films for Solid Oxide Fuel Cell Interconnection Application’. ChemInform v. 28(25), pp. 248-250
21. Singhal, S. C. (1999) ‘Progress in Tubular Solid Oxide Fuel Cell Technology’, in Singhal, S. C. and Dokiya, M.(ed.) *Solid oxide fuel cells: (SOFC VI) : proceedings of the Sixth International Symposium*. Pennington, NJ: Electrochemical Society
22. Takeuchi, H., Nishiyama, H. and Ueno, A. (1999) ‘Current Status of SOFC Development by Wet Process’, in Singhal, S. C. and Dokiya, M.(ed.) *Solid oxide fuel cells: (SOFC VI) : proceedings of the Sixth International Symposium*. Pennington, NJ: Electrochemical Society
23. Aizawa, M., Kuroishi, M. and Ueno,A.(1997) ‘Performance of a tubular SOFC with thin YSZ film at medium temperatures’, in Stimming, U. Singhal, S.C. and Tagawa, H. (ed.). *Proceedings of the Fifth International Symposium on Solid Oxide Fuel Cells (SOFC-V).* Pennington, NJ: Electrochemical Society.
24. Kaneko,S., Gengo, T. and Uchida, S. (1991) *Proc. 2nd Int. Symp. Solid Oxide Fuel Cells (SOFC-II)*, Brussels: The European

25. Mori, H., Omura, H. and Hisatome, N.(1999) ‘Pressurized 10 kW Class Module of SOFC’, in Singhal, S. C. and Dokiya, M.(ed.) *Solid oxide fuel cells: (SOFC VI) : proceedings of the Sixth International Symposium*. Pennington, NJ: Electrochemical Society
26. Kakigani, S., Kurihara, T. and Hisatome, N.(1997) ‘Development of SOFC module’, in Stimming, U. Singhal, S.C. and Tagawa, H. (ed.). *Proceedings of the Fifth International Symposium on Solid Oxide Fuel Cells (SOFC-V).* Pennington, NJ: Electrochemical Society.
27. Vincenzini, P. (ed.) (1998). I*nnovative materials in advanced energy technologies: Proceedings of Topical Symposium VII - "Innovative Materials in Advanced Energy Technologies" of the Forum on New Materials of the 9th CIMTEC-World Ceramics Congress and Forum on New Materials*, Florence, Italy: Techna.
28. Gardner, F. J., Day, M. J. and Brandon, N. P. (2000) ‘SOFC technology development at Rolls-Royce’. Journal of Power Sources, v.86, pp. 122-129.
29. Minh, N. Q. (1993), ‘Ceramic Fuel Cells’. Journal of the American Ceramic Society, v. 76, pp. 563–588.
30. Singhal, S. C. and Kendall, K. (2003). *High-temperature Solid Oxide Fuel Cells: Fundamentals, Design and Applications*. Burlington: Elsevier.
31. Anderson, H. U., Kuo, J. H. and Sparlin,D.M. (1989) ‘Review of Defect Chemistry of $LaMnO_3$ and $LaCrO_3$’, in: Singhal, S. C. (ed.) Proceedings of the First International Symposium on Solid Oxide Fuel Cells, Pennington, N.J. (10 S. Main St., Pennington 08534-2896: Electrochemical Society.
32. Yamamoto, O. (1987). ‘Perovskite-type oxides as oxygen electrodes for high temperature oxide fuel cells’. Solid State Ionics v.22, pp. 241-246.
33. Lau, S. K. and Singhal, S. C. (1985) ‘Potential electrode / electrolyte interactions in solid oxide fuel cells’, Corrosion v. 85, pp.1-9
34. Yamamoto,O., Takeda,Y. and Kanno, R. (1989) ‘in proceedings of the first international symposium on Solid Oxide Fuel Cells’, in Singhal, S. C.(ed.) The Electrochemical Society, Pennington, NJ.
35. Fuel cell materials by Nextech materials. August 2001.

36. Bard, A. J. and Faulkner, L. R. (2001) *electrochemical methods: fundamentals andapplications,* 2nd edition, New York: Wiley.
37. Tsujimura, S., Wadano, A. and Kano, K. (2001) 'Photosynthetic bio electrochemical cell utilizing cyanobacteria and water-generating oxidase'. Enz. Microb.Technol. v.29, pp. 225–231.
38. Li, J.L., Wang, S.R. and Wang, Z.R.(2006) 'Effect of the cathode structure on the electrochemical performance of anode-supported solid oxide fuel cells'. Journal Of Solid State Electrochemistry v.14(4), pp. 579-583
39. Montinaro, D., Sglavo, V.M. and Bertoldi, M. (2006) 'Tape casting fabrication and co-sintering of solid oxide "half cells" with a cathode–electrolyte porous interface'. Solid State Ionics v.177(19), pp. 2093-2097
40. Appleton, W. and Pira International. (1994). *Screen printing: A literature review.* Leatherhead, England: Pira International.
41. Kurten, R. A. (1992) 'Advantages and disadvantages of screen printing over other printing processes', Siebdruck *v.*38(4), pp.120-122
42. Noteboom, E. (1992) 'Screen printing: where did it all begin?'. Screen Print v.82(10), pp. 52-56
43. Wang, Z.R., Qian, J.Q. and Cao, J.D. (2007) 'A study of multilayer tape casting method for anode-supported planar type solid oxide fuel cells (SOFCs)'. Journal of Alloys and Compounds v.437, pp.264-268
44. Zhou, X.L., Sun, K.N. and Gao, J. (2009) 'Microstructure and electrochemical characterization of solid oxide fuel cells fabricated by co-tape casting'. *Journal Of Power Sources,* v.191(2), pp. 528-533
45. Mistler, R. E. and Twiname, E. R. (2000). *Tape casting: Theory and practice.* Westerville, OH: American Ceramic Society.
46. Howatt, G. N., Breckenridge, R. G. and Brownlow, J. M. (1947) 'Fabrication of thin ceramic sheets for capacitors'. Journal of the American Ceramic Society v.30 (8), pp. 237-242.
47. Park, J. L. Jr. (1961) 'Manufacture of Ceramics', U.S. Patent 2,966,719.
48. Howatt, G. N. (1952) 'Method of producing High Dielectric High Insulation Ceramic Plate', U.S. Patent 2,582993.

49. Malghan, S.G. (1991) ‘Characterization of Ceramic Powders’, in Schneider, S. J. (ed.) *Engineered Materials Handbook*, *Ceramics and Glasses.* Newbury: OH
50. Shanefield, D. J. (1995) *Organic Additives and Ceramic Processing,* Boston: Kluwer Academic Publishers.
51. Boch, P. and Chartier, T. (1991) ‘Tape casting and Properties of Mullite and Zirconia- Mullite Ceramics’, *J. Am. Ceram. Soc.* V.74(10), pp. 2448-2452
52. Horn, R. G. (1995) ‘Particle Interactions in Suspensions’, in Terpstra,R. A., Pex, P. P. A. C. and DeVries, A. H.(ed.) *Ceramic Processing,* London: Chapman & Hall.
53. Chartier, T. and Bruneau, A. (1993) ‘Aqueous Tape Casting of Alumina Substrates’, J. Eur. Ceram. Soc. v.12, pp. 243-247
54. Hayashi, T. (1991) *Surface Chemistry of Ceramic Shaping Processes*, *Annual Report for Overseas Readers,* Japan Fine Ceramic Association
55. Han, M. F., Tang, X. L. and Yin, H.Y. (2007) ‘Fabrication, microstructure and properties of an YSZ electrolyte for SOFCs’. Journal of Power Sources v.165(2), pp.757-763
56. ZHOU, W., SHI, H., and RAN, R. (2008) ‘Fabrication of an anode-supported yttria-stabilized zirconia thin film for solid-oxide fuel cells via wet powder spraying’. Journal of Power Sources v.184 (1), pp. 229-237.
57. LI, C., LI, C. and XING, Y. (2006) ‘Influence of YSZ electrolyte thickness on the characteristics of plasma-sprayed cermet supported tubular SOFC’. Solid State Ionics v.177, pp. 2065-2069.
58. Shi, H., Ran, R. and Shao, Z. (2012) ‘ Wet powder spraying fabrication and performance optimization of IT-SOFCs with thin-film ScSZ electrolyte’. International Journal of Hydrogen Energy v.37 (1), pp. 1125-1132.
59. Choy, K.L. (2003) ‘Chemical vapour deposition of coatings’. Progress in Materials Science v.48, pp. 57–170
60. Do, T. C., Pucci, A., & Wandelt, K. (2009). *Physics and engineering of new materials*. Berlin: Springer.

61. Meng, G., Song, H. and Dong, Q. (2004) ‘Application of novel aerosol-assisted chemical vapour deposition techniques for SOFC thin films’. Solid State Ionics v.175, pp.29-34.
62. Schlupp, M. V. F., Kurlov, A. and Hwang, J. (2013) ‘Gadolinia Doped Ceria Thin Films Prepared by Aerosol Assisted Chemical Vapour Deposition and Applications in Intermediate-Temperature Solid Oxide Fuel Cells’. Fuel Cells v.13, pp. 658–665.
63. Bobrenok, O. F. and Predtechenskii, M. R. (2010) ‘Solid oxide fuel cells with film electrolytes prepared by chemical vapour deposition’. Russian Journal of Electrochemistry v.46 (7), pp. 798-804.
64. Meng, B., He, X. and Sun, Y. (2008) ‘Preparation of YSZ electrolyte coatings for SOFC by electron beam physical vapour deposition combined with a sol infiltration treatment’. Materials Science and Engineering: B v.150 (2), pp.83-88.
65. Gannon, P., Deibert, M. and White, P. (2008) ‘Advanced PVD protective coatings for SOFC interconnects’. International Journal of Hydrogen Energy v. 33(14), pp.3991-4000.
66. He, X., Meng, B. and Sun, Y. (2008) ‘Electron beam physical vapour deposition of YSZ electrolyte coatings for SOFCs’. Applied Surface Science v.254(22), pp.7159-7164.
67. Heiroth, S., Frison, R. and Rupp, J. L. M. (2011) ‘Crystallization and grain growth characteristics of yttria-stabilized zirconia thin films grown by pulsed laser deposition’. Solid State Ionics v.191 (1), pp. 12-23.
68. Stöver, D., Hathiramani, D. and Vaßen, R. (2006) ‘Plasma_sprayed components for SOFC applications’. Surface and Coatings Technology v.201 (5), pp. 2002-2005.
69. White, B., Kesler, O. and Rose, L. (2008) ‘Air plasma spray processing and electrochemical characterization of SOFC composite cathodes’. Journal of Power Sources v.178 (1), pp.334-343.
70. White,B., Kesler, O. and Rose, L. (2007) ‘Electrochemical Characterization of Air Plasma Sprayed LSM/YSZ Composite Cathodes on Metallic Interconnects

Cathode Materials, Processing, and Performance'. *ECS Transactions* v.7 (1), pp.1107-1114

71. Besra, L. and Liu, M. (2007) 'A review on fundamentals and applications of electrophoretic deposition (EPD)'. Progress in Materials Science v.52 (1), pp.1-61.
72. Matsuda, M., Hosomia, T. and Murata, K. (2007) 'Fabrication of bilayered YSZ/SDC electrolyte film by electrophoretic deposition for reduced-temperature operating anode-supported SOFC'. Journal of Power Sources v.165 (1), pp. 102-107.
73. Santillán, M. J., Caneiro, A. and Quaranta, N. (2009) 'Electrophoretic deposition of $La_{0.6}Sr_{0.4}Co_{0.8}Fe_{0.2}O_{3-\delta}$ cathodes on $Ce_{0.9}Gd_{0.1}O_{1.95}$ substrates for intermediate temperature solid oxide fuel cell (IT-SOFC)'. Journal of the European Ceramic Society v.29 (6), pp. 1125-1132.
74. Gilissen, R., Erauw, J. and Smolders, A., (2000) 'Gelcasting, a near net shape technique'. Materials and Design v.21 (4), pp. 251-257.
75. Dong, D., Gao, J. and Liu, X. (2007) 'Fabrication of tubular NiO/YSZ anode-support of solid oxide fuel cell by gelcasting'. Journal of Power Sources v.165 (1), pp. 217-223.
76. Wang, H. T., Liu, X. Q. and Zheng, H. (1999) 'Gelcasting of $La_{0.6}Sr_{0.4}Co_{0.8}Fe_{0.2}O_{3-\delta}$ from oxide and carbonate powders'. Ceramics International v.25 (2), pp.177-181.
77. Li, G., Ren, R. and Wu, Z. (2004) 'Preparation of green body of La0.8Sr0.2MnO3 by gelcasting forming process'. Materials Letters v.58 (21), pp.2583-2585.
78. Carter, S., Selcuk, A. and Chater, R. J. (1992) 'Oxygen transport in selected nonstoichiometric perovskite-structure oxides'. Solid State Ionics: Part 1 v.53, pp. 597-605.
79. Jiang, S. P. and Wang, W. (2005) 'Effect of Polarization on the Interface between $(La, Sr)MnO_3$ Electrode and $Y_2O_3ZrO_2$ Electrolyte'. Electrochemical, Solid State Lett v.8 (2), pp. A115-A118

80. Bidrawn, F., Vohs, J. M. and Gorte, R. J. (2010) ‘Fabrication of LSM–YSZ Composite Electrodes by Electrodeposition’. Journal of the Electrochemical Society v.157(11), pp. B1629-B1633
81. Labrincha, J. A., Frade, J. R. and Marques, F. M. B. (1993) ‘$La_2Zr_2O_7$ formed at ceramic electrode/YSZ contacts’. Journal of Materials Science v.28(14), pp.3809-3815.
82. Badwal and Hughes, (1991) *Proceedings of the second international symposium on solid oxide fuel cells*, Brussels: Commission of the European Communities.
83. Kim, S. H., Ohshima, T. and Shiratori, Y. (2007) ‘Effect of Water Vapour and SOx in Air on the Cathodes of Solid Oxide Fuel Cells’. Mrs Proceedings v.1041.
84. Hagen, A., Chen, M. and Neufeld, K. (2009) ‘Effect of humidity in air on performance and long-term durability of SOFCs’. ECS Transactions v.25, pp.439-446.
85. Nielsen, J., Hagen, A. and Liu, Y. L. (2010) ‘Effect of cathode gas humidification on performance and durability of Solid Oxide Fuel Cells’. Solid State Ionics v.181, pp.517-524.
86. Babaei, A., Zhang, L. and Liu, E. (2011) ‘Performance and stability of $La_{0.8}Sr_{0.2}MnO_3$ cathode promoted with palladium based catalysts in solid oxide fuel cells’. Journal of Alloys and Compounds v.509 (14), pp. 4781-4787.
87. Zhang, X., Lin, B. and Ling, Y. (2010) ‘An anode-supported micro-tubular solid oxide fuel cell with redox stable composite cathode’. International Journal of Hydrogen Energy v.35 (16), pp. 8654-8662.
88. Orui, H., Watanabe, K. and Chiba, R. (2004) ‘Application of $LaNi(Fe)O_3$ as SOFC Cathode’. Journal of The Electrochemical Society v.151 (9), pp. A1412-A1417
89. Fouquet, D., Müller, A. C. and Weber, A. (2003) ‘Kinetics of Oxidation and Reduction of Ni/YSZ Cermets’. Ionics v.9, pp. 103-108
90. Waldbillig, D., Wood, A. and Ivey, D. (2005) ‘Thermal analysis of the cyclic reduction and oxidation behaviour of SOFC anodes’. Solid State Ionics v.176, pp.847-859.

91. Klemensø, T., Chung, C. and Larsen, P.H. (2005) ‘The Mechanism Behind Redox Instability of Anodes in High-Temperature SOFCs’. Journal of the Electrochemical Society v.152 (11), pp. A2186–A2192
92. Robert, G., Kaiser, A. and Batawi, E. (2004) ‘Anode substrate design for redox-stable ASE cells’, *in* Mogensen, M. (ed.), *Proceedings of the 6th European SOFC Forum*, Lucerne, Switzerland.
93. Tietz, F., Arul Raj, I. and Stöver, D. (2004) ‘Statistical design of experiments for evaluation of Y–Zr–Ti oxides as anode materials in solid oxide fuel cells’. British Ceramic Transactions V.103(5), pp. 202-210
94. Tao, S. and Irvine, J. T. (2003) ‘A redox-stable efficient anode for solid-oxide fuel cells’. Nature Materials v. 2, pp. 320-323.
95. Marina, O. A., Canfield, N. L. and Stevenson, J. W. (2002) ‘Thermal, electrical, and electrocatalytical properties of lanthanum-doped strontium titanate’. Solid State Ionics v.149, pp. 21-28.
96. S.Q. Hui, A. Petric, J. Electrochem. Soc. 149 (2002) J1. Hui, S. and Petric, A. (2002) ‘Electrical Properties of Yttrium-Doped Strontium Titanate under Reducing Conditions’. Journal of the Electrochemical Society v.149 (1), pp. J1-J10
97. Bevilacqua, M., Montini, T. and Tavagnacco, C. (2007) ‘Preparation, Characterization, and Electrochemical Properties of Pure and Composite LaNi0.6Fe0.4O3-Based Cathodes for IT-SOFC’. Chemistry of Materials v.19 (24), pp. 5926-5936.
98. Nielsen, J., Jacobsen, T. and Wandel, M. (2011) ‘Impedance of porous IT-SOFC LSCF:CGO composite cathodes’. Electrochimica Acta v.56 (23), pp. 7963-7974.
99. Bossel, U. (ed.) (1994). *First European Solid Oxide Fuel Cell Forum: 3-7 October 1994*, Lucerne, Switzerland : proceedings. Baden: European SOFC Forum Secretariat.
100. Mallory, G. O. and Hajdu, J. B. (1990) *Electroless plating: Fundamentals and applications*. Orlando, Fla: AESF.
101. Okinaka, Y. and Osaka, T. (1994) ‘Electroless Deposition Processes: Fundamentals and Applications’, in Gerischer, H. and Tobias,C.(ed.)

Advances in Electrochemical Science and Engineering, New York: *VCH Publishers*

102. Djoki´c, S. S. (2002) 'Electroless Deposition of Metals and Alloys', in Conway, B. E. and White, R.E.(ed.), *Modern Aspects of Electrochemistry*, New York: Kluwer Academic/Plenum Publishers,

103. Zhou, W., Ran, R. and Shao, Z. (2008) 'Electrochemical performance of silver-modified $Ba_{0.5}Sr_{0.5}Co_{0.8}Fe_{0.2}O_{3-\delta}$ cathodes prepared via electroless deposition'. Electrochimica Acta v.53 (13), pp. 4370-4380.

104. Baba, N. B. and Davidson, A. (2011) 'Investigation of Ni-YSZ SOFC Anode Fabricated Via Electroless Nickel Co-Deposition'. Procedia Engineering v.23, pp. 474-478.

105. Djokić, S. S. (ed.) (2010). *Electrodeposition: Theory and practice*, New York: Springer.

106. Kanani, N. (2004). *Electroplating: Basic principles, processes and practice*. Oxford: Elsevier Advanced Technology.

107. Ebnesajjad, S. (2011). *Handbook of adhesives and surface preparation: Technology, applications and manufacturing.* Amsterdam: William Andrew/Elsevier.

108. University of California. *Introduction to Energy Dispersive X-ray Spectrometry (EDS). [online],* http://cfamm.ucr.edu/documents/eds-intro.pdf *, available at October,2014*

109. Lasia, A. (1999) 'Electrochemical Impedance Spectroscopy and Its Applications', in Conway, B. E., Bockris, J. and White, R.E.(ed.) *Modern Aspects of Electrochemistry*, New York: Kluwer Academic / PlenumPublishers.

110. Bevilacqua, M., Montini, T. and Tavagnacco, C. (2007) 'Preparation, Characterization, and Electrochemical Properties of Pure and Composite $LaNi_{0.6}Fe_{0.4}O_3$-Based Cathodes for IT-SOFC'. Chemistry of Materials v.19 (24), pp. 5926-5936.

111. Jørgensen, M. J., Primdahl, S. and Mogensen, M. (1999) 'Characterisation of composite SOFC cathodes using electrochemical impedance spectroscopy'. Electrochimica Acta v.44 (24), pp. 4195-4201.

112. Nwosu, N. O. E., (2013) ‘Optimisation of electroless co-deposited solid oxide fuel cell electrodes’. Ph.D. thesis, Edinburgh Napier University.

113. Macdonald, J. R. (1992) ‘Impedance spectroscopy’. Annals of Biomedical Engineering v. 20(3), pp. 289-305

114. Mori, M., Yamanoto, T. and Itoh, H. (1998) ‘Thermal Expansion of Nickel‐Zirconia Anodes in Solid Oxide Fuel Cells during Fabrication and Operation’. J. Electrochem. Soc v.145 (4), pp.1374-1381

115. Tietz, F. (1999) ‘Thermal expansion of SOFC materials’. Ionics v.5 (1-2), pp. 129-139.

116. Stodolny, M. K. Boukamp, B. A. and Blank, D. H. A. (2012) ‘Impact of Cr-poisoning on the conductivity of different $LaNi_{0.6}Fe_{0.4}O_3$ cathode microstructures’. Solid State Ionics, v. 225(2), pp. 136-140.

117. Weber,A. Manner,R. and Waser,R.(1996) ‘Interaction between microstructure and electrical properties of screen printed cathodes in SOFC single cells’. Denki Kagaku oyobi KogyoButsuri Kagaku v.64(6), pp. 582-589

118. Virkar, A.V. Chen, J. and Tanner,C. (2000) ‘The role of electrode microstructure on activation and concentration polarizations in solid oxide fuel cells’. Solid State Ionics v.131 (1-2), pp.189 -198